IDŐJÁRÁS

QUARTERLY JOURNAL
OF THE HUNGARIAN METEOROLOGICAL SERVICE

CONTENTS

****

http://omsz.met.hu/english/ref/jurido/jurido_en.html

VOL. 107 * NO. 2 * APRIL–JUNE 2003

IDŐJÁRÁS

Quarterly Journal of the Hungarian Meteorological Service

Editorial Office: P.O. Box 39, H-1675 Budapest, Hungary or
Gilice tér 39, H-1181 Budapest, Hungary
E-mail: prager.t@met.hu or *antal.e@met.hu*
Fax: (36-1) 346-4809

Subscription by

mail: IDŐJÁRÁS, P.O. Box 39, H-1675 Budapest, Hungary
E-mail: prager.t@met.hu or *antal.e@met.hu*; *Fax: (36-1) 346-4809*

Dr. Pál Ambrózy is 70

Dr. Pál Ambrózy has recently celebrated his 70th birthday. On this occasion we wish to congratulate him and also express our greatest honour for the enormous work he has completed during his carrier for the Hungarian meteorology and the society of Hungarian meteorologists.

He was born in 1933 in Rimaszombat. He completed his studies at the secondary school in Nyiregyháza, then he obtained a meteorologist diploma at the Eötvös Loránd University of Sciences (Budapest) in 1955. He obtained his university doctor degree in 1963. He devoted his entire life to the service of the Meteorological Service of Hungary and also the Hungarian Meteorological Society, for which he has been the President from 1991.

Just after finishing his studies he begins to work at the Meteorological Service. In the first years he works in a research team dealing with dynamical meteorology, where

he soon becomes the head. There he plays a significant role in the domestic implementation of numerical and graphic methods of weather forecasting, which were in the frontline of development of meteorological science at that time. He also participates in the establishment of objective methods of storm forecasting at Lake Balaton. In 1968 he spent one year in the United States and in the Soviet Union as a UN sponsored scholar. He serves as the head of the Central Office of the Service, then in 1974 he was appointed as the director of the Central Meteorological Institute. At that time this was the basic unit of the Service, whose tasks included the countrywide meteorological observations, data collection, and also climatological research. Under his direction many high quality scientific results were achieved in this institute, the recounting of that is beyond the limit of this short greeting note. The main thing is that he personally participates in scientific work and has many outstanding scientific results, like the mapping of climatic resources in Hungary, or the redaction of Climate Atlas of Hungary. He is one of the co-authors of the book "Register of small geographical regions of Hungary", which then won an Academic Award. The number of his scientific publications is over one hundred, and his name is fixed in the local macrosynoptic classification Ambrózy-Bartholy-Gulyás. He retired from the Service in 1991, but we cannot call this a retirement, because he is a most active worker of the Service even now.

He is the member of the Hungarian Meteorological Society from 1952. Under his presidency, as was mentioned before, the Society, which is an NGO, succeeded to survive the difficult period of the 1990's and now continues to work and develop properly, serving this way the interests of everybody, who is interested in the science of meteorology in Hungary. The Society now is a member of the European Meteorological Society, where he was elected as a council member.

For us Hungarian meteorologists a very important medium is the periodical "Légkör" ("Atmosphere") for which he is the Editor-in-Chief from 1978. Under his talented (I may say genial) supervision this periodical became and remains a central forum of distribution of information about meteorology for meteorologists and non-meteorologists in Hungary. It is a real pleasure to look at and read through every single issue of this journal.

Finally, we wish to mention, that he was awarded by the Steiner Lajos Memorial Prize in 1975, then with the Hungarian Scientific Societies Award in 1999, finally with the highest possible award for Hungarian meteorologists, the Schenzl Guido Award in 2000.

In the name of myself and the whole editorial board of the Időjárás I would like to wish "uncle Pali" good health and many further years of fruitful work for the interest of Hungarian meteorology.

Tamás Práger

IDŐJÁRÁS

Quarterly Journal of the Hungarian Meteorological Service
Vol. 107, No. 2, April–June 2003, pp. 85–114

Application of a cloud model in simulation of atmospheric sulfate transport and redistribution Part I. Model description

Vlado Spiridonov[1] and **Mladjen Ćurić**[2]

[1]*Institute of Physics, Faculty of Natural Sciences and Mathematics,*
St. Cyril and Methodius University,
Branislav Nusic 11-1/17, 1000 Skopje, Macedonia
E-mail: vspiridonov@meteo.gov.mk

[2]*Department of Meteorology, Faculty of Physics, University of Belgrade,*
11000 Belgrade, P.O. Box 550, Yugoslavia
E-mail: curic@ff.bg.ac.yu

(Manuscript received December 7, 2001; in final form September 25, 2002)

Abstract–The authors have incorporated the sulfur chemistry in a rather sophisticated three-dimensional compressible meso-scale cloud model with a standard bulk parameterization of microphysics. The governing equations of the model include momentum conservation equations, thermodynamic and pressure equations, four continuity equations for the various water substances, and the subgrid scale (SGS) turbulent kinetic energy equation (TKE). The chemical part is formulated in terms of the continuity equations in the gaseous, aqueous, and ice phases within the cloud. The absorption of a gas phase chemical species in the cloud water and rainwater is determined either by the equilibrium according to Henry's law or by mass transfer limitation calculations in order to include the possible non-equilibrium states. After dissolution into cloud water and rain, follows the transfer of a soluble compound through the microphysical processes that affect the parent hydrometeor. All dissolved compounds are retained during the conversion of liquid drops to frozen hydrometeors. Melting of ice, snow, or hail again totally transfers the dissolved matter to cloud water and rain. During sublimation of hail and snow, dissolved scalar is retained in the hail or snow, unless all hydrometeor mass is converted to gas phase. The calculation of the cloud water pH and rainwater pH is based on the equilibrium hydrogen ion concentration for $[H^+]$, which is given by the simple charge balance equation.

Part I of the paper gives the detailed description of the model including the chemistry. Results of case studies with the model are described in Part II of the present article, which will be published in a later issue of this journal.

Key-words: scavenging, oxidation, sulfate transport, redistribution, wet deposition.

1. Introduction

The interactions between clouds, atmospheric aerosols, and gases have important effects on the chemical composition of atmospheric hydrometeors and on the long-range transport of air pollutants. Deep convection significantly contributes to the transport and vertical redistribution of atmospheric pollutants (e.g., *Isaac et al.*, 1982, 1983). Many studies have been devoted to these issues in the past. Most of the early models are one-dimensional (e.g., *Hales,* 1982; *Walcek* and *Taylor,* 1986; *Taylor,* 1989a,b) constraining the physical interpretation of the model results. *Sarma* (1986) examined the in-cloud conversion of SO_2 for a single case using a two-dimensional Eulerian model. Studies by *Tremblay* and *Leighton* (1986) and *Niewiadomski* (1989) apply three-dimensional cloud chemistry models and their applications to redistribution of chemical species during convection, but they primarily focus on warm convective clouds. On the other hand, *Wang* and *Chang,* (1993a,b) have developed a three-dimensional cloud chemistry model focused on deep convection and chemical processes related to in-cloud transformations and redistribution of pollutants. *Flossmann* and *Wobrock* (1996), *Kreidenweis et al.* (1997) studied the transport of SO_2 in convective clouds and chemical reactions. *Skamorock et al.* (2000) have examined tracer transport in three-dimensional simulations using the Klemp-Wilhemson model. *Crutzen* and *Lawrence* (2000) used a three-dimensional global model to examine the impact of convective and large scale precipitation scavenging on the transport of trace gases. More recently *Barth et al.* (2001) examined the redistribution of gases with various solubility during deep convection, while *Yin et al.* (2001) examined the trace gas redistribution using a two-dimensional dynamic cloud model with detailed microphysics and spectral treatment of gas scavenging. *Table 1* gives a short review of studies, focused on deep convection and transport of various species, using cloud chemistry models with different dynamical, microphysical, and chemical frameworks.

Part I is focused on cloud model formulation and description of model dynamics, thermodynamics, and microphysics (Section 2). The microphysical and chemical processes of the sulfuric compounds are illustrated in Section 3. Chemical reactions of these compounds, their mass transfer between gas and liquid phases, and also their mass transfer between cloud hydrometeors, and finally calculation of pH are described.

2. Cloud model formulation and description

The present version of the model is a three-dimensional, nonhydrostatic, time-dependant, compressible system which is based on the *Klemp* and *Wilhelmson*

(1978) dynamics, *Lin et. al.* (1983) microphysics, *Orville* and *Kopp* (1977) thermodynamics, and *Taylor* (1989b) sulfate chemistry. The governing equations of the model include momentum conservation equations, thermodynamic and the pressure equations, four continuity equations for the water substances, a subgrid scale (SGS) turbulent kinetic energy equation (TKE), and continuity equations for chemical species associated with various cloud water species.

Table 1. A review of studies with brief description of their cloud-chemistry model formulations

Authors of separate studies→	***Taylor*** **(1989a,b)**	***Tremblay*** **and** ***Leighton*** **(1986)**	***Wang*** **and** ***Chang*** **(1993b)**	***Crutzen*** **and** ***Lawrence*** **(2000)**	***Barth et al.,*** **(2001)**	***Yin et al.*** **(2001)**	***Spiridonov*** **and** ***Curič*** **(present model)**
The basic characteristic of the model	1-D dimensional cumulus cloud model	3-D (warm cumulus cloud model)	3-D non-hydrostatic cloud model	3-D global model (MATCH)	3-D non-hydrostatic cloud model	2-D non-hydrostatic cloud model	3-D non-hydrostatic cloud model
Model dynamics and thermodynamics	1.5 D Eulerian model cloud TKE Local turbulent Kinetic energy	Compressible Cloud model	Compressible cloud model Ice-liquid potential temperature 1-order closure scheme	Global model for chemical transport	Compressible cloud model	Slab-symmetric	Compressible cloud model TKE 1- order closure scheme Prognostic equation for entropy
Model microphysics	Bulk-water microphysics	A simply bulk-parameterization warm microphysics	Semi-spectral microphysics scheme	Semi-explicit cloud microphysics scheme	Mixed phase. Particle microphysics	Detail microphysics. Method of multi moments	Bulk-water parameterization with significant improvements
Model chemistry	Sulfate chemistry parameterization	Liquid-gas phase chemistry	Gas phase and liquid-ice phase chemical reactions	Transport trace- gases Scavenging and dissolution in liquid phase	Transport and scavenging of tracers (highly soluble and passive tracers)	Spectral treatment of scavenging and redistribution of gases (tracers)	Liquid-ice phase chemical reactions (sulfate chemistry) inside clouds

2. 1 The model dynamics

2.1.1 The momentum equations

The momentum equations are derived from the Navier-Stokes equations with the aid of the moist equation of state:

$$p = \rho R_d T(1 + 0.608 q_v), \tag{1}$$

where p is the pressure; ρ is the density of moist air; R_d is the gas constant for dry air; T is the temperature; and q_v is the mixing ratio of water vapor. Re-written in terms of non-dimensional pressure or the Exner function Π :

$$\Pi = \left(\frac{p}{p_0} \right)^{R_d / c_p} = \left(\frac{R_d}{p_0} \rho \theta_v \right)^{R_d / c_v} \tag{2}$$

Here p_0 is the basic state pressure at the ground and θ_v is the virtual potential temperature. Using the Boussinesq-approximation for homogeneous and rotating fluid, taking into account advection, turbulent transport, buoyancy (either due to warming or loading hydrometeors), and pressure gradient force, the tensor form of the momentum equations could be written as:

$$\frac{d\vartheta_i}{dt} + c_p \theta_{\vartheta 0} \frac{\partial \pi'}{\partial x_i} = \left(\frac{\theta'}{\theta_0} + 0.608 q_{\vartheta}' - q_c - q_r \right) g \delta_{i3} - \varepsilon_{i3l} f \vartheta_l + F_{ui}. \tag{3}$$

In this equation ϑ_i $(i = 1,2,3)$ is the wind speed component along the ith coordinate axis; c_p is the specific heat at constant pressure of dry air; $\theta_{\vartheta 0} = c_p \theta_0 (1 + 0.608 q_{\vartheta 0})$; π' is the deviation of non-dimensional pressure or Exner function from the initial unperturbed state Π_0; θ' and q_{ϑ}' are the perturbations of the initial potential temperature and mixing ratio of water vapor; θ_0 is equilibrium value of the potential temperature; q_c and q_r are the mixing ratios of cloud water and rainwater, respectively; δ_{i3} is the delta function; g is the gravitational acceleration; ε_{i3l} is the appropriate tensor of third rang; f is the Coriolis parameter; and F_{ui} represents contribution of subgrid-scale processes to ϑ_i.

2.1.2 The pressure equation

The pressure equation is derived by taking substantial derivative of Eq. (2) using the compressible continuity equation,

$$\frac{\partial \rho}{\partial t} = -\frac{\partial}{\partial x_j}\overline{\rho u_j} - \frac{\partial}{\partial x_j}\overline{\rho'' u_j''}, \tag{4}$$

to eliminate $d\rho/dt$, and thermodynamic equation to eliminate $d\theta/dt$. The final equation has the following form:

$$\frac{\partial \pi'}{\partial t} + \frac{\bar{c}^2}{c_p \bar{\rho}\bar{\theta}_v^{\,2}}\frac{\partial}{\partial x_j}(\bar{\rho}\bar{\theta}_v u_j) = -u_j\frac{\partial \pi}{\partial x_j} + \frac{R_d \pi}{c_v}\frac{\partial u_j}{\partial x_j} + \frac{c^2}{c_p \theta_v^{\,2}}\frac{d\theta_v}{dt} + D_\pi . \tag{5}$$

Using the parallel tensor notation in the equations, $u_j\,(j=1,2,3)$ are the velocities u, v, w; $(\partial/\partial x_j)$ are partial derivatives along the axes (x,y,z); c is the speed of sound given by $c^2 = c_p R_d \Pi \theta_v / c_v$, and D_π is the subgrid scale contribution term for π'.

2.1.3 The thermodynamic equation

In the thermodynamic equation, the potential temperature derived by *Orville* and *Kopp* (1977) is used as a conservative variable for adiabatic processes. The flux-conserving form of the equation is

$$\begin{aligned}\frac{\partial \varphi'}{\partial t} &= -\vec{\vartheta}\cdot\nabla\varphi' + K_h\nabla\varphi' + \frac{L_f}{c_P T_{00}}(P_g' + P_s') + \frac{c_W}{T_{00}}(T - T_0)\,(P_{GMLT} + P_{SMLT}) \\ &- \frac{c_W}{T_{00}}\left[q_{CW}\vec{\vartheta}\cdot\nabla T + q_R(\vec{\vartheta} - \vec{k}U_R)\cdot\nabla T\right] - \frac{c_I}{c_P T_{00}}\delta\left[q_{CI}\vec{\vartheta}\cdot\nabla T + q_G(\vec{\vartheta} - \vec{k}U_G)\cdot\nabla T\right. \\ &\left. + q_S(\vec{\vartheta} - \vec{k}U_S)\cdot\nabla T\right],\end{aligned} \tag{6}$$

where φ' is the specific entropy of the moist air; K_h is the heat eddy coefficient; L_f is the latent heat of freezing; P_g' is the total production rate of hail; P_s' is the total production rate of snow; C_W is the specific heat of water; T_0 is the melting temperature; P_{GMLT} is the production rate of rain from melting of hail; P_{SMLT} is the production rate of rain from melting snow; $q_{CW}, q_{CI}, q_R, q_G, q_S$ are the mixing ratios of cloud water, cloud ice, rain, hail,

and snow; C_I is the specific heat of ice; and U_r, U_g, U_s represent terminal velocities for rain, hail, and snow, respectively. The first two terms on the right-hand side of Eq. (6) represent the advection and turbulent mixing effects. The third term shows the heating effect of liquid water freezing, or the cooling effect of melting. The fourth term indicates the energy needed to warm the melted hail and snow from 0°C to the ambient temperature. The last two terms represent the energy changes due to the various hydrometeors coming into thermal equilibrium with the environment as they move through a layer with changing temperature gradient.

2.1.4 The subgrid scale parameterization

The parameterization of subgrid scale fluxes is based on the solution of the turbulent kinetic energy (TKE) equation given in the form

$$\frac{\partial E}{\partial t}+\overline{\vartheta}_K\frac{\partial E}{\partial x_K}=\delta_{I3}g\,\overline{\vartheta_I'\left(\frac{\theta''}{\theta_0}+0.608q_v''-q_C'\right)}-\overline{\vartheta_I'\vartheta_K'}\frac{\partial\overline{\vartheta}_I}{\partial x_K}$$

$$-\frac{\partial}{\partial x_K}\overline{[\vartheta_K(E+c_p\theta_{v0}\Pi'')]}-\nu\,\overline{\frac{\partial\vartheta_I'}{\partial x_K}\frac{\partial\vartheta_I'}{\partial x_K}}, \tag{7}$$

where

$$E=\frac{1}{2}\overline{(\vartheta_i')^2} \tag{8}$$

is the subgrid-scale kinetic energy per unit mass. The terms on the right-hand side of Eq. (7) represent the effects of buoyancy, shear, diffusion, and dissipation. Eq. (7) is derived from momentum equation, Eq. (3), for incompressible fluid ($\rho = \text{const}$), performing Reynolds averaging on each of the prognostic variables and applying the first-order closure to the nearly conservative variables. Heat eddy coefficient is assumed to be proportional to the momentum eddy coefficient. Details could be found in study by *Klemp* and *Wilhemson* (1978).

2.2 Cloud microphysics

For the parameterization of the microphysical processes we use the integrated (bulk) water parameterization by *Lin et al.* (1983), with significant improvement of hail growth parameterization. Instead of using the hail size spectrum from zero to infinity (idealized spectrum), *Curic* and *Janc* (1995, 1997) proposed considering the hail size spectrum which includes only hail sized parti-

cles (larger than 0.5 cm in diameter; hereafter called realistic hail spectrum). Six types of water substances are included: water vapor, cloud water, cloud ice, rain, snow, graupel, and hail. Cloud water and cloud ice are assumed to be monodisperse, with zero terminal velocities. Cloud water droplets have identical mass $M_w = 4.19 \times 10^{-9}$ g, while cloud ice crystals have mass $M_i = 4.19 \times 10^{-10}$ g. Rain, hail, and snow have Marshall-Palmer type size distributions with fixed intercept parameters: $n_{0R} = 8 \times 10^{-2}$ cm^{-4}, $n_{0H} = 4 \times 10^{-4}$ cm^{-4}, and $n_{0S} = 3 \times 10^{-2}$ cm^{-4}. The assumed values for density of rain, hail, and snow are 1 g cm^{-3}, 0.9 g cm^{-3}, and 0.1 g cm^{-3}. The density of air is separately calculated. These six forms of the water substances interact mutually.

Four continuity equations for the various water substances

$$\frac{\partial q}{\partial t} = -\vec{\vartheta} \cdot \nabla q + \nabla \cdot K_h \nabla q - P_R - P_S - P_G , \tag{9}$$

$$\frac{\partial q_R}{\partial t} = -\vec{\vartheta} \cdot \nabla q_R + \nabla \cdot K_m \nabla q_R + P_R + \frac{1}{\rho} \frac{\partial}{\partial z} (U_R q_R \rho) , \tag{10}$$

$$\frac{\partial q_G}{\partial t} = -\vec{\vartheta} \cdot \nabla q_G + \nabla \cdot K_m \nabla q_G + P_G + \frac{1}{\rho} \frac{\partial}{\partial z} (U_G q_G \rho) , \tag{11}$$

$$\frac{\partial q_S}{\partial t} = -\vec{\vartheta} \cdot \nabla q_S + \nabla \cdot K_m \nabla q_S + P_S + \frac{1}{\rho} \frac{\partial}{\partial z} (U_S q_S \rho) , \tag{12}$$

where $q = r + q_{CW} + q_{CI}$; q_{CW}, q_{CI}, q_R, q_G, q_S, and r are the mixing ratios for cloud water, cloud ice, rain, hail/graupel, snow, and water vapor, respectively; K_h is the eddy heat diffusion coefficient; K_m is the eddy momentum diffusion coefficient; U_R, U_G, U_S are terminal velocities for rain, hail/graupel, and snow, and P_R, P_G, and P_S are production terms for rain, hail, and snow.

The source reference for the scheme to allow coexistence of cloud water and cloud ice in the temperature region of –40 to 0°C is derived from *Hsie et al.* (1980). Condensation and deposition of water vapor produce cloud water and cloud ice, respectively. Conversely, evaporation and sublimation of cloud water and cloud ice maintain saturation. Natural cloud ice is normally initiated by using a Fletcher-type equation for the ice nuclei number concentration. In this version of the model, cloud ice may also be produced by the Hallett-

Mossop ice multiplication. Bergeron-Findeisen process transforms some of the cloud water into cloud ice and, to a certain extent, both of them into snow.

Rain is produced by the auto-conversion of cloud water, melting of snow and hail, and shedding during the wet growth of hail.

Hail is produced by the auto-conversion of snow, interaction of cloud ice and snow with rain, and by immersion freezing of rain.

Snow may be produced by the auto-conversion, Bergeron-Findeisen growth of cloud ice, and interaction of cloud ice and rain. All types of precipitation elements grow by different forms of accretion. Evaporation (sublimation) of all types of hydrometeors is also simulated.

3. Microphysics and chemical processes of the sulfuric compounds

The chemical model is based on the sulfate chemistry taken from *Taylor* (1989b) and represents an extension of already published work concerning warm clouds from *Tremblay* and *Leighton* (1986).

To study the interactions between clouds, aerosols, and gases participating in sulfate production, the model is formulated in terms of continuity equations. If the concentration of the *i*th pollutant is expressed by the mixing ratio in the air, cloud water and cloud ice by $q_{i,a}$, rain by $q_{i,r}$, graupel or hail by (q_{i,g_h}), and snow by $q_{i,s}$, then the local change of each component separately is given by the following conserving forms which are consistent with the dynamics and thermodynamics formulations:

$$\frac{\partial q_{i,a}}{\partial t} + \vec{\vartheta} \cdot \nabla q_{i,a} = E_{i,a} + SM_{i,a} + Sq_{i,a} \qquad j = 1, 2, 3, \tag{13}$$

$$\frac{\partial q_{i,r}}{\partial t} + \vec{\vartheta} \cdot \nabla q_{i,r} - SF_{i,r} = E_{i,r} + SM_{i,r} + Sq_{i,r}, \tag{14}$$

$$\frac{\partial q_{i,g\_h}}{\partial t} + \vec{\vartheta} \cdot \nabla q_{i,g\_h} - SF_{i,g\_h} = E_{i,g\_h} + SM_{i,g\_h} + Sq_{i,g\_h}, \tag{15}$$

$$\frac{\partial q_{i,s}}{\partial t} + \vec{\vartheta} \cdot \nabla q_{i,s} - SF_{i,s} = E_{i,s} + SM_{i,s} + Sq_{i,s}, \tag{16}$$

where $\vec{\vartheta}$ is the wind velocity vector with components (u, v, w); $E_{i,a}$, $E_{i,c}$, $E_{i,r}$, E_{i,g_h}, and $E_{i,s}$ are the subgrid contribution terms; $SM_{i,a}$, $SM_{i,r}$, SM_{i,g_h}, and $SM_{i,s}$ are redistribution terms induced by microphysical conversion processes given by the relation

$$SM_{i,w} = q_{i,w}\, q_m(\mathrm{w} \rightarrow \mathrm{i})/q_w\,, \tag{17}$$

where $q_m(\mathrm{w} \rightarrow \mathrm{i})$ is the rate of microphysical transformation derived from the microphysical scheme. During transformation the water "w" is considered to lose mass and the category "i" to gain mass. $q_{i,w}$ is the mixing ratio of pollutant "i" associated with water "w" and q_w is the mixing ratio of water. $Sq_{i,a}$, $Sq_{i,r}$, Sq_{i,g_h}, and $Sq_{i,s}$ denote the chemical transformation terms, while the falling rates for hydrometeors $SF_{i,r}$, SF_{i,g_h}, and $SF_{i,s}$ are given by

$$SF_{i,r,g\_h,s} = \frac{1}{\bar{\rho}\rho}\frac{\partial}{\partial x_3}(\bar{\rho}\, U_{r,g\_h,s}\; q_{i,r,g\_h,s})\,, \tag{18}$$

where $\bar{\rho}$ is the initial unperturbed value of air density, $U_{r,g\_h,s}$ are terminal velocities of rain, graupel or hail, and snow, respectively.

3.1. The mass transfer between gas and liquid phases

The absorption of a gas phase chemical species in the cloud water and rainwater is determined either by the equilibrium according to Henry's law or by mass transfer limitation calculations in order to include the possible non-equilibrium states.

Gases (with an effective Henry's law constant $K_H^{*} < 10^3$ mol dm^{-3} atm^{-1}) in cloud water and rain are assumed to be in equilibrium with the local gas-phase concentrations. These liquid-phase concentrations of each chemical component "**i**" are calculated according to Henry's law, i.e.,

$$[\mathbf{i}] = K_H\, p_{\mathbf{i}}\,, \tag{19}$$

where **[i]** is given in units of mol **i**/L H_2O (M); K_H is the Henry's law coefficient (M atm^{-1}); and p_{i} is the partial pressure of the species "**i**" given in units atm. All equilibrium constants and oxidation reactions are temperature dependent according to van't-Hoff's relation

$$K_T = K_{T0} \exp\left(-\Delta H/R\,(1/T - 1/T_0)\right), \tag{20}$$

where ΔH is the increase of enthalpy induced by chemical reactions; K_{T0} is the equilibrium constant at a standard temperature T_0=298 K; and R is the universal gas constant. However, a chemical species may not attain equilibrium on the time scales of the cloud model because of slow mass transfer between phases. In that case a fully kinetic calculation of gas dissolution into the cloud droplets and raindrops is included in the model. The rate of mass transfer among gas species "**i**", spectra of drops with diameter α, and number concentration N_α (per mole air) could be expressed by the following relation by *Yin et al.* (2001):

$$\frac{dq_{d,i,a}}{dt} = \frac{12\eta D_{g,i} N_{Sh,i}}{RT\alpha^2}\left(V_\alpha N_\alpha P_i - \frac{q_{d,i,\alpha}}{K_H^*}\right), \tag{21}$$

where $q_{d,i,\alpha}$ is the rate of molar mixing ratio of gas species inside drops with diameter α to that in the air; K_H^* is the effective Henry's law constant of species "**i**"; R is the universal gas constant; T is the temperature; $D_{g,i}$ is the diffusivity of gases "**i**" in air which are taken from *Pruppacher* and *Klett* (1997); V_α is the volume of drops with diameter α; P_i is the partial pressure of gas species "**i**" in the environment; $N_{Sh,i}$ is the mass ventilation coefficient (Sherwood number); and η is a factor which is a function of the Knudsen-number K_n and sticking coefficient γ_i of gas species "**i**" on spherical drops.

3.2. Mass transfer between cloud hydrometeors

After dissolution into cloud water and rain, follows the transfer of a soluble compound through the microphysical processes that affect the parent hydrometeor.

The present cloud modeling study includes a freezing transport mechanism of chemical species based on *Rutledge et al.* (1986). Similar approach could be found in studies (e.g., *Wang* and *Chang*, 1993a; *Chen* and *Lamb*, 1994; *Kreidenweis et al.*, 1997).

It is assumed that all dissolved compounds are retained during the conversion of liquid drops to frozen hydrometeors. Melting of ice, snow, or hail again totally transfers the dissolved matter to cloud water and rain. During sublimation of hail and snow, dissolved scalar is retained in the hail or snow, unless all hydrometeor mass is converted to gas phase.

3.3. The sulfate chemistry parameterization terms

Microphysical processes and chemical conversions for SO_4^{2-} in air and different water substances, and the names associated with each of them in the model are demonstrated in *Fig. 1*. The equilibrium chemical reactions and reaction constants for these processes as well as for S (IV) oxidations (see 3.4) are listed in *Table 2*.

(1) PS1(SUL1) – S(IV) solution in cloud water

The total concentration of the S(IV) species for pH ≤ 5.5, which is typical for cloud and rain water, is predominantly in the form of $[HSO_3^-]$. Thus the concentration of $[HSO_3^-]$ is given by

$$[HSO_3^-] = (K_1 K_2 p_{SO_2}) / [H^+]. \tag{22}$$

By substitution of the rate coefficients, and using expression for the partial pressure of SO_2 (in Pascal's) given by

$$p_{SO_2} = p q_{SO_2} / \left(\frac{M_{SO_2}}{M_d} + q_{SO_2} \right), \tag{23}$$

the rate, at which SO_2 is removed from the atmosphere or return in gaseous phase, is written as

$$\text{PS1(SUL1)} = \frac{K_1 K_2}{[H_C^+]} p q_{SO_2} \frac{M_{SO_2}}{M_{HSO_3^-}} \frac{\delta q_c}{\delta t}, \tag{24}$$

where p is the air pressure; $(\delta q_c / \delta t)$ is condensation rate for cloud water; and $[H_C^+]$ is the equilibrium hydrogen ion concentration in cloud water. The molecular weights M_{SO_2} and $M_{HSO_3^-}$ for SO_2 and $[HSO_3^-]$ are included since SUL1 is a sink term for SO_2.

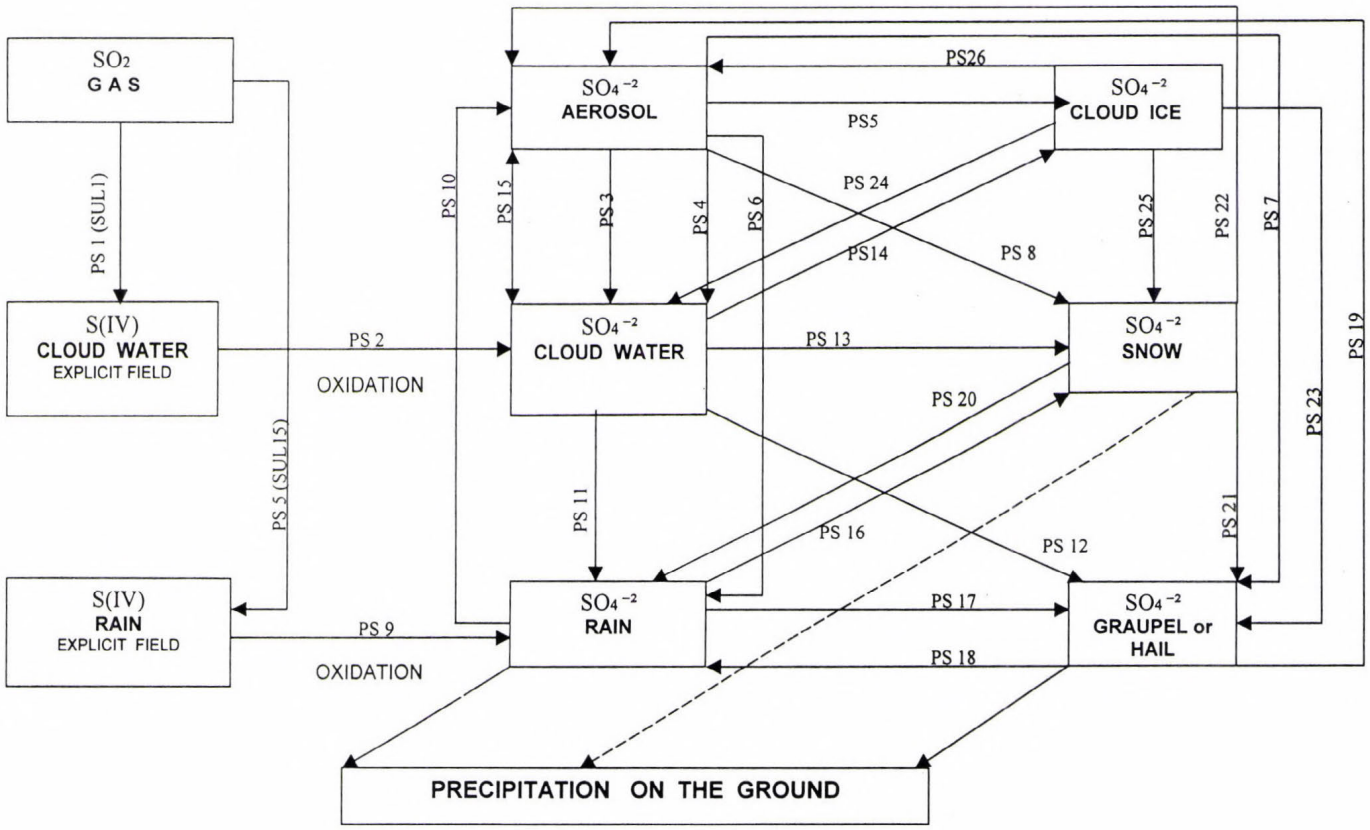

Fig. 1. Scheme of microphysics- and chemistry-related conversions for SO_4^{2-} in air and different water categories, and the names associated with each of them in the model.

Table 2. Equilibrium reactions, rate coefficients, S (IV) oxidations, and the corresponding coefficients

No.	Reactions	K_{298} (M or M atm^{-1})	$-H_{298}/R(K)$	References
1	SO_2 (g) $\Leftrightarrow$ SO_2 (aq)	1.2	3135	(1)
2	SO_2 (aq) $\Leftrightarrow$ $HSO_3^- + H^+$	1.3×10^{-2}	2000	(2)
3	$HSO_3^- \Leftrightarrow SO_3^{-2} + H^+$	6.3×10^{-8}	1495	(3)
4	O_3 (g) $\Leftrightarrow$ O_3 (aq)	1.13×10^{-2}	2300	(4)
5	H_2O_2 (g) $\Leftrightarrow$ H_2O_2 (aq)	7.1×10^4	6800	(5)
6	NH_3 (g) $\Leftrightarrow$ NH_4OH (aq)	75	3400	(6)
7	HNO_3 (g) $\Leftrightarrow$ HNO_3 (aq)	2.1×10^5	8700	(7)
8	CO_2 (g) $\Leftrightarrow$ CO_2 (aq)	3.4×10^{-2}	2420	(8)
9*	S(IV) + $O_3 \rightarrow$ S(VI) + O_2	3.7×10^5	5530	(9)
10*	S(IV) + $H_2O_2 \rightarrow$ S(VI) + H_2O	7.45×10^7	4751	(10)

* In case of non-equilibrium reactions 9 and 10 in the head of columns 2 and 3 ΔK_{298} (M s^{-1}) and $-\Delta H_{298}/R$ (K) should be understood;

(1), (2), (3), (9), and (10) are derived from values given by Hoffmann and Calvert (1985);

(4), (6), and (8) by *Pandis* and *Seinfeld* (1989); (5) by *Martin* and *Damaschen* (1981), and (7) by *Schwartz* and *While* (1981)

(2) PS2 - Oxidation by O_3 and H_2O_2 to SO_4^{2-} in cloud water

As it is listed in *Table 2*, PS2 term is a combination of oxidation reactions. In pH range of interest, S(IV) is predominately in form of HSO_3. Thus the oxidation of O_3 and H_2O_2 could be expressed by rate equation

$$\frac{d}{dt}[SO_4^{2-}] = K_{S(IV)} \left\{ [HSO_3^-][O_{3_{aq}}] + [HSO_3^-][H_2O_{2_{aq}}] \right\} . \tag{25}$$

The term $K_{S(IV)}$ is a modified Henry's law coefficient given by relation

$$K_{S(IV)} = K_1 \left(1 + \frac{K_2}{[H_C^+]} \right). \tag{26}$$

Here $[O_3\,aq]$ and $[H_2O_2\,aq]$ concentrations are calculated using Henry's law coefficients given in *Table 2*, respectively:

$$\begin{aligned} [O_3\,aq] &= K_9 p_{O_3}\,, \\ [H_2O_2\,aq] &= K_{10} p_{H_2O_2}\,, \end{aligned} \tag{27}$$

where p_{O_3} is the partial pressure. Taking into account this relation and the conversion factor $q_{SO_4^{2-}} = 0.0961[SO_4^{2-}]q_c$ given in *Taylor* (1989), the total rate of S(IV) conversion to SO_4^{2-} is given by

$$PS2 = K_{S(IV)} \frac{K_1 K_2}{[H_C^+]} p q_{SO_2} / \left(\frac{M_{SO_2}}{M_d} + q_{SO_2} \right) \{ K_9 p_{O_3} + K_{10} p q_{H_2O_{2C}} \} 0.0961 q_c \quad (28)$$

(3) PS3 - Nucleation scavenging of SO_4^{2-} aerosol by CCN

The term for nucleation scavenging of SO_4^{2-} aerosol by CCN simply shows primary activation of cloud condensation nuclei (CCN), based on numerical integration of the droplet growth equation. According to *Jensen* and *Charlson* (1984), in typical continental cloud condensation nuclei, most primary activation occurs few hundred meters of cloud basis. Also their work shows high nucleation efficiency, 80–100% of total aerosol mass is activated and incorporated into cloud drops. *Taylor* (1989b) has been approximated this process by following expression:

$$PS3 = \begin{cases} \dfrac{\varepsilon_{SO_4^{2-}} q_{SO_4^{2-}a}}{\delta t}, & \delta qc > 0 \\ 0, & \delta qc \le 0 \end{cases}, \quad (29)$$

where $\varepsilon_{SO_4^{2-}} = 0.55$ is the fractional nucleation efficiency; δqc is the condensation of cloud drops during the current time step in the model. Secondary activation of CCN is not included in the model since we use a bulk water parameterization and fixed droplet number in cloud model.

(4a) $PS4_{CB}$ - Scavenging of SO_4^{2-} aerosol by Brownian diffusion in cloud drops

Stationary drops capture aerosol particles by simple Brownian diffusion. The $PS4_{CB}$ term on this way approximates to

$$PS4_{CB} = 4\pi D_p N_C q_{SO_4 a} \alpha_C \bar{f}_p, \quad (30)$$

where D_p is the diffusion coefficient set to $D_p = 1.56 \times 10^{-8}$ m^2 s^{-1}, (*Pruppacher* and *Klett,* 1997), N_C is the cloud droplet concentration; α_C is the mean cloud droplet diameter; and $\overline{f}_p$ is the mean ventilation coefficient .

(4b) $PS4_{IB}$ - Scavenging of SO_4^{2-} aerosol by Brownian diffusion in cloud ice

This term is similar to previous term $PS4_{CB}$ but is related to cloud ice and scavenging of SO_4^{2-} aerosol by Brownian diffusion. This term is approximated as

$$PS4_{IB} = 4\pi D_p N_I q_{SO_4 a} \alpha_I \bar{f}_p , \tag{31}$$

where D_p is the diffusion coefficient set to $D_p = 1.56 \times 10^{-8}$ m^2 s^{-1} (*Pruppacher* and *Klett,* 1997); N_I is the cloud ice concentration; α_I is the mean cloud ice diameter; and $\overline{f}_p$ the mean ventilation coefficient.

(5) PS5 - Nucleation scavenging of SO_4^{2-} aerosol by ice nuclei (IN)

Although the effects of the nucleation scavenging by ice crystals have not been studied in field, the term for nucleation scavenging of SO_4^{2-} aerosol by ice nuclei (IN), is conditionally computed in an analogous fashion to PS3:

$$PS5 = \begin{cases} \dfrac{\varepsilon_{SO_4^{2-}} q_{SO_4^{2-}a}}{\delta t} , & \delta qI > 0 \\ 0, & \delta qI \le 0 \end{cases} , \tag{32}$$

where $\varepsilon_{SO_4^{2-}} = 0.55$ is the fractional nucleation efficiency; δqI is the initiating the ice phase during the current time step in the model.

(6) PS6 - Impact scavenging of SO_4^{2-} aerosol by rain

The impact scavenging of SO_4^{2-} by rain is computed for continuos collection processes

$$-\frac{\partial q_{SO_4a}}{\partial t} = \int_0^\infty \frac{\pi}{4} \alpha_R{}^2 U_R(\alpha_R) q_{SO_4a} \varepsilon_R n_d(\alpha_R, t) d\alpha_R \,. \tag{33}$$

Assuming exponential size distributions for the precipitation particles, PS6 is reduced:

$$\text{PS6} = \frac{\pi}{4} \Gamma(3.5) \varepsilon_R U_R n_{0R} \alpha_R{}^{3.5} q_{SO_4} \,, \tag{34}$$

where n_{0R} is the slope intercept parameter of the rain; α_R is the diameter of rain; U_R is the mass-weighted mean terminal velocity of rain; and ε_R is the collection efficiency.

(7) PS7 - Impact scavenging of SO_4^{2-} aerosol by graupel

Similar as previous term, impact scavenging of SO_4^{2-} aerosol by graupel is calculated assuming continuos collection, i.e.,

$$\text{PS7} = \frac{3\pi}{7} \varepsilon_G U_G N_{TG} \alpha_G{}^2 q_{SO_4a} \,, \tag{35}$$

where N_{TG} is the total number of graupels; α_G is the diameter of graupel; U_G is the mass-weighted mean terminal velocity of graupel; and ε_G is the collection efficiency.

(8) PS8 - Impact scavenging of SO_4^{2-} aerosol by snow

Impact scavenging of SO_4^{2-} aerosol by snow is computed on similar way to terms PS6 and PS7:

$$\text{PS8} = \frac{\pi}{4} \varepsilon_S U_S N_{TS} \alpha_S{}^2 q_{SO_4a} \,, \tag{36}$$

where N_{TS} is the total number of snow; α_S is the diameter of graupel; U_S is the mass-weighted mean terminal velocity of snow; and ε_S is the collection efficiency.

(9) PS9 - Oxidation of S(IV) by O_3 and H_2O_2 to SO_4^{2-} in rainwater

The term PS9, which represents oxidation of S(IV) in rain, is computed on similar way as term PS2:

$$PS9 = K_{S(IV)} \frac{K_1 K_2}{[H_R^+]} pq_{SO_2} / \left(\frac{M_{SO_2}}{M_d} + q_{SO_2} \right) \left\{ K_9 p_{O_3} + K_{10} pq_{H_2O_2 p} \right\} 0.0961 q_c \quad (37)$$

Here $[H_R^+]$ is the hydrogen ion concentration in rain; while $q_{H_2O_2 R}$ is the hydrogen peroxide rain water mixing ratio.

(10) PS10 - S(IV) Evaporation of rain

This term calculates the rate at which SO_2 returns to the atmosphere during evaporation of rain. Since the pH range of cloud and rain water S(IV) is predominantly in form of $[HSO_3^-]$, now the conversion from $[HSO_3^-]$ to SO_2 gas during evaporation of rain, could be expressed by relation

$$PS10 = \frac{K_1 K_2}{[H_R^+]} pq_{SO_2} \frac{M_{SO_2}}{M_{HSO_3^-}} P_{REVP}, \quad (38)$$

where P_{REVP} is the evaporation from rain.

(11) PS11 - SO_4^{2-} transfer from cloud water to rain

This term follows the microphysical transition and transfers SO_4^{2-} from cloud water to rain SO_4^{2-}.

$$PS11 = \frac{q_{SO_4 C}}{q_C} (P_{RAUT} + P_{RACW} + P_{SACW}), \quad (39)$$

where P_{RAUT}, P_{RACW}, and P_{SACW} are autoconversion of cloud water to form rain, accretion of cloud water by rain, and accretion of cloud water by snow, respectively producing snow if $T < T_0$ or rain if $T \geq T_0$. Also enhances snow melting for $T \geq T_0$.

(12) PS12 - SO_4^{2-} transfer from cloud water to graupel

This term follows the microphysical transition and transfers SO_4^{2-} from cloud water to graupel SO_4^{2-}:

$$PS12 = \frac{q_{SO_4C}}{q_C} P_{GACW}, \tag{40}$$

where P_{GACW} is accretion of cloud water by graupel.

(13) PS13 - SO_4^{2-} transfer from cloud water to snow

This term parallels the microphysical transition and transfers SO_4^{2-} from cloud water to snow SO_4^{2-}:

$$PS13 = \frac{q_{SO_4C}}{q_C} (P_{SACW} + P_{SFW}), \tag{41}$$

where P_{SFW} is the Bergeron process (deposition and riming) transferring cloud water to snow; and P_{SACW} is explained in the previous part.

(14) PS14 - SO_4^{2-} transfer from cloud water to cloud ice

This term follows the microphysical transition and transfers SO_4^{2-} from cloud water to cloud ice SO_4^{2-}:

$$PS14 = \frac{q_{SO_4C}}{q_C} (P_{IDW} + P_{IHOM}), \tag{42}$$

where P_{IDW} and P_{IHOM} are depositional growth of cloud ice at expense of cloud water, and homogeneous freezing of cloud water to form cloud ice, respectively.

(15) PS15 - SO_4^{2-} transfer from cloud water to aerosol

This term transfer the cloud droplet SO_4^{2-} to aerosol during evaporation of

cloud droplets. This transfer occurs in the model when mean cloud droplet diameter falls below 1 μm:

$$PS15 = \frac{q_{SO_4C}}{\delta t}. \tag{43}$$

(16) PS16 - SO_4^{2-} transfer from rain to snow

On analogous fashion, this term follows the microphysical transition and transfers SO_4^{2-} from rain to snow SO_4^{2-}:

$$PS16 = \frac{q_{SO_4R}}{q_R}(P_{IACR} + P_{SACR}), \tag{44}$$

where P_{IACR} is the accretion of rain by cloud ice, producing snow or graupel depending on the amount of rain and accretion of rain by snow; and P_{SACR} represents accretion of rain by snow. For $T < T_0$, it produces graupel if rain or snow exceeds threshold; if not, it produces snow. For $T \geq T_0$, the accreted water enhances snow melting.

(17) PS17 - SO_4^{2-} transfer from rain to graupel

Similarly to the computation of the term PS16, this term follows the microphysical transition and transfers SO_4^{2-} from rain to graupel SO_4^{2-}:

$$PS17 = \frac{q_{SO_4R}}{q_R}(P_{GACR} + P_{GFR} + P_{IACR} + P_{SACR}), \tag{45}$$

where P_{GACR} and P_{GFR} are the accretion of rain by graupel, and probabilistic freezing of rain to form graupel, respectively.

(18) PS18 - Transfer of SO_4^{2-} from graupel to rain

On analogous fashion, this term follows the microphysical transition and transfers SO_4^{2-} from graupel to rain SO_4^{2-}:

$$PS18 = \frac{q_{SO_4G}}{q_G} P_{GMLT}, \tag{46}$$

where P_{GMLT} is the melting of graupel to form rain, $T \geq T_0$. (In this regime, P_{GACW} is assumed to be shed as rain).

(19) PS19 - SO_4^{2-} transfer from graupel to aerosol

This term represents the microphysical transition and transfers SO_4^{2-} from graupel to SO_4^{2-} aerosol:

$$\text{PS19} = \frac{q_{SO_4G}}{q_G} P_{GSUB}, \tag{47}$$

where P_{GSUB} is the sublimation of graupel.

(20) PS20 - Transfer of SO_4^{2-} from snow to rain

On analogous fashion, this term follows the microphysical transition and transfers SO_4^{2-} from snow to rain SO_4^{2-}:

$$\text{PS20} = \frac{q_{SO_4S}}{q_S} P_{SMLT}, \tag{48}$$

where P_{SMLT} is the melting of snow to form rain, $T \geq T_0$.

(21) PS21 - Transfer of SO_4^{2-} from snow to graupel

The term PS21 follows the microphysical transition and transfers SO_4^{2-} from snow to graupel SO_4^{2-}:

$$\text{PS21} = \frac{q_{SO_4S}}{q_S} (P_{GAUT} + P_{GACS} + P_{RACS}) \tag{49}$$

where P_{GAUT}, P_{GACS}, P_{RACS} are the autoconversion (aggregation) of snow to

form graupel, accretion of snow by graupel, and accretion of snow by rain, respectively; produces graupel if rain or snow exceeds threshold and $T < T_0$.

(22) PS22 - Transfer of SO_4^{2-} from snow to aerosol

The term PS22 parallels the microphysical transition and transfers SO_4^{2-} from snow to SO_4^{2-} aerosol:

$$\mathrm{PS22} = \frac{q_{\mathrm{SO_4}S}}{q_S}(P_{SSUB} + P_{SDEP}), \tag{50}$$

where P_{SSUB} and P_{SDEP} are the sublimation of snow, and depositional growth of snow, respectively.

(23) PS23 - SO_4^{2-} transfer from cloud ice to graupel or hail

On analogous fashion, this term follows the microphysical transition and transfers SO_4^{2-} from cloud ice to graupel or hail SO_4^{2-}:

$$\mathrm{PS23} = \frac{q_{\mathrm{SO_4}I}}{q_I}(P_{GACI} + P_{RACI}), \tag{51}$$

where P_{GACI} and P_{RACI} are the accretion of cloud ice by graupel, and accretion of cloud ice by rain, respectively, producing snow or graupel depending on the amount of rain.

(24) PS24 - Transfer of SO_4^{2-} from cloud ice to cloud water

On analogous fashion, this term follows the microphysical transition and transfers SO_4^{2-} from cloud ice to cloud water SO_4^{2-}:

$$\mathrm{PS24} = \frac{q_{\mathrm{SO_4}I}}{q_I} P_{IMLT}, \tag{52}$$

where P_{IMLT} the melting of cloud ice to form cloud water, $T \geq T_0$.

(25) PS25 - SO_4^{2-} transfer from cloud ice to snow

This term parallels the microphysical transition and transfers SO_4^{2-} from cloud ice to snow SO_4^{2-}:

$$\mathrm{PS25} = \frac{q_{\mathrm{SO}_4 I}}{q_I}(P_{SAUT} + P_{SACI} + P_{SFI} + P_{RACI}), \tag{53}$$

where P_{SAUT}, P_{SACI}, and P_{SFI} are the autoconversion (aggregation) of cloud ice to form snow, accretion of cloud ice by snow, and transfer rate of cloud ice to snow through growth of Bergeron process embryos, respectively.

(26) PS26 - SO_4^{2-} transfer from cloud ice to aerosol

This term transfers the cloud ice SO_4^{2-} to aerosol during evaporation of cloud ice. This transfer occurs in the model when mean cloud ice diameter falls below 1 μm:

$$\mathrm{PS26} = \frac{q_{\mathrm{SO}_4 I}}{\delta t}. \tag{54}$$

3.4 Hydrogen peroxide, ozone, and sulfur dioxide source terms

The scheme of H_2O_2, O_3 and SO_2 reactions are presented in *Fig. 2*. The source terms for H_2O_2 and O_3 include: equilibration between gas and aqueous phases using Henry's law, reduction due to oxidation of S(IV) in cloud drops and rain, as well as the set of microphysical transfer and conversions among different water categories. SO_2 field is explicitly treated in the model. The source terms of S(IV) are solution in cloud water and rain water, and microphysical conversions.

(1) PH1, OHP1, SUL1 - Equilibration of H_2O_2, O_3, and SO_2 in cloud droplets

As SUL1 is a sink term for SO_2 described before, PH1 and OHP1 are terms representing equilibration of H_2O_2 and O_3 concentrations in cloud droplets. According to Henry's law, these terms could be expressed as

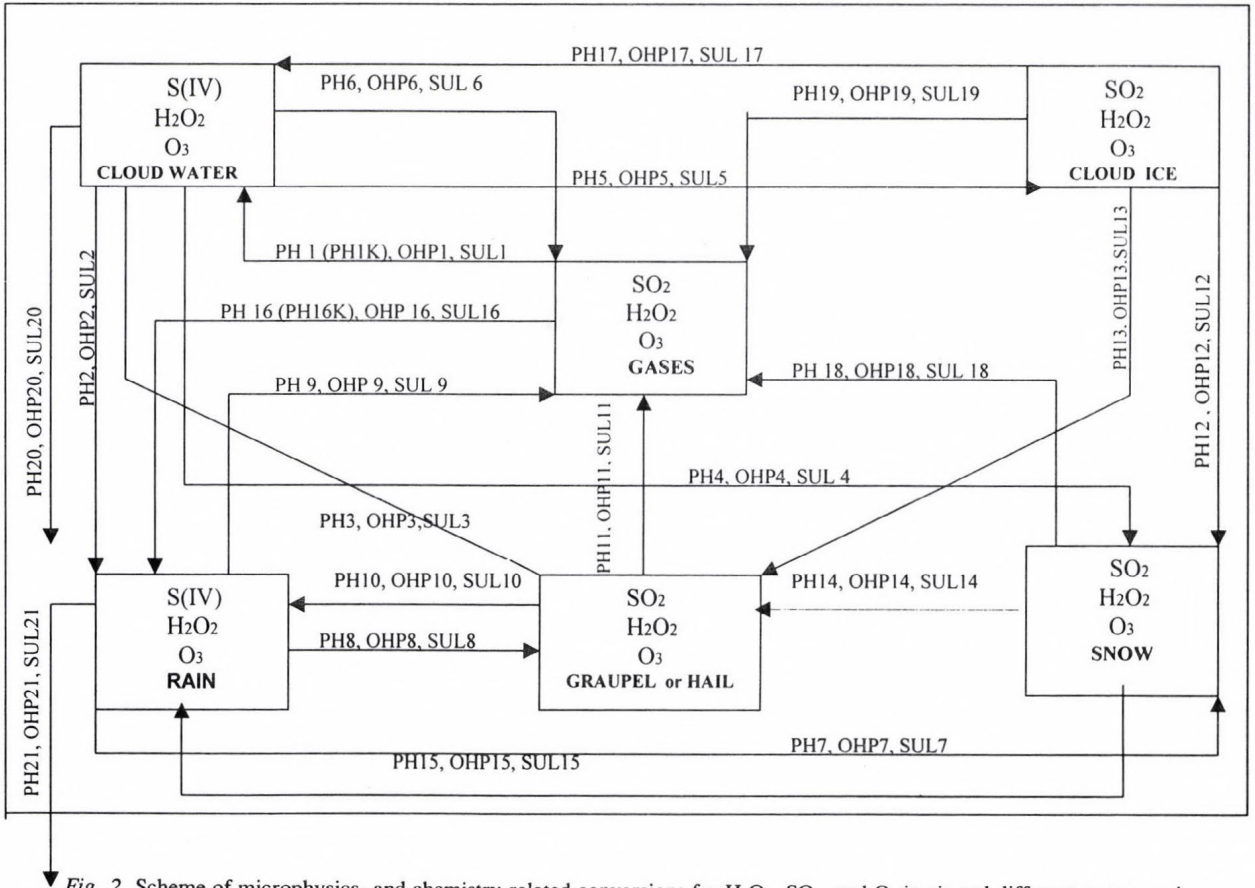

Fig. 2. Scheme of microphysics- and chemistry-related conversions for H_2O_2, SO_2, and O_3 in air and different water carriers, and the names associated with each of them in the model.

$$\mathrm{PH1,OHP1} = K_4 p q_{\mathrm{H_2O_2,O_3}C} \frac{\delta q_C}{\delta t}. \tag{55}$$

If condensation rate $\frac{\delta q_C}{\delta t} < 0$, in the computation of PH1 and OHP1 we take maximum available amounts of H_2O_2 or O_3, which is returned to the environment (*Taylor*, 1989), i.e.,

$$\mathrm{PH1,OHP1} = \max\left[K_4 p q_{\mathrm{H_2O_2,O_3}C} \frac{\delta q_C}{\delta t}, \frac{q_{\mathrm{H_2O_2,O_3}C}}{\delta t} \right]. \tag{56}$$

(2) PH2, OHP2, SUL2 - H_2O_2, O_3, and SO_2 transfer from cloud water to rainwater

This term follows the microphysical transition and transfers of H_2O_2, O_3, and SO_2 from cloud water to rain H_2O_2, O_3, and SO_2.

$$\mathrm{PH2,OHP2,SUL2} = \frac{q_{\mathrm{H_2O_2,O_3,SO_2}C}}{q_C} (P_{RAUT} + P_{RACW} + P_{SACW}), \tag{57}$$

where P_{RAUT}, P_{RACW}, and P_{SACW} are autoconversion of cloud water to form rain, accretion of cloud water by rain, and accretion of cloud water by snow; it produces snow if $T < T_0$, or rain if $T \geq T_0$. Also enhances snow melting for $T \geq T_0$.

(3) PH3,OHP3, SUL3 - H_2O_2, O_3, and SO_2 transfer from cloud water to graupel

$$\mathrm{PH3,OHP3,SUL3} = \frac{q_{\mathrm{H_2O_2,O_3,SO_2}C}}{q_C} P_{GACW}. \tag{58}$$

(4) PH4,OHP4,SUL4 - H_2O_2, O_3, and SO_2 transfer from cloud water to snow

$$\mathrm{PH4,OHP4,SUL4} = \frac{q_{\mathrm{H_2O_2,O_3,SO_2}C}}{q_C} (P_{SACW} + P_{SFW}). \tag{59}$$

(5) PH5,OHP5,SUL5 - H_2O_2, O_3, and SO_2 transfer from cloud water to cloud ice

$$\mathrm{PH5,OHP5,SUL5} = \frac{q_{\mathrm{H_2O_2,O_3,SO_2}C}}{q_C}\left(P_{IDW} + P_{IHOM}\right). \tag{60}$$

(6) PH6,OHP6, SUL6 - H_2O_2, O_3, and SO_2 transfer to gas phase from cloud water

$$\mathrm{PH6,OHP6,SUL6} = \frac{q_{\mathrm{H_2O_2,O_3,SO_2}\,G}}{\delta t}. \tag{61}$$

(7) PH7,OHP7,SUL7 - H_2O_2, O_3, and SO_2 transfer from rain to snow

In an analogous fashion, this term follows the microphysical transition and transfers H_2O_2, O_3, and SO_2 from rain to snow:

$$\mathrm{PH7,OHP7,SUL7} = \frac{q_{\mathrm{H_2O_2,O_3,SO_2}\,S}}{q_S}\left(P_{IACR} + P_{SACR}\right), \tag{62}$$

where P_{IACR} is the accretion of rain by cloud ice; produces snow or graupel depending on the amount of rain and accretion of rain by snow, and P_{SACR} represents accretion of rain by snow. For $T < T_0$, produces graupel if rain or snow exceeds threshold; if not, produces snow. For $T \geq T_0$, the accreted water enhances snow melting.

(8) PH8, OHP8, SUL8 - H_2O_2, O_3, and SO_2 transfer from rain to graupel

$$\mathrm{PH8,OHP8,SUL8} = \frac{q_{\mathrm{H_2O_2,O_3,SO_2}R}}{q_R}\left(P_{GACR} + P_{GFR} + P_{IACR} + P_{SACR}\right). \tag{63}$$

(9) PH9, OHP9, SUL9 - H_2O_2 evaporation from rain to aerosol

$$\mathrm{PH9,OHP9,SUL9} = \frac{q_{\mathrm{H_2O_2,O_3,SO_2}R}}{q_R}P_{REVP}. \tag{64}$$

(10) PH10, OHP10, SUL10 - Transfer of H_2O_2, O_3, and SO_2 from graupel to rain

$$PH10,OHP10,SUL10 = \frac{q_{H_2O_2,O_3,SO_2\,G}}{q_G} P_{GMLT} \cdot \quad (65)$$

(11) PH11, OHP11, SUL11 - H_2O_2, O_3, and SO_2 transfer from to gas phase graupel

$$PH11,OHP11,SUL11 = \frac{q_{H_2O_2,O_3,SO_2G}}{q_G} P_{GSUB} \cdot \quad (66)$$

(12) PH12,OHP12,SUL12 - H_2O_2, O_3, and SO_2 transfer from cloud ice to snow

$$PH12,OHP12,SUL12 = \frac{q_{H_2O_2,O_3,SO_2I}}{q_I} (P_{SAUT} + P_{SACI} + P_{SFI} + P_{RACI}) \cdot \quad (67)$$

(13) PH13 - H_2O_2, O_3, and SO_2 transfer from cloud ice to graupel

$$PH13,OHP13,SUL13 = \frac{q_{H_2O_2,O_3,SO_2\,I}}{q_I} (P_{GACI} + P_{RACI}) \cdot \quad (68)$$

(14) PH14,OHP14,SUL14 - Transfer of H_2O_2, O_3, and SO_2 from snow to graupel

$$PH14,OHP14,SUL14 = \frac{q_{H_2O_2,O_3,SO_2\,S}}{q_S} (P_{GAUT} + P_{GACS} + P_{RACS}) \cdot \quad (69)$$

(15) PH15, OHP15, SUL15 - H_2O_2, O_3, and SO_2 transfer from snow to rain

These terms transfer the snow H_2O_2, O_3, and SO_2 to rain during melting of snow:

$$PH15,OHP15,SUL15 = \frac{q_{H_2O_2,O_3,SO_2\,S}}{q_S} P_{SMLT} \cdot \quad (70)$$

(16) PH16, OHP16, SUL16 - Equilibration of H_2O_2, O_3, and SO_2 in rain drops

Like PH1, OHP1, these terms follows Henry's law equilibration between H_2O_2, O_3, SO_2, and rain drops,

$$PH16, OHP16, SUL16 = \max\left[K_{4,7,1}\ pq_{H_2O_2,O_3,SO_2R} P_{REVP}, \frac{q_{H_2O_2,O_3,SO_2R}}{\delta t} \right]. \tag{71}$$

The second term limits the amounts returning to the atmosphere through evaporation of rain drops.

(17) PH17, OHP17, SUL17 - Transfer of H_2O_2 from cloud ice to cloud water

$$PH17, OHP17, SUL17 = \frac{q_{H_2O_2,O_3,SO_2I}}{q_I} P_{IMLT}. \tag{72}$$

(18) PH18, OHP18, SUL18 - Transfer of H_2O_2, O_3, and SO_2 from snow gas phase

These terms transfer H_2O_2, O_3, and SO_2 from snow to gas phase:

$$PH18, OHP18, SUL18 = \frac{q_{H_2O_2,O_3,SO_2S}}{q_S} (P_{SSUB} + P_{SDEP}). \tag{73}$$

(19) PH19, OHP19, SUL19 - Transfer of H_2O_2, O_3, and SO_2 from cloud ice to gas phase

$$PH19, OHP19, SUL19 = \frac{q_{H_2O_2,O_3,SO_2S}}{\delta t}. \tag{74}$$

(20) PH20, OHP20, SUL20 - Reduction of H_2O_2 and O_3 in cloud droplets by SO_2

A part of the S(IV) conversion to SO_4^{2-} is due to oxidation in cloud drops and rain by H_2O_2. On this way, H_2O_2 is being reduced in cloud droplets and rain by SO_2. According to (*Taylor,* 1989), H_2O_2 is destroyed in aqueous reaction

$$HSO_3^- + H_2O_2 \Leftrightarrow O_2SOOH^- + H_2O. \tag{75}$$

The rate at which H_2O_2 is destroyed is parameterized in the same manner as for oxidations terms PS2 and PS9 formulated in the sulfate production:

$$\mathrm{PH20,OHP20} = K_{\mathrm{S(IV)}} \frac{K_1 K_2}{[\mathrm{H}_C^+]} pq_{\mathrm{SO_2}} \frac{M_{\mathrm{H_2O_2,O_3}}}{M_{\mathrm{SO_2}}} K_{4,7} pq_{\mathrm{H_2O_2,O_3}C} \cdot \qquad (76)$$

(21) PH21,OHP21, SUL21 – Reduction of H_2O_2 and O_3 in rain by SO_2

On similar way, parameterization of H_2O_2 destruction in rain is given by

$$\mathrm{PH21,OHP21} = K_{\mathrm{S(IV)}} \frac{K_1 K_2}{[\mathrm{H}_R^+]} pq_{\mathrm{SO_2}} \frac{M_{\mathrm{H_2O_2,O_3}}}{M_{\mathrm{SO_2}}} K_{4,7} pq_{\mathrm{H_2O_2,O_3}R} \cdot \qquad (77)$$

In addition, cloud and raindrops contain dissolved ammonium sulfate $(NH_4)_2SO_4$, which is not created or destroyed in the chemical reactions. The only transitions of $[NH_4^+]$ aerosol are from scavenging and those following the microphysical transfers (*Taylor*, 1989b).

3.5 Calculation of pH

The calculation of the cloud water pH and rainwater pH is based on the equilibrium hydrogen ion concentration for $[H^+]$, which is given by the simple charge balance equation (*Taylor*, 1989b):

$$[H^+] = 0.5\left\{2[SO_4^{2-}] - [NH_4^+] + \left((2[SO_4^{2-}] - [NH_4^+])^2 + 4K_H{}^* p_{SO_2} + 4K_W\right)^{0.5}\right\}. \qquad (78)$$

4. Summary and conclusions

We have developed and incorporated the chemical packet into a three-dimensional compressible cloud model combined with bulk water microphysics. The governing equations of the model include momentum conservation equations, thermodynamic and pressure equations, four continuity equations for the various water substances, subgrid scale (SGS) turbulent kinetic energy equation (TKE), and continuity equations for chemical species associated with various cloud water species.

The microphysics and chemistry modules have been formulated in terms of continuity equations, which represent the average microphysical and chemical properties of the cloud and cloud environment within elementary well-

mixed volumes. The simple sulfur chemistry and parameterization of chemical species included in sulfate budget are considered in detail. Processes occurring on smaller scales are parameterized in terms of these average properties. The utilized cloud-chemistry model uses explicit treatment of gases, and specifically, mass transfer limitation calculations for highly soluble gases. The set of three-dimensional runs with mixed phase microphysics and the modification of the hail growth equation in the microphysics parameterization scheme are also novel aspects of the model.

Acknowledgements–First of all we acknowledge to *Mr. Bosko Telenta*, for his support, giving insights and explanations concerning the technical aspects of this model. We also wish to express our gratitude to *Ms. Marija Andreevska* from Hydrometeorological Institue of Macedonia, for her help with some useful explanations of chemical aspects of the paper. The anonymous referees have made many substantial remarks that increased the completeness and clarity of the manuscript. We would like to express our special gratitude to *Dr. Tamás Práger*, for his important contribution giving constructive comments during final revision of the paper and allowance its publishing.

References

Barth, M.C., Stuart, A.L., and *Skamorock, W.C., 2001*: Numerical simulation of the July 10 Stratospheric-Tropospheric Experiment: Radiation, Aerosols, and Ozone/Deep Convection storm: Redistribution of soluble tracers. *J. Geophys. Res. 106*, 12, 381-12,400.

Chen, J.P. and *Lamb, D.*,1994: Simulation of cloud microphysics and chemical processes using a multicomponent framework, I. Description of the microphysical model. *J. Atmos. Sci. 51*, 2613-2630.

Crutzen, P.J. and *Lawrence, M.G.*, 2000:The impact of precipitation scavenging on the transport of trace gases: A three-dimensional model sensitivity study. *J. Atmos. Chem. 37*, 81-112.

Ćurić, M. and *Janc, D.*, 1995: On the sensitivity of the continuous accretion rate equation used in bulk-water parameterization schemes. *Atmos. Res. 39*, 313-332.

Ćurić, M. and *Janc, D.*,1997: On the sensitivity of hail accretion rates in numerical modeling. *Tellus 49A*, 100-107.

Flossman, A.I. and *Wobrock, W.*, 1996:Venting of gases by convective clouds. *J. Geophys. Res. 101*, 18,639-18,649.

Hales, J.M., 1982: Mechanistic analysis of precipitation scavenging using a one-dimensional time variant model. *Atmos. Environ. 16*, 177-1783.

Hoffmann, M.R. and *Calvert, J.G.*, 1985: *Chemical Transformation Modules for Eulerian Acid Deposition Models, Vol. 2.* The aqueous phase chemistry. Rep. EPA/600/3-85/017, U.S. Environ. Prot. Agency, Research Triangle Park. N. C.

Hsie, E.Y., Farley, R.D., and *Orville, H.D.*, 1980: Numerical simulation of ice-phase convective cloud seeding. *J. Appl. Meteor. 19*, 950-977.

Isaac, G.A., Strapp, J.W., Wiebe, H.A., Leaitch, W.R. Kerr, J.B., Anlauf, K.G., Summers, P.W., and *McPherson, J.I.*, 1982: The role of cloud dynamics in redistributing pollutants and the implications for scavenging studies. In *Precipitation Scavenging, Dry Deposition and Resuspension*. (Coords.: *H.R. Pruppacher, R.G. Semonin*, and *W.G.N. Slinn*). *Elsevier*, pp. 1-13.

Isaac, G.A., Joe, P.J., and *Summers, P.W.*, 1983: The vertical transport and redistribution of pollutants by clouds. In *The Meteorology of Acid Deposition*. (ed.: *P.J. Samson*). Air Pollution Control Association, pp. 496-512.

Klemp, J.B. and *Wilhelmson, R.B.*, 1978: The simulation of three-dimensional convective storm dynamics. *J. Atmos. Sci. 35*, 1070-1096.

Kreidenweis, S.M., Zhang, M., and *Taylor, G.R.*, 1997: The effects of clouds on aerosol and chemical species production and distribution 2. Chemistry model description and sensitivity analysis. *J. Geophys. Res. 102*, 23867-23882.

Lin, Y.L. Farley, R.D., and *Orville, H.D.*, 1983: Bulk water parameterization in a cloud model. *J. Climate Appl. Meteor. 22*, 1065-1092.

Martin, L R. and *Damaschen, D.E.*, 1981: Aqueous oxidation of sulfur dioxide by hydrogen peroxide at low pH. *Atmos. Environ. 15*, 191-195.

Niewiadomski, M., 1989: Sulfur dioxide and sulfate in a three-dimensional field of convective clouds: Numerical simulations. *Atmos. Environ. 23(2)*, 477-487.

Orville, H.D. and *Kopp, F.J.*, 1977: Numerical simulation of the history of a hailstorm. *J. Atmos. Sci. 34*, 1596-1618.

Pandis, S.N. and *Seinfeld, J.H.*, 1989: Sensitivity analysis of a chemical mechanism for aqueous-phase atmospheric chemistry. *J. Geophys. Res. 94(D1)*, 1105-1126.

Pruppacher, H.R. and *Klett, J.D.*, 1997: *Microphysics of Clouds and Precipitation*. 2nd ed. Kluwer Acad., Norwell, Mass.

Rutledge, S.A., Hegg, D.A., and *Hobbs, P.V.*, 1986: A numerical model for sulfur and nitrogen scavenging in narrow cold-frontal rainbands. Part 1: Model description and discussion of microphysical fields. *J. Geophys. Res. 91*, 14 385-14 402.

Sarma, R.A., 1986: *Numerical Simulation of the Formation and Transport of Sulfate in Convective Clouds. Ph.D. dissertation*. South Dakota School of Mines and Technology, Rep. No. SDSMT/IAS/R-86/04, 188 pp.

Skamorock, W.C. et al., 2000: Numerical simulation of the July 10 Stratospheric-Tropospheric Experiment: Radiation, Aerosols, and Ozone/Deep Convection experiment convective system: Kinematics and transport. *J. Geophys. Res. 105*, 19, 973-19,990.

Schwartz, S.E. and *White, W.H.*, 1981: *Solubility equilibrium of the nitrogen oxides and oxyacids in dilute aqueous solution*. In *Advances in Environmental Science and Engineering*, Vol. 4, (eds: *J.R. Pfafflin* and *E.N Ziegler*), 1-45. Gordon and Breach Science Publishers, NY.

Taylor, G.R., 1989a: Sulfate production and deposition in midlatitude continental cumulus clouds, Part I, Cloud model formulation and base run analysis. *J. Atmos. Sci. 46*, 1971-1990.

Taylor, G.R., 1989b: Sulfate production and deposition in midlatitude continental cumulus clouds, II, Chemistry model formulation and sensitivity analysis. *J. Atmos. Sci. 46*, 1991-2007.

Tremblay, A. and *Leighton, H.*, 1986: A three-dimensional cloud chemistry model. *J. Climate Appl. Meteor. 25*, 652-671.

Walcek, C.J. and *Taylor, G.R.*, 1986: Theoretical method for computing vertical distributions of acidity and sulfate production within cumulus clouds. *J. Atmos. Sci. 43*, 339-355.

Wang, C. and *Chang, J.S.*, 1993a: A three-dimensional numerical model of cloud dynamics, microphysics and chemistry, Part IV. Cloud chemistry and precipitation chemistry. *J. Geophys. Res. 98*, 116,799-16,808.

Wang, C. and *Chang, J.S.*, 1993b: A three-dimensional numerical model of cloud dynamics, microphysics, and chemistry, Part I. Concepts and formulation. *J. Geophys. Res. 98*, 14,827-17,844.

Yin, Y., Parker, D.J. and *Carslaw, K.S.*, 2001: Simulation of trace gas redistribution by convective clouds-Liquid phase processes. *Atmos. Chem. Phys. 1*, 19-36.

IDŐJÁRÁS

Quarterly Journal of the Hungarian Meteorological Service
Vol. 107, No. 2, April–June 2003, pp. 115–132

Validation of the Eulerian dispersion model MEDIA at the Hungarian Meteorological Service

Zita Ferenczi[1] and **István Ihász**[2]

Hungarian Meteorological Service
[1]*P.O. Box 39, H-1675 Budapest, Hungary; E-mail: ferenczi.z@met.hu*
[2]*P.O. Box 38, H-1525 Budapest, Hungary; E-mail: ihasz.i@met.hu*

(Manuscript received October 24, 2002; in final form May 16, 2003)

Abstract–This paper presents adaptation of the Eulerian dispersion model – MEDIA – at the Hungarian Meteorological Service. The model is part of the emergency response system of the Hungarian Meteorological Service, which can be operated by forecaster on request. The model calculates air concentration fields at 10 different sigma layers in lower and middle troposphere, and deposition field (dry and wet) for every 6 hours. The lead-time depends on the forecasting time of the driving numerical weather prediction model. Some new results of the investigation work are presented which provide the decision makers with new information about the time evolution of the polluted material. The influence of dry and wet deposition was examined separately. Model was launched without dry and wet deposition, and the final concentration fields were compared to the normal simulation. The influence of heavy rain was studied, and the concentration and deposition fields were compared to normal simulations as well. An interesting weather situation was selected to demonstrate our results.

Key-words: dispersion model, radioactive pollutant, concentration fields, dry/wet deposition, meteorological workstation, time series, vertical distribution, regional and continental scale transport.

1. Introduction

The aim of this paper is to describe a dispersion model, which has been used at the Hungarian Meteorological Service (HMS) in case of nuclear/industrial accident. Since 1990, foreward and backward trajectories have been calculated in emergency situation (*Ihász,* 1992, 1999). After the serious accident happened in Chernobyl, several air pollution models were developed in

Europe. The so-called MEDIA model was developed by Meteo France in 1989, and it was adapted by the HMS in 1997. Its aim is to provide forecasts for the dispersion of pollution in case of accidental release of potentially dangerous materials into the atmosphere. Since 1999, the model has been part of the emergency response system of the HMS, which can be operated on request. The model can be used in real time mode. The forecaster can choose the coordinate of the source point, the time of release, the type of pollutant, and the interval of emission. In Hungary the model is driven by meteorological input data provided by the ALADIN or ECMWF numerical weather prediction models (*Ihász,* 2000).

ALADIN is a short-range limited area model making weather forecasts up to 48 hours. ALADIN was developed by international co-operation of several European countries by leadership of France (ALADIN is French abbreviation: Aire Limitee Adaptation Dynamique Developement International (*Horányi et al.*, 1996). ECMWF (European Centre for Medium Range Weather Forecasts) is an international organization supported by 24 European countries, Hungary has a co-operation agreement since 1994. ECMWF operationally provides medium range deterministic and ensemble forecasts up to 10 days for its member states and co-operating states (resolution of deterministic model is 40 km, i.e., approximately 0.4 degrees) (*White*, 2000a-e).

All the simulations of MEDIA model that were performed reveal that the quality of the atmospheric transport model strongly depends on the quality of the driving numerical weather prediction model. Meteorological input data from the ALADIN/HU (version of ALADIN model running at the Hungarian Meteorological Service) numerical weather prediction model are used for the developing aim. The space resolution of these meteorological data are 0.1 by 0.15 degrees in latitude and longitude, the time resolution is 1 hour, so these data sets are much better for examination purposes than the data coming from ALADIN/LACE (LACE means Limited Area Model for Central Europe) or ECMWF models. ALADIN/LACE model was planned to be terminated on December 31, 2002, so in the future only ALADIN/HU model can be used on very high resolution. In this paper we will present some new results of the development work at the HMS and some interesting case studies.

2. Short description of MEDIA

Dispersion models can belong to two types, namely the Eulerian and Lagrangian models, or some kind of combination of them. Galmarini (*Galmarini et al.*, 2002) gives a summary about recently available dispersion models in Europe. If nuclear or chemical accident happens quite far from our

reception point, a continental or global model should be used, if it happens not so far from our reception point, fine mesh regional model can be preferable.

MEDIA is a three dimensional Eulerian type dispersion model for medium and long-range transport of emitted pollutant in the atmosphere. In this paper we give only a short review of the transport model. A complete description and validation of the model can be found in *Piedelievre et al.* (1990). The governing equation of the model is the diffusion equation, which is based on the mass conservation of the polluted material in the atmosphere in vectorial form:

$$\frac{\partial C}{\partial t} + \mathbf{V}(\nabla C) = \nabla(\mathbf{K}\nabla C) + \dot{S}_0 - \dot{S}_i \,, \tag{1}$$

$$\frac{\partial C}{\partial t} + u\frac{\partial C}{\partial x} + v\frac{\partial C}{\partial y} + w\frac{\partial C}{\partial z} = +\frac{\partial}{\partial x}\left(K_x \frac{\partial C}{\partial x}\right) + \frac{\partial}{\partial y}\left(K_y \frac{\partial C}{\partial y}\right) + \frac{\partial}{\partial z}\left(K_z \frac{\partial C}{\partial z}\right) + \dot{S}_0 - \dot{S}_i \,, \tag{2}$$

where C [Bq m^{-3}] is the air concentration of the pollutant at a given point at time t, u, v, w are three components of the wind velocity vector (**V**) [m s^{-1}], K_x, K_y ,K_z horizontal and vertical turbulent diffusion coefficients (diagonal elements of the **K** turbulent diffusion tensor), $\dot{S}_0$ and $\dot{S}_i$ are source and sink terms. The rate of decay of a radionuclide is described by its activity, namely by the number of atoms that decay per unit time. The unit of activity is becquerel (Bq), which is defined unit in International System (SI), defined as one disintegration or nuclear transform per second: 1 Bq = 1 s^{-1}.

2.1 Advection

The pollutant concentration is transported by the horizontal wind fields coming from the driving numerical prediction model.

2.2 Turbulent diffusion

The diffusion represents the mixing of the pollutant in the atmosphere due to the turbulent motions. In order to simplify the procedure and make it coherent with coupling model, the diffusion is modeled using exchange coefficients (first order closure). This choice means that the pollutant is assumed to be diffused in the same way as water vapor. In that case, **K** tensor is diagonal:

$$\nabla(\mathbf{K}\nabla C) = \frac{\partial}{\partial x}K_x\frac{\partial C}{\partial x} + \frac{\partial}{\partial y}K_y\frac{\partial C}{\partial y} + \frac{\partial}{\partial z}K_z\frac{\partial C}{\partial z} \,. \tag{3}$$

The diffusion is solved using the *K*-theory with horizontal coefficients (K_x, K_y) dependent on the grid size, and vertical coefficient (K_z) related to the stability of the layer according to *Louis* (1979), as follows:

$$K_z = l^2 \frac{\partial |\mathbf{V}_h|}{\partial z} F(Ri), \tag{4}$$

where $\mathbf{V}_h$ is the horizontal wind vector, l is the mixing length, Ri is bulk Richardson number,

$$l = \frac{\kappa z}{1 + \frac{\kappa z}{150}} \tag{5}$$

in which: κ is the Karman constant (0.4),

$$Ri = \frac{g}{\theta} \frac{\partial \theta}{\partial z} \left(\left(\frac{\partial u}{\partial z} \right)^2 + \left(\frac{\partial v}{\partial z} \right)^2 \right)^{-1}, \tag{6}$$

here: θ is the potential temperature, g is the gravitational acceleration.

$$F(Ri) = \frac{1}{1 + 3b\, Ri (1 + dRI)^{1/2}} \qquad \text{if } Ri > 0, \tag{7}$$

$$F(Ri) = \frac{1}{1 + 3bc \left[l^2 Ri^{1/2} / (z^2 \sqrt{27}) \right]} \qquad \text{if } Ri < 0, \tag{8}$$

where $b = c = d = 5$.

2.3 Sinks

Sinks can be wet and dry deposition and radioactive decay for radioactive pollutant.

2.4 Wet deposition

Wet deposition due to scavenging by precipitation is computed using a global coefficient of air-to-water transfer, which roughly describes dilution or catching. Despite its simplicity, this solution is generally used and is well

adapted to accuracy of precipitation predicted by the model. The rate of wet deposition D_W (Bq m^{-2} s^{-1})can be written in the next form:

$$D_w = \frac{C_m E P_r}{p_w} , \tag{9}$$

where C_m is average concentration in precipitating layer in concentration units (Bq m^{-3} for a radioactive cloud), $E=10^4$ is scavenging ratio, P_r is rate of precipitation (kg m^{-2} s^{-1}), p_w is specific mass of water (kg m^{-3}).

Since in coupling model precipitation fluxes are only available at ground level, we assume that the thickness of the precipitating layer is 3000 m, and that the scavenging is uniformly active in this part of the atmosphere. In the vertical it is distributed proportionally to the concentration. Four different types of precipitation can be defined in the model: rain and snow, which can be large scale or convective.

2.5 Dry deposition

Dry deposition describes uptake of a pollutant at the earth's surface by soil, water, or vegetation. This process is modeled using a coefficient that is dimensionally equal to a deposition velocity. The downward flux of radioactive material D_{dsoil} (Bq m^{-2} s^{-1}) can be written in the following way:

$$D_{dsoil} = V_d C_{soil} , \tag{10}$$

where C_{soil} is concentration in air near the ground (Bq m^{-3}), V_d is dry deposition velocity (m s^{-1}).

2.6 Radioactive decay

In case of a radioactive pollutant, the other factor of depletion is the radioactive decay, which is formulated by the well-known equation

$$\frac{dC}{dt} = -KC , \tag{11}$$

where $K = \ln 2/T$ is the splitting constant and T is the radioactive half-life time of the pollutant.

2.7 Source

In the source mesh, Gaussian distribution describes the diffusion on a subgrid scale:

$$\frac{dC}{dt} = \frac{Q(t)}{2\pi\sigma_n^2 H} \exp \frac{(-d^2)}{2\sigma_n^2}, \tag{12}$$

where d is distance from the source (m), Q is emission term (Bq s^{-1}), H is vertical extension of the pollutant cloud (m), σ_n^2 is surface of the mesh which includes the source (m^2).

The model has ten σ levels in the vertical ($\sigma = \frac{p}{p_s}$, where p is pressure and p_s is surface pressure in so-called Phillips terrain following co-ordinate system). Equidistant σ levels are located between 1 and 0.5 (*Table 1*).

Table 1. Relation between the σ levels of MEDIA and the typical heights above surface

σ levels of MEDIA	**Typical heights above surface level in m if p_s is 1013 hPa**
0.99	10.1
0.94	495.3
0.88	1004.5
0.83	1540.6
0.77	2106.8
0.71	2707.3
0.66	3347.2
0.60	4032.6
0.54	4771.6
0.49	5574.4

3. Description of the simulation

MEDIA dispersion model has been working operationally since 1999 at the HMS. The model was also tested in an accident happened in Algeciras, Spain, in May 1998. Several case studies have been investigated, now we will show a situation connecting to an interesting weather situation, when benefit of very fine mesh coupling numerical forecasting model can be specially seen.

The Hungarian a nuclear power plant near the town of Paks (46.8°N, 18.6°E) has been operating since 1982. This location was the source point in our experiment running. Four different geographical points were selected for the analysis of the time series. The first point is located near the source point in the path of the maximum concentration values. The other three points are

around the source point in different directions. Location of the source point and the four detection points can be seen in *Fig. 1.*

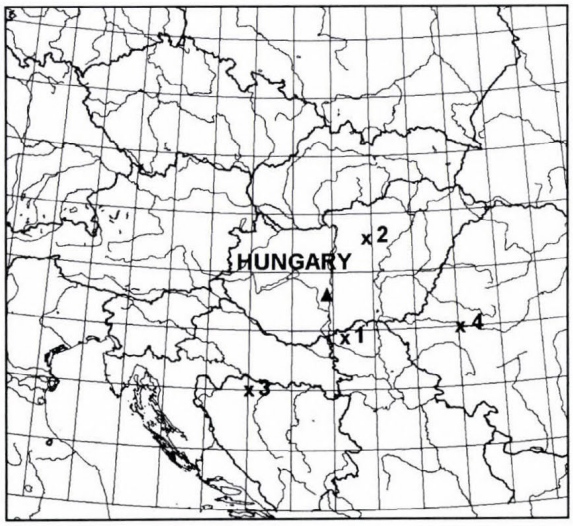

Fig. 1. Location of the source point and detection points (▲ indicates the source point, while the ×-s are the detection points).

The supposed release started at 00 UTC, December 11, 2001, and there was 2-hour explosion with an average hourly rate 5×10^{14} Bq h^{-1}. In the case of the extremely dangerous accident happened at Chernobyl, in April 26, 1986, maximum release was in this magnitude (*Piedelivre et al.*, 1990). The height of release was 10 to 120 m. The simulation was carried out for ^{137}Cs (the half time is 30 years). The dry deposition velocity was chosen to be equal to 10^{-3} m s^{-1}, which is compatible with the size of Caesium nuclides. The space resolution of the ALADIN/HU forecasted meteorological data were 0.1 by 0.15 degree in latitude and longitude, and the time resolution was 1 hour. The integration time step was 300 s, and the integration domain covers an area between 42.9° and 51.4°N; 6.4° and 24.55°E.

Weather situation in Central Europe at December 11, 2001:

There was an anticyclone in Europe, but over the eastern part of Europe there was a cyclone with an occluded front (*Fig. 2*). This frontal zone left Hungary late afternoon. In the territory of the Carpathian Basin, the weather was cold

and cloudy, there was snowing on many places. The wind was blowing from northwest to southeast. The wind speed near the ground level (at about 10 m height) was about 2–3 m s^{-1} (*Fig. 3*). In the upper air (at about 500 m height), the wind direction turned right and the wind speed was 3-4 m s^{-1} (*Fig. 4*). The wind moved the polluted material in the southeast direction. In the west part of Hungary, intensity of the precipitation was 2–3 mm day^{-1} (*Fig. 5*).

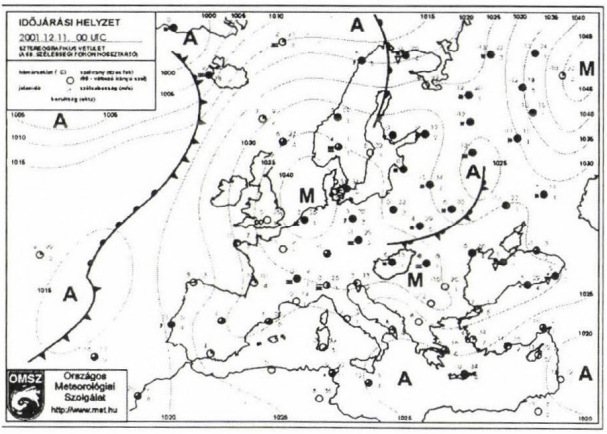

Fig. 2. Synoptic chart at 00 UTC, December 11, 2001.

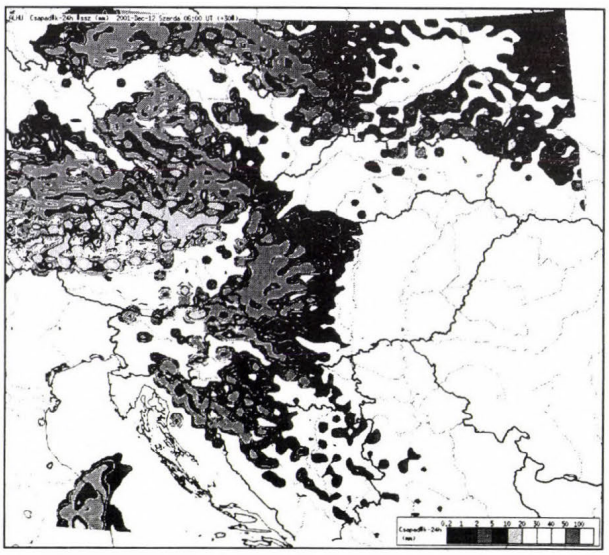

Fig. 3. Precipitation field between 00 UTC, December 11, 2001 and 00 UTC, December 12, 2001.

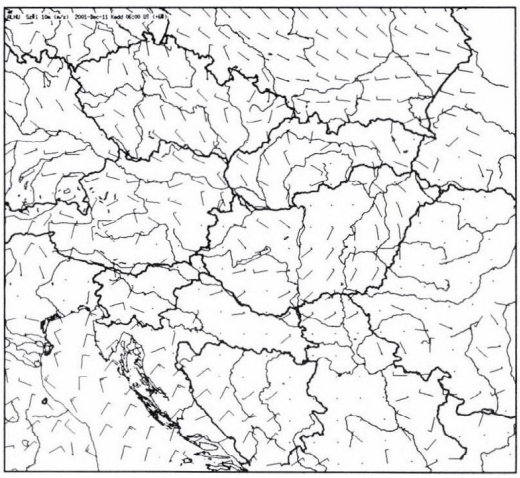

Fig. 4. Wind field at the 10 m height 00 UTC, December 11, 2001.

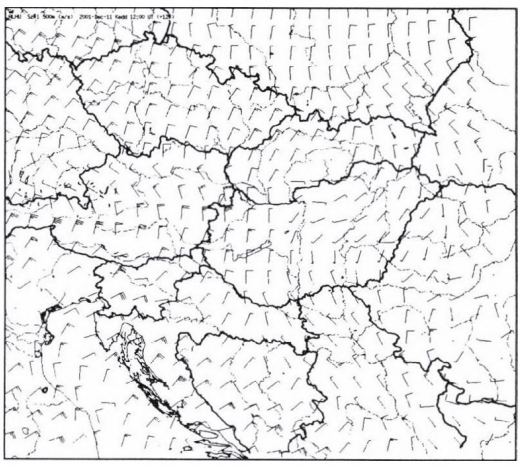

Fig. 5. Wind field at the 500 m height at 00 UTC, December 11, 2001.

4. Concentration fields at different vertical layers

The effect of horizontal and vertical wind fields and horizontal and vertical diffusion was studied in different vertical layers (*Figs. 6* and *7*). During postprocessing of the model, mean air concentration was determined for the standard layer (the average of concentration fields of the 2–5th sigma layers).

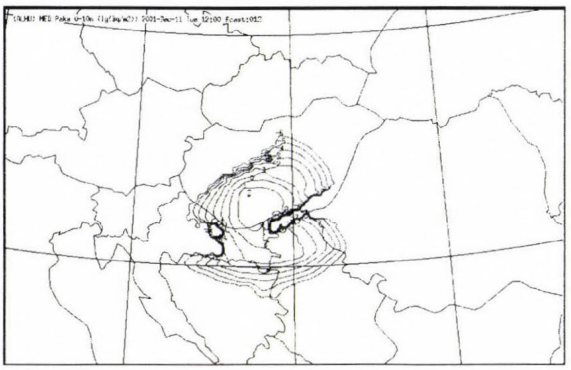

(a) first sigma level, maximum concentration is: 2.00 Bq m^{-3}

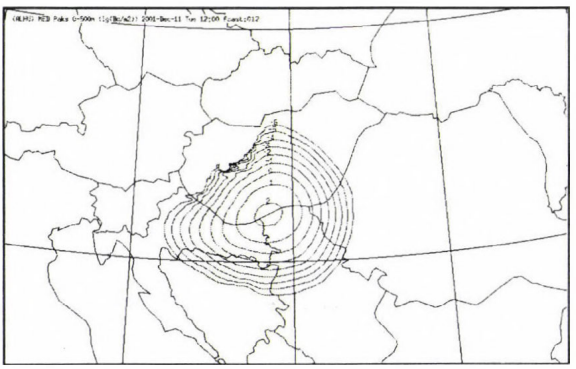

(b) second sigma level, maximum concentration is: 2.18 Bq m^{-3}

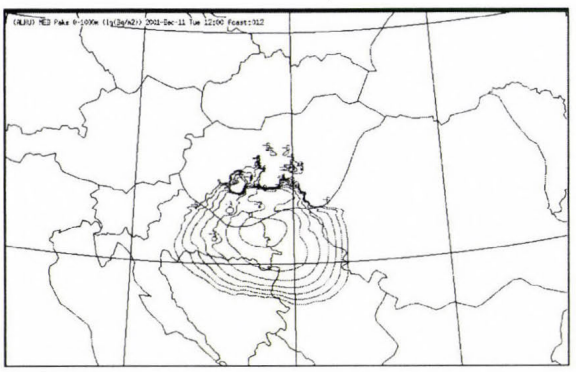

(c) third sigma level, maximum concentration is: 0.62 Bq m^{-3}

Fig. 6. Concentration fields 12 hours after the release at different vertical layers (isolines are $\log_{10}$C, and unit is in Bq m^{-3}) at 12 UTC, December 11, 2001.

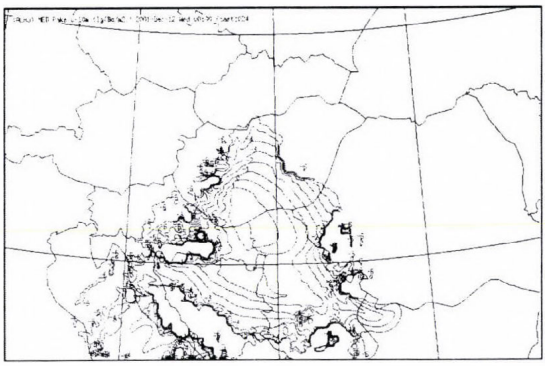

(a) first sigma level, maximum concentration is: 1.69 Bq m^{-3}

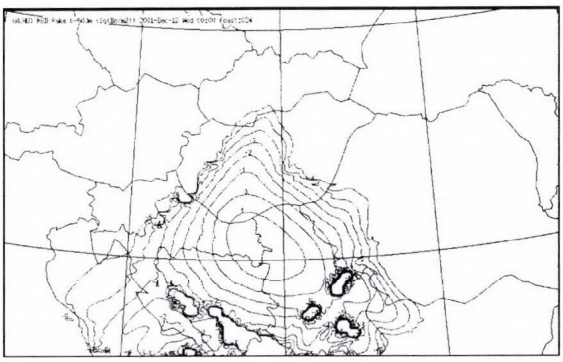

(b) second sigma level, maximum concentration is: 1.85 Bq m^{-3}

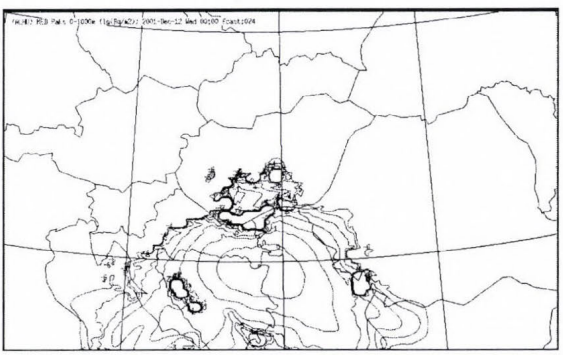

(c) third sigma level, maximum concentration is: 0.72 Bq m^{-3}

Fig. 7. Concentration fields 24 hours after the release at different vertical layers (isolines are $\log_{10}C$, and unit is in Bq m^{-3}) at 00 UTC, December 12, 2001.

In this experiment, this wide layer was divided to four sublayers (the 2nd, 3rd, 4th, and 5th sigma layers were separated). Dividing technique could be important near the surface layer (10–1000 m), because the concentration values here can be much higher than the mean values valid for the standard layer, and this concentration field influences directly the human beings.

The first three sigma layers were analyzed in detail. The effects of the terrain and wind field are reflected in the concentration field of the first sigma layer. 12 hours after the release, the plume covered almost the whole area of Hungary, and caused more than 10^{-10} magnitude of the concentration. 24 hours after the release, the situation in Hungary did not change essentially, but the contamination increased considerably in the countries, which are located in the south direction to Hungary. In the west part of Hungary, there was a significant amount of precipitation during the examination time. 24 hours after the release, the concentration field reflected the effect of wet deposition. The effect of wet and dry deposition will be examined in detail in section 6.

In the upper levels, the effect of the terrain is lower and lower, whilst the effect of the wind field becomes more and more important.

The maximum concentration values decrease continually in the first and second level 6 hours after the release. The situation is much more complex at the upper levels. This complexity can be observed in *Fig. 8*, in the case of station 1 (location of the station can be seen in *Fig. 1*) at the third and forth sigma level. At these upper levels, the shapes of the curves are not Gaussian, like in the lower levels, but they reflect the effect of vertical motion and diffusion.

As it was mentioned in the previous section, in MEDIA the value of the horizontal turbulent diffusion coefficient (K_x, K_y) is consistent with the grid resolution in metres (*Piedelievre et al.*, 1990). Parameterization of horizontal turbulent diffusion coefficient gives an universal solution in this way, when the time and spatial resolution of the driving numerical weather prediction models are different. In the previous version of the model, the values of these coefficients were fixed ($K_x=K_y=10^5$ m^2 s^{-1}) (*Bompay,* 1998). In the long-range dispersion models it is necessary to increase the horizontal diffusion, in order to include the advection fluctuations non-resolved by large-scale meteorological models (*Piedelievre et al.*, 1990). This effect is reflected in our case, when we used MEDIA in regional scale, so our horizontal turbulent diffusion coefficient must be smaller than 10^5 m^2 s^{-1}. In our experiment the grid resolution was 0.1 by 0.15 degrees in latitude and longitude, the north border was 51.4°N, the south border was 42.9°N of the driving model. This model resolution resulted in an $1.04\ 10^4$ - $1.22\ 10^4$ m^2 s^{-1} horizontal diffusion coefficient interval.

Parameterisation of the vertical turbulent diffusion coefficient (K_z) is better known than the horizontal diffusion coefficients. In MEDIA, this parameter depends on the stability of the layer. Determination of $F(R_i)$ is different when the value of R_i is higher (stable) or lower (instable) than zero (Eqs. 7–8). This thing causes that the values of the vertical turbulent diffusion coefficient change in wide scale. In our case, the magnitude of K_z changed from 10^{-15} to 10 $m^2 s^{-1}$.

5. Time series of the concentration values in specified geographical points

Four different geographical points were selected for the analysis of the time series. The first point is located southeast to the source point in the path of the maximum concentration values. The other three points are located 150–250 km far from the source point in different directions (southwest, east and northeast). Location of the source point and the four detection points can be seen in *Fig. 1*.

The figures with concentration fields give complex information about the situation of the pollution. Time series of the concentration values in discrete geographical points can be much more informative than the concentration fields, if we would like to know the time when the polluted cloud reaches or leaves a given town. With this program option we can predict the time series of the concentration values at different vertical levels. The original version of the model did not contain this option, but there were considerable claims to develop this tool. *Figs. 8* and *9* show some examples of application of this useful tool.

The highest values and concentrations were found in the first detector point (*Fig. 8*). In this point the highest concentration was detected at the second sigma layer 11 hours after the release, and after this time the concentration values decreased. The plume moved up in the 500 m height immediately, and from this layer the polluted material mixed up to the higher and lower layers. At every station the highest concentrations were detected at the 500 m height.

At the level of 500 m height, the concentration values were much higher than in the surface layer in the 22 hours interval after the release. After this time the situation was changed, the maximum values of the concentration of polluted material were at the surface layer. The diagrams show the concentration values at the 1000 m and 1500 m heights as well. At these levels the magnitude of concentration values is ten and hundred (or more) times lower than at the surface layer, except at station 3. At this station the highest values were detected at the third sigma layer.

The diagrams pointed that the considerable layer is the second sigma layer. This means that the concentration fields of this level should be visualized. The other important level is the surface level, where the concentrations can be dangerous for the biomass.

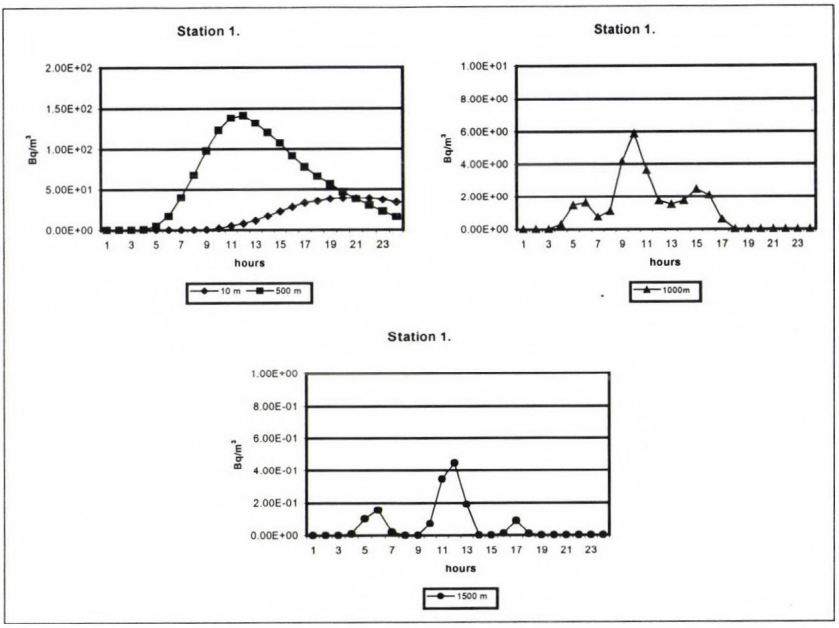

Fig. 8. Time series of calculated concentration on four different levels at station 1.

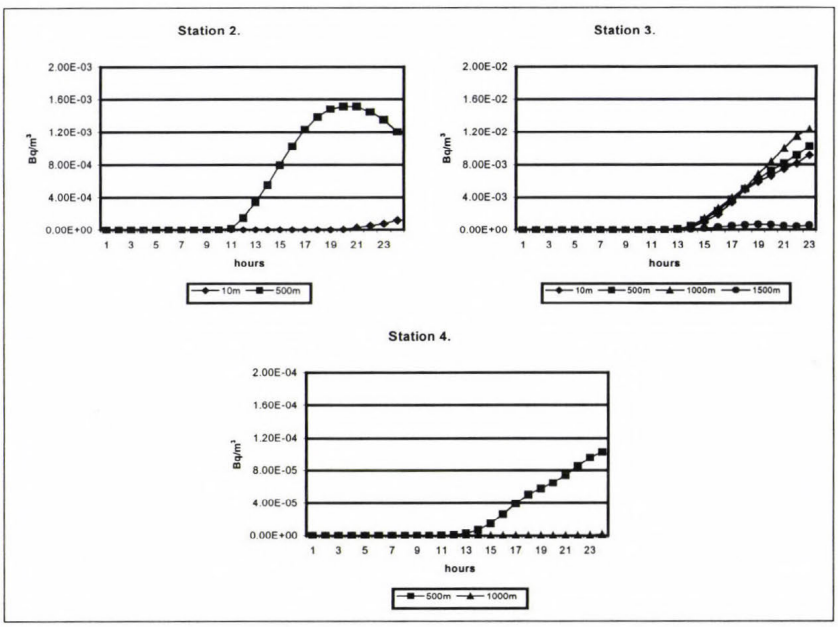

Fig. 9. Time series of calculated concentration on some selected levels at stations 2, 3, and 4.

6. Effects of wet and dry deposition

The deposition of airborne material to the underlying surface can follow two main pathways: dry and wet deposition. A further depletion process, where radionuclides are involved is, of course, the radioactive decay. Removal of material at the surface leads to plume depletion with distance, and to a modified vertical distribution of air concentration.

Dry deposition is the removal of gaseous or particulate material from the atmosphere by the surface or vegetation (or even water surfaces) through processes like absorption, implication, and sedimentation. For the pollutant plume is in contact with the ground, all the particles in the turbulent atmospheric boundary layer constitute a reservoir from which material can be deposited to the surface. This is calculated by means of a deposition velocity, which is related to the resistance of the underlying surface to the transfer. The parameterization of this process was described in section 2. Before running MEDIA, the value of deposition velocity must be set for a given radioactive nuclide emitted into the air.

Wet deposition – the removal of the radionuclides by the action of rain or snow – is a much more important process, and everyone is familiar with the notion of "hot spots" formed where a radioactive plume is intercepted by a burst of rain. There are two processes involved in wet deposition, washout: where pollutants are swept out of the air by falling rain, and the more efficient process of rainout, where the pollutant is taken up by the growing cloud droplets and is subsequently precipitated out. Representative coefficients for scavenging processes for large-scale and convective precipitation were given in the model. The model developers determined these coefficients and we have not changed their values.

In this experiment the influence of wet and dry deposition was studied. In the original version of the model only total (wet+dry) deposition field was produced at the final time step. After modifying the postprocessing scheme, it was possible to study the wet and dry deposition separately. It was found that in case of big amount of precipitation, wet deposition is the determinant process. This was the case in our investigated weather situation. The result can be seen in *Fig. 10.*

In the other case the dry deposition velocity was set to 0 and precipitation was set to 0 mm/12h as well in the grid points of the domain. Air concentration values were significantly higher in any vertical layers, than in normal case. Differences between the maximum concentration values became higher and higher in time.

In this experiment we found that the values of the dry deposition velocity and the intensity of precipitation are determinant in connection with the

concentration and deposition fields. It means that we have to set the value of dry deposition velocity and the intensity of precipitation as accurate as possible to get the best result of simulation.

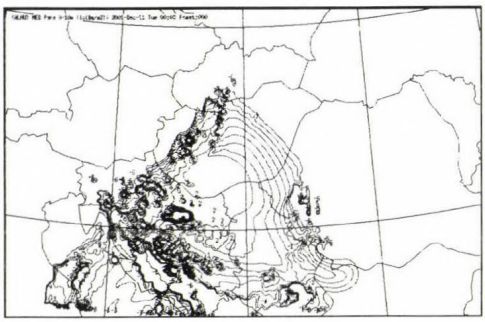

(a) Total deposition

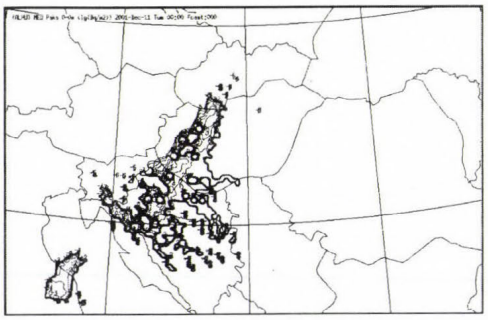

(b) Wet deposition

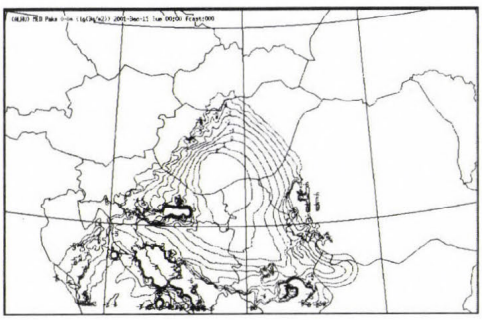

(c) Dry deposition

Fig. 10. Total, wet, and dry, 24-hour deposition fields (isolines are $\log_{10}$C, and unit is in Bq m^{-2}) between 00 UTC, December 12, 2001 and 00 UTC, December 12, 2002.

7. Conclusions

This study demonstrated the capability of MEDIA Eulerian type model to predict the time-evolution of a polluted material in the air considering wet and dry depositions.

Increasing the time and grid resolution of meteorological fields provided an improvement in the time and space resolution of the prediction of concentrations. This information is very important in case of emergency response applications. In the every day routine, ALADIN/LACE or ECMWF numerical weather prediction model results have been used as input meteorological data to drive MEDIA. Since the ALADIN/HU model gives data only for 36 hours with 1 hour time resolution; it could be very important in case of an emergency situation in regional scale, while deterministic ECMWF forecast can be preferable especially in continental scale. Due to the fact that computing capacity was significantly increased at the HMS in 2002, in the near future there is an opportunity to develop ensemble version of MEDIA dispersion model coupled by ECMWF ensemble model.

Acknowledgements–The authors gratefully acknowledge support and encouragement of *Francois Bompay* in Toulouse, and financial support of EU and the French government. Two anonymous referees are thanked for their insightful comments that helped improve the quality of manuscript.

References

Bompay, F., 1998. Evaluation of the METEO-FRANCE response in ETEX release 1. *Atmospheric Environment 32,* 4351-4357.

Galmarini, S., Bianconi R., Bellasio, R., and *Klug, W.*, 2002: ENSEMBLE: A system for ensemble dispersion forecast in case of nuclear emergencies. In *IRPA 2002*, Florence, 8-11 Oct., 2002.

Horányi, A., Ihász, I., and *Radnóti, G.*, 1996: ARPEGE-ALADIN: A numerical weather prediction model for Central-Europe with the participation of the Hungarian Meteorological Service. *Időjárás 100,* 277-300.

Ihász, I., 1992: Isobaric and isentropic objective analysis of meteorological fields for regional and continental scale trajectories. *Időjárás 96,* 81-91.

Ihász, I., 1999: The application of MEDIA dispersion model and 3D trajectory model using ALADIN/LACE, ALADIN/HU and ECMWF model products at the Hungarian Meteorological Service. *Proceedings of the 7th International ALADIN Workshop: Recent and planned operational exploitation of ALADIN model. Operational use and applications, verification. MAP.* 17-19 November 1999, Ljubljana, Slovenia.

Ihász, I., 2000: Large scale modelling of chemical and radioactive pollutant by joint use of ALADIN, ECMWF numerical weather forecasting models and MEDIA dispersion model at the Hungarian Meteorological Service (in Hungarian). In *Meteorológiai Tudományos Napok, 2000: A levegőkörnyezet monitoringja, állapotának értékelése és szabályozása*. Országos Meteorológiai Szolgálat, Budapest, 119-124.

Louis, J.F., 1979: A parametric model of vertical eddy fluxes in the atmosphere. *Boundary Layer Meteorology 17,* 187-202

Piedelievre, J.P., Musson-Genon, L., and *Bompay, F.,* 1990: MEDIA – An eulerian model of atmospheric dispersion: first validation on Chernobyl release. *J. of Applied Meteorology 29,* 1205-1220.

White, P., 2000a: IFS Documentation Part I: Observation Processing (CY21R4). *Meteorological Bulletin M1.5/2,* ECMWF, Shinfield Park, Reading, March 2000.

White, P., 2000b: IFS Documentation Part II: Data Assimilation (CY21R4). *Meteorological Bulletin M1.5/3*, ECMWF, Shinfield Park, Reading, February 2000.

White, P., 2000c: IFS Documentation Part III: Dynamics and Numerical Procedures (CY21R4). *Meteorological Bulletin M1.6/4*, ECMWF, Shinfield Park, Reading, March 2000.

White, P., 2000d: IFS Documentation Part V: The Ensemble Prediction System (CY21R4). *Meteorological Bulletin M1.6/6*, ECMWF, Shinfield Park, Reading, March 2000.

White, P., 2000e: IFS Documentation Part VI: Technical and Computational Procedures (CY21R4). *Meteorological Bulletin M1.6/7*, ECMWF, Shinfield Park, Reading, March 2000.

IDŐJÁRÁS

Quarterly Journal of the Hungarian Meteorological Service
Vol. 107, No. 2, April–June 2003, pp. 133–152

Surface ozone observations over Egypt

F. M. El-Hussainy[1], **W. M. Sharobiem**[2], and **M. D. Ahmed**[2]

[1]*Faculty of Science, Al-Azhar University, P.O. Box 11884, Cairo, Egypt; E-mail: el_hussainy@hotmail.com*

[2]*Meteorological Authority, P.O. Box 11784, Cairo, Egypt; E-mail: wafiek@yahoo.com*

(Manuscript received June 22, 2001; in final form January 21, 2002)

Abstract—Hourly data of surface ozone measurements at Cairo, Sidi Branni, and Hurghada were taken to compare the ozone concentration of polluted area with that of rural areas. The study showed that the maximum value of surface ozone concentration appears in the afternoon in all regions. While the maximum concentration of surface ozone appears in spring at Sidi Branni, and in summer at Cairo and Hurghada. Also, daily and monthly relationships between surface ozone and some meteorological elements were performed. Strong relationships between surface ozone and solar radiation were found for Cairo and Hurghada. Also, positive trend for surface ozone against wind speed was found in all regions.

Key-words: tropospheric ozone, regional pollution.

1. Introduction

Like water, ozone can be useful or dangerous atmospheric component, depending on the place and amount of it. Ozone in the stratosphere is very important as it acts as a shield for the mother planet, the Earth, and protects us against harmful UV-B radiation coming from the sun. However, the ozone in the atmosphere is a greenhouse gas, trapping the long wave radiation in 9.6 μm band, affecting the energy budget of the earth-atmosphere system. It is also a pollutant that is produced as a result of antropogenic activities such as fossil fuel burning, and has potential to affect human health (*Lippman,* 1989; *Tilton*, 1989), vegetation (*Woodman*, 1987) and animals (*Costa et al.*, 1989), if it is allowed to attain high concentration. It has been observed that the amount of ozone at the surface is increasing while in the stratosphere is decreasing with anthropogenic activities, and it is a serious problem (*Randriambelo et al.*, 1999).

Ozone close to the ground is produced on the account of photochemical reactions involving oxides of nitrogen, hydrocarbons, and sunlight. High ozone concentration at a particular place depends on the concentration of oxides of nitrogen and hydrocarbons. The source of oxides of nitrogen may be local or they can be transported from another source areas. Therefore, the monitoring of ozone concentration is very important, as it provides information about its formation, scavenging, and transport at a site or within an area (*Jain* and *Arya*, 2000).

Ozone measurements in the Mediterranean region (*Butkovic et al.*, 1990) indicate serious problems of photochemical air pollution in areas with more sunny days per year than in Central Europe. The special meteorological conditions, dominating almost in the whole year over the eastern Mediterranean (intensive sunlight, high temperatures, etc.), can enhance photochemistry and biogenic volatile organic compound emission into the atmosphere, and combined with low deposition velocities over the sea, they result in high ozone levels (*Kouvarakis et al.*, 2000; *Johnson et al.*, 2000).

Tropospheric ozone concentration in the tropics is believed to be low as compared to those in middle latitudes, because of inactive transport from stratosphere to troposphere (*Routhier et al.*, 1980). However, tropospheric ozone is supplied by photochemical reactions as well as transport from the stratosphere. We expect high photochemical activity in the tropics, where the solar radiation is intense. The land area provides potential sources for the precursor species of surface ozone formation in the tropics (*Crutzen et al.*, 1985), while the ocean does not seem to be a source (*Helas* and *Warneck*, 1981). Tropospheric ozone data imply that the marine air is lean in ozone (*Piotrowice et al.*, 1986).

Ozone formation in the greater Cairo (Egypt) area was studied in 1990 in a three weeks measurement period performed at three sites (Shoubra El-Khema, Mokattam Hill, and Helwan), covering a north–south direction of 27 km long. In 1991, from the beginning of April until the end of October, ozone was studied by measuring the seasonal variation of ozone at one site at El-Quobba (*Gusten et al.*, 1994). The sinusoidal shape in the diurnal volume fraction plots with peak values of 120 ppb and daily mean value of 50 ppb throughout the year indicates a substantial contribution of photochemical reactions to the ozone content of the atmosphere. Ozone is produced predominantly over the industrial area in the north and in the center of Cairo, and transported southward by the prevailing northerly winds. Contrary to many urban areas in Europe and North America, fairly high average ozone levels of 40 ppb are observed during the night in spring and summer. This may imply that health hazards and crop damages are higher in the greater Cairo area than in Central Europe.

This paper presents a comparative study between the formation and variation of surface ozone in a polluted area (Cairo) and rural areas (Sidi Branni and Hurghada). Also, it discusses the relationships between the surface ozone and each of the solar radiation, air temperature, wind, and relative humidity.

2. Observation sites and data

Hourly data of surface ozone (measured by Ozone Analyzer Model 49 manufactured by Thermo Environmental Inc.), solar radiation (measured by Epply Pyranometer), relative humidity, surface wind, and temperature at Cairo, Sidi Branni, and Hurghada are taken in the periods indicated in *Table 1*.

Table 1. Measuring period of the data with the latitude, longitude, and altitude of the stations

Stations	Latitude	Longitude	Altitude	Period
Cairo	30°02'N	31°12'E	16 meters	January–December 1999
Sidi Branni	31°22'N	25°32'E	24 meters	September 1999–August 2000
Hurghada	27°17'N	33°45'E	06 meters	October 1995–September 1996

Fig. 1 shows the location of surface ozone stations (Hurghada lies at the Red Sea and Sidi Branni at the Mediterranean Sea).

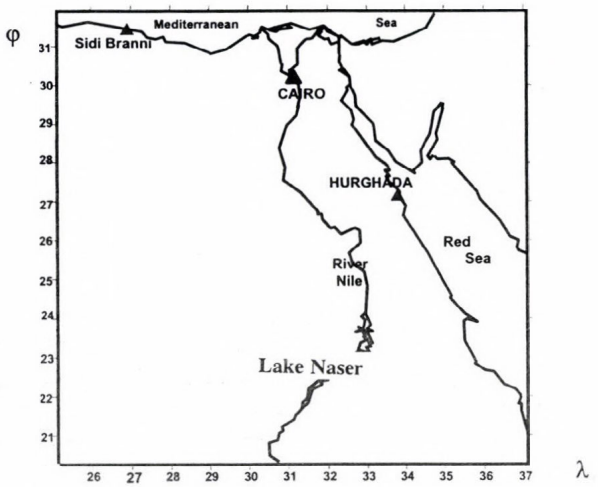

Fig. 1. Surface ozone stations in Egypt.

The Cairo station situates inside the buildings of Cairo University. Cairo encompasses 27% of the Egyptian population, 64% of the industry, and 45% of the motor vehicles. It is clear that the population of Cairo is exposed to an alarming level of air pollution (*Gusten et al.*, 1994). Hurghada station lies near the Red Sea, south from the natural gas burning at Ras Garb, Ras Shocker, and Oil Gulf regions, which extend from 70 to 150 km. Sidi Branni is a flat sandy area at the coast of the Mediterranean Sea. There is no industry in Sidi Branni with small population and few cars and trucks.

Table 2a–c represent the descriptive statistics for all measurements at Cairo, Sidi Branni, and Hurghada, respectively.

Table 2a. Descriptive statistics for daily data measured at Cairo

Elements	Number of valid obs.	Std. deviation	Mean value	Maximum value	Minimum value
Solar radiation (MJ/m^2/day)	256	6.61	19.43	29.00	4.90
Wind speed (m/s)	256	1.59	4.00	8.10	0.90
Rel. humidity (%)	256	7.13	65	89	47
Temperature (°C)	256	5.70	22.50	32.20	12.40
Surface ozone (ppb)	256	23.09	40.40	97.49	5.00

Table 2b. Descriptive statistics for daily data measured at Sidi Branni

Elements	Number of valid obs.	Std. deviation	Mean value	Maximum value	Minimum value
Solar radiation (MJ/m^2/day)	366	8.01	21.41	33.20	1.60
Wind speed (m/s)	366	2.49	4.23	16.80	1.00
Rel. humidity (%)	366	11.31	44	80	16
Temperature (°C)	366	4.90	21.60	34.70	10.60
Surface ozone (ppb)	366	6.58	48.56	70.59	27.90

Table 2c. Descriptive statistics for daily data measured at Hurghada

Elements	Number of valid obs.	Std. deviation	Mean value	Maximum value	Minimum value
Solar radiation (MJ/m^2/day)	365	7.43	22.55	32.68	1.96
Wind speed (m/s)	365	1.54	5.87	9.60	2.90
Rel. humidity (%)	365	12.76	39	75	14
Temperature (°C)	365	5.80	23.40	36.30	13.00
Surface ozone (ppb)	365	7.88	41.94	62.80	21.20

3. Results and discussion

Surface ozone has been measured on round the clock basis. According to *Table 1*, ozone was measured during different periods at the different locations using ozone analyzer to study diurnal as well as seasonal variation.

3.1 Diurnal variation of surface ozone concentration

The diurnal variation of surface ozone observed at Cairo, Sidi Branni and Hurghada is depicted in *Figs. 2a–e*. *Fig. 2a* represents the diurnal variation of average surface ozone concentration, while *Figs. 2b–e* represent the diurnal variation of seasonal surface ozone concentration in spring, summer, autumn, and winter, respectively.

There is a wide range between the day and night values of ozone at Cairo comparing to the other stations. This is due to the urbanization effect at Cairo (big industrial area) including the increasing vehicular traffic and big industries. Whereas Sidi Branni and Hurghada are considerable as rural regions with less human activities.

Generally, the minimum value of ozone concentration occurs in the early morning hours (before dawn at Hurghada), and its maximum occurs at around noon (late afternoon at Sidi Branni). The pattern of diurnal variation of surface ozone at Cairo results from daytime photochemical production and downward transport of ozone rich air from above, combined with ozone loss by dry deposition and reaction with nitric oxide (NO) at night, when photochemical production ceases and vertical transport is inhibited by an inversion of the normal temperature profile. In locations near large sources of NO (e.g., Cairo), the nighttime minimum in ozone can be quite pronounced (see *Table 2a*), because of the rapid reaction between ozone and NO. In fact, in many urban areas the NO source is strong enough to cause the complete nighttime disappearance of ozone (*Seinfeld* and *Spyros,* 1998). In addition to variations over a diurnal cycle, ozone concentration at these locations also can vary significantly from one day to the next, in particular, Cairo location has the maximum variation as indicated in *Table 2a*. It is not uncommon, for the daily maximum ozone concentration at an urban site (like Cairo), for instance, can vary by factor 2 or 3 from day to day, as local meteorological conditions change.

The maximum of the diurnal variation of surface ozone at Hurghada occurs at around 12:00 GMT. This is a typical type but its variation is not so big as in Cairo, which indicates that the photochemical activity is smaller. The diurnal variation changes from day to day due to advected ozone that produced from sources in north Hurghada (natural gas burning). Whereas, the diurnal variation of surface ozone in Sidi Branni is very little. This is because the

photochemical activity is smaller due to clean air conditions in this region (no human activities). But it is mainly vertically transported from the upper troposphere and has no definite pattern.

(a)

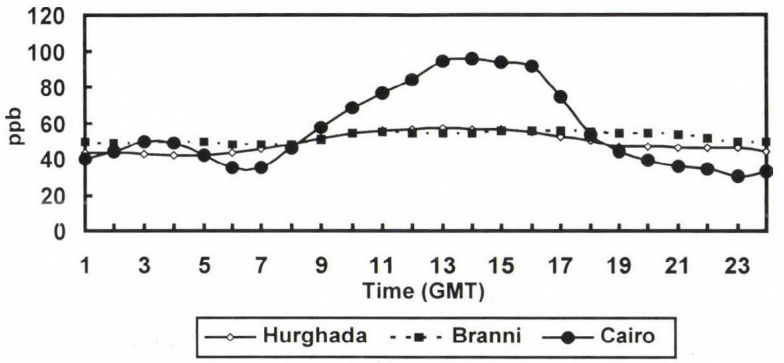

(b)

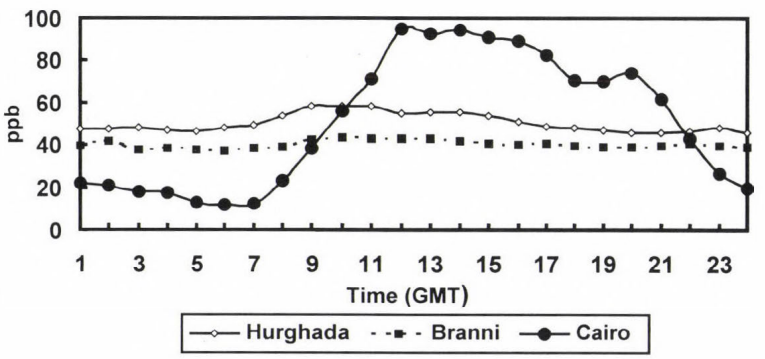

(c)

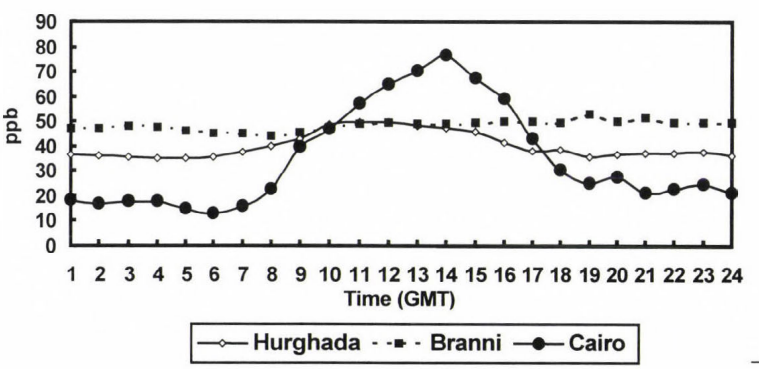

→

(d)

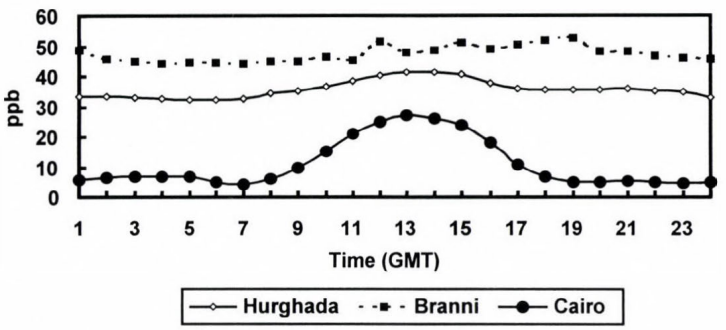

Fig. 2. Diurnal variation of surface ozone in Egypt (*a*) in spring, (*b*) in summer, (*c*) in autumn, (*d*) in winter.

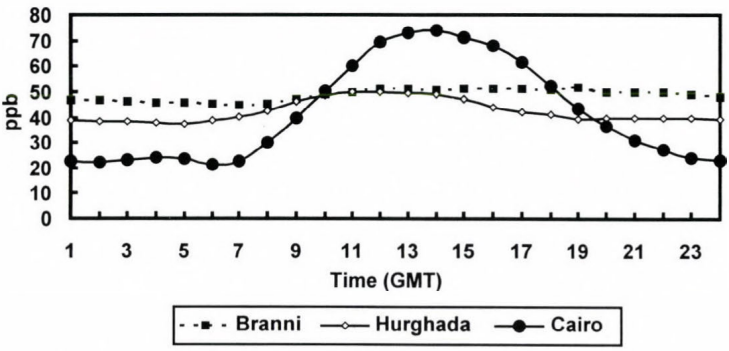

Fig. 2e. Diurnal variation of average surface ozone in Egypt.

On seasonal basis, surface ozone has small concentration at Cairo in wintertime. This is due to low solar radiation intensity and high emissions of reductive substances like NO. The latter characterizes the city all year. In contrast, the other stations do not depend on the effect of photochemical reactions as mentioned before. In spring, the pattern for Cairo goes up to higher concentrations, in particular daytime, due to the increasing solar radiation intensity. In summer and autumn the patterns of surface ozone concentration at Cairo seem to be the same.

3.2 Monthly variation of surface ozone concentration

The monthly average variation of surface ozone concentration at Cairo, Sidi Branni, and Hurghada are depicted in *Fig. 3a*. The variation of maximum and minimum values of surface ozone concentration at Cairo, Sidi Branni, and Hurghada are depicted in *Figs. 3b* and *3c*.

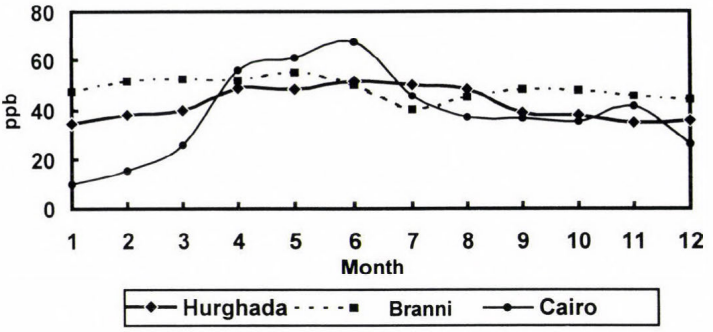

Fig. 3a. Monthly variation of average surface ozone in Egypt.

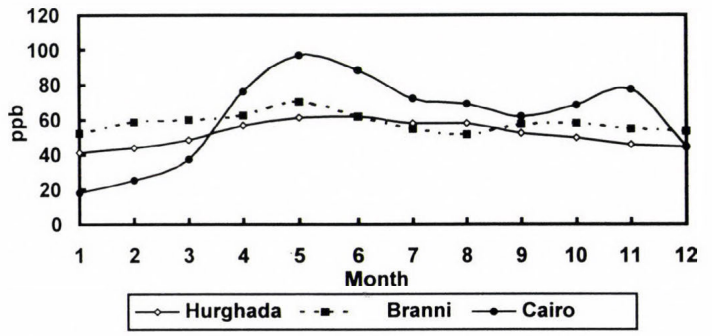

Fig. 3b. Monthly variation of maximum surface ozone in Egypt.

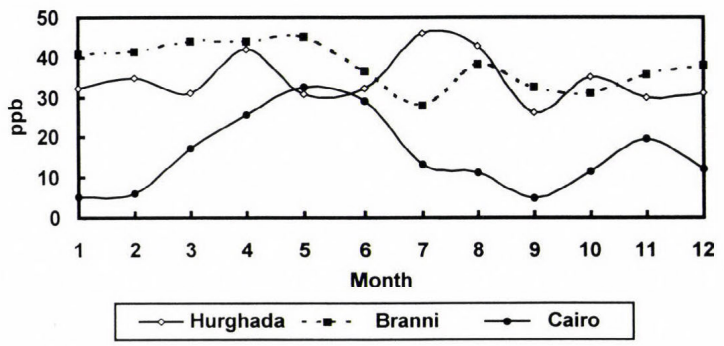

Fig. 3c. Monthly variation of minimum surface ozone in Egypt.

Fig. 3a shows that Cairo has a maximum concentration in June and the minimum occurs in January. This follows the seasonal solar radiation cycle.

A secondary maximum in November seems to appear occasionally, due to rice straw burning in 1999. Monthly variation at Hurghada mainly depends on solar intensity change from summer to winter. Sidi Branni has a maximum in spring, and the minimum occurs in July. The spring maximum follows the seasonal variation of total amount of ozone in middle latitudes, while the minimum occurs due to northerly wind, which blows from the Mediterranean Sea.

It can be noticed, that Cairo has the same pattern with large amplitude (see *Figs. 3b* and *3c*). The maximum pattern for Hurghada and Sidi Branni takes the same shape as the average pattern, but the minimum pattern for each station has no definite aspect.

In spite of low human activity at Sidi Branni, the concentration of surface ozone is higher than the background stations in Europe, which varies from 20 to 40 ppb. This is due to the permanent subtropical high pressure with the subsidence of air, which causes the intrusion of surface ozone from higher altitudes to the surface.

3.3 Relationship between surface ozone and solar radiation

As proposed by *Frenkiel* (1959), the main source reaction for photochemically produced ozone is photodissociation of NO_2 by solar radiation with wavelength $\lambda < 400$ nm

$$NO_2 + h\nu \rightarrow NO + O\,(^3P) \qquad \lambda < 400 \text{ nm}. \tag{1}$$

This reaction provides the needed O atoms for ozone production. The UV (ultraviolet) portion is about 3–4% of total global radiation. Strong relationship between UV radiation and global solar radiation over Cairo was found by *El-Hussainy* (1986). Therefore, global solar radiation can be used because UV radiation measurements are not available at all stations in Egypt.

Figs. 4.a1, 4.b1, and *4.c1* show the monthly variation of surface ozone concentration and solar radiation at Cairo, Sidi Branni, and Hurghada, respectively, while *Figs. 4.a2, 4.b2*, and *4.c2* represent the relation between surface ozone concentration and solar radiation at these stations.

Table 3 gives the daily correlation between surface ozone concentration and global solar radiation at Cairo, Sidi Branni, and Hurghada. There is a significant relation at Cairo and Hurghada with 1% significance level, while for Sidi Branni there is no significant relation (with 5% significance level). This indicates that the surface ozone concentration in Cairo and Hurghada depend on the photochemical reactions producing surface ozone. Also, the family of curves (*Figs. 4.a1, 4.b1, 4.c1*) and trends (*Figs. 4.a2, 4.b2, 4.c2*) are ascertained the above fact. The trend line for Sidi Branni shows that the vertical transport of ozone from the upper troposphere is the effective source.

(a1)

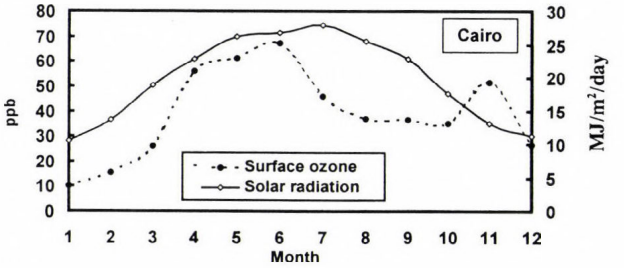

(b1)

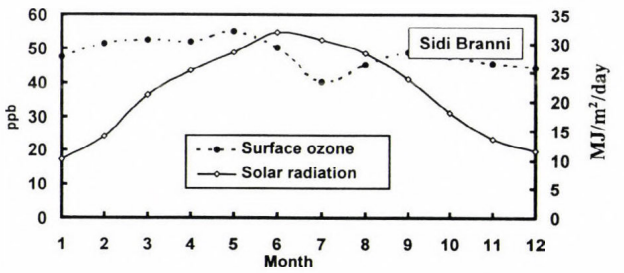

(c1)

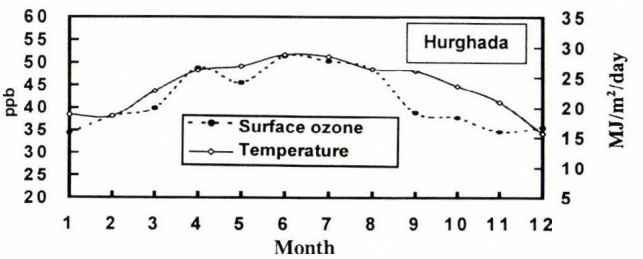

Fig. 4.a1–c1. Monthly variation of surface ozone and solar radiation at Cairo, Sidi Branni, and Hurghada.

(a2)

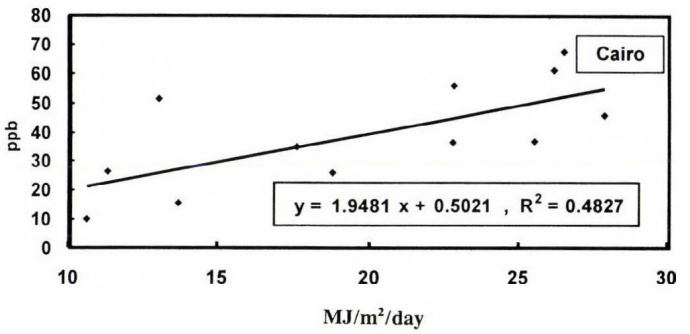

→

(b2)

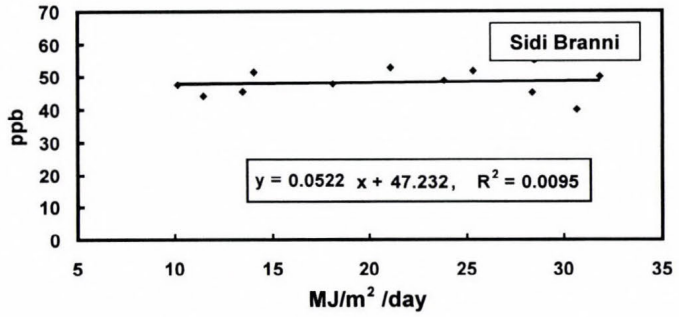

(c2)

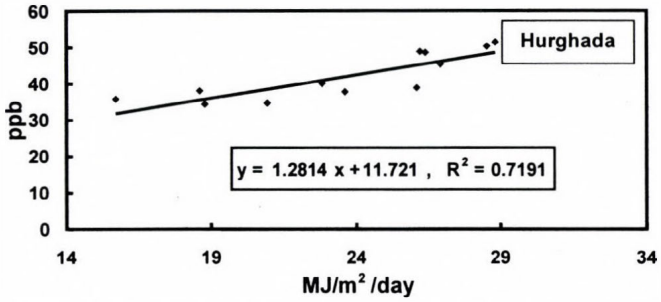

Fig. 4.a2–c2. Relation between surface ozone and solar radiation at Cairo, Sidi Branni, and Hurghada.

Table 3. Correlation coefficients between surface ozone against relative humidity, wind speed, temperature and solar radiation at Cairo, Sidi Branni, and Hurghada

Daily correlation	Rel. humidity	Wind speed	Temperature	Solar radiation	All*
Ozone (Cairo)	-0.26	+0.37	+0.54	+0.59	0.61
Ozone (Sidi Branni)	-0.12	+0.11	-0.27	+0.05	0.40
Ozone (Hurghada)	-0.54	+0.15	+0.53	+0.53	0.40

*All: multiple correlation for all elements with surface ozone

3.4 Relationship between surface ozone and surface wind

We are aware that surface wind is only a rough approximation of horizontal transport of ozone and its precursors. The situation becomes even more complicated, because solar radiation should play an important role in the photochemical ozone production. *Figs. 5.a1, 5.b1*, and *5.c1* represent the monthly variation of surface ozone and wind speed at Cairo, Sidi Branni, and

Hurghada, respectively, while *Figs. 5.a2, 5.b2*, and *5.c2* show the relation between surface ozone and wind speed at the same stations. On monthly basis, it is noticed from these figures, that there is a positive correlation between the surface ozone concentration and surface wind speeds in the range of 2–7 m/s. The noticeably clear correlation at Cairo is due to several existing sources of pollutants. On daily basis, it is noticed from *Table 3* that there is a negative correlation with a significant level better than 1 % for Cairo and Hurghada, and there is no significant correlation for Sidi Branni.

(a1)

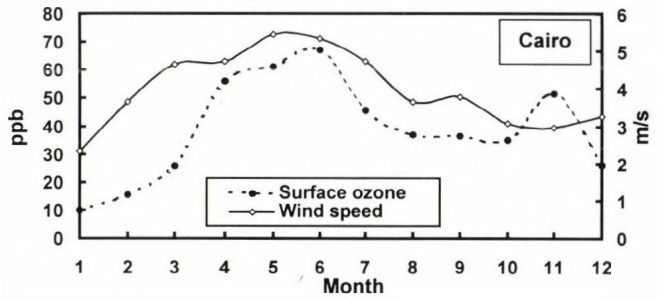

(b1)

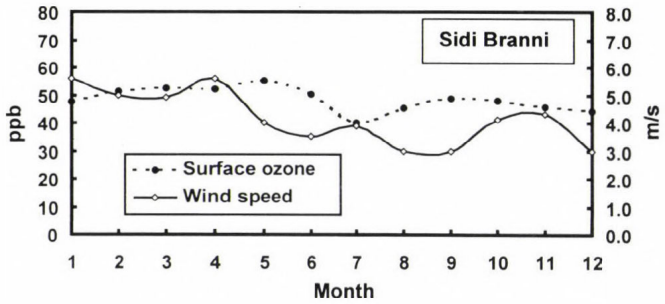

(c1)

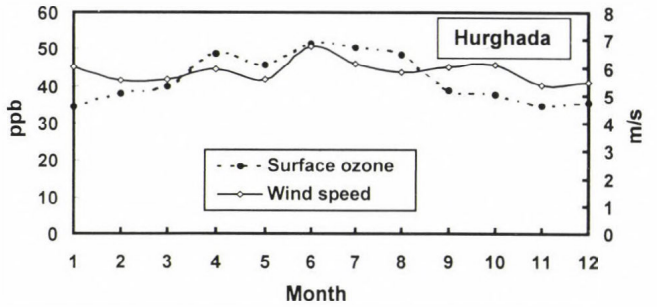

Fig. 5.a1–c1. Monthly variation of surface ozone and wind speed at Cairo, Sidi Branni and Hurghada.

(a2)

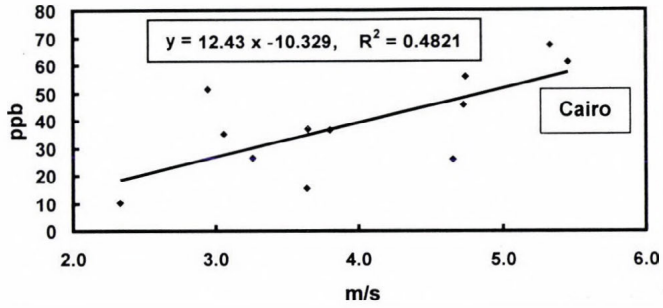

(b2)

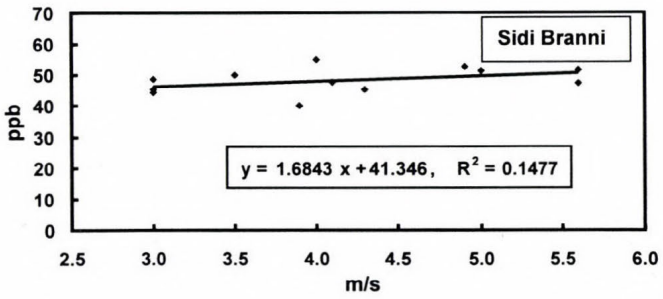

(c2)

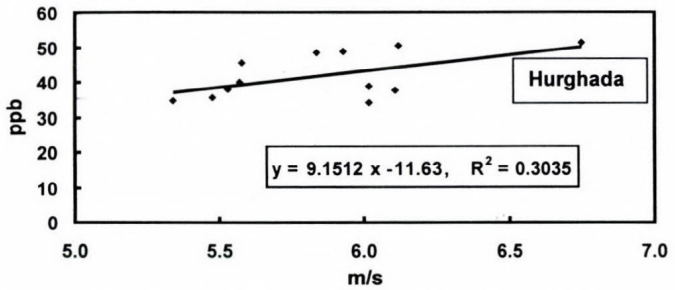

Fig. 5.a2–c2. Relation between surface ozone and wind speed at Cairo, Sidi Branni, and Hurghada.

Fig. 5d shows that for Hurghada the surface ozone concentration takes high values when the wind direction is northeast, while low values of surface ozone concentration occur when the wind is northwest. At Sidi Branni, the surface ozone concentration takes low values when the wind direction is north or northeast, and high values occur when the wind is southeast or northwest. The wind direction is not significant for concentration of surface ozone at Sidi Branni. For Cairo, high values of surface ozone concentration occur when the wind direction is northwest and low values occur at northeast, wind (see *Gusten et al.*, 1994).

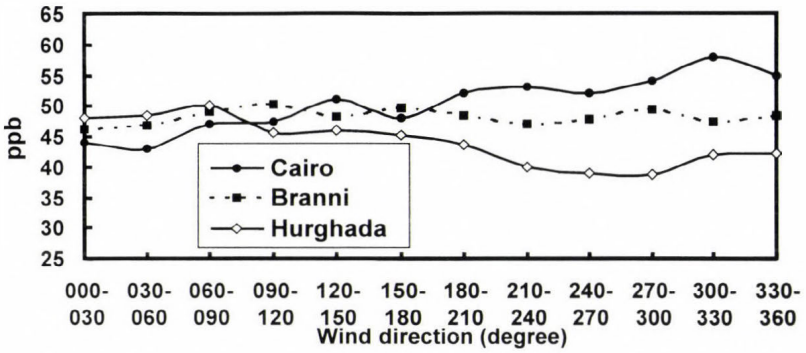

Fig. 5d. Variation of surface ozone and wind direction at Egypt.

3.5 Relationship between surface ozone and relative humidity

The principal photochemical sink of O_3 in the troposphere can be written by the following reactions:

$$O_3 + h\nu \rightarrow O(^1D) + O_2, \quad (2)$$

$$O(^1D) + M \rightarrow O + M, \quad (3)$$

$$O(^1D) + H_2O \rightarrow 2OH. \quad (4)$$

Since this removal path depends on the concentration of water vapor, it is most effective at low latitudes and low altitudes, where the radiation is intense and the humidity is high. Ozone destruction occurs whenever an $O(^1D)$ reacts with H_2O, since this removes $O(^1D)$ from the system; otherwise $O(^1D)$ is just quenched back to O in reaction (2), and O immediately reforms O_3 by reaction:

$$O + O_2 + M \rightarrow O_3 + M, \quad (5)$$

where M represents N_2, O_2 or another third molecule that absorbs the excess vibrational energy and thereby stabilizes the O_3 molecule formed (*Seinfeld* and *Spyros*, 1998).

Figs. 6.a1, 6.b1, and *6.c1* represent the monthly variation of surface ozone and relative humidity at Cairo, Sidi Branni, and Hurghada, respectively, while *Figs. 6.a2, 6.b2*, and *6.c2* show the relation between surface ozone and relative humidity at the same stations. There is a negative trend for the surface ozone against relative humidity, which is in agreement with the findings by *Seinfeld* and *Spyros* (1998).

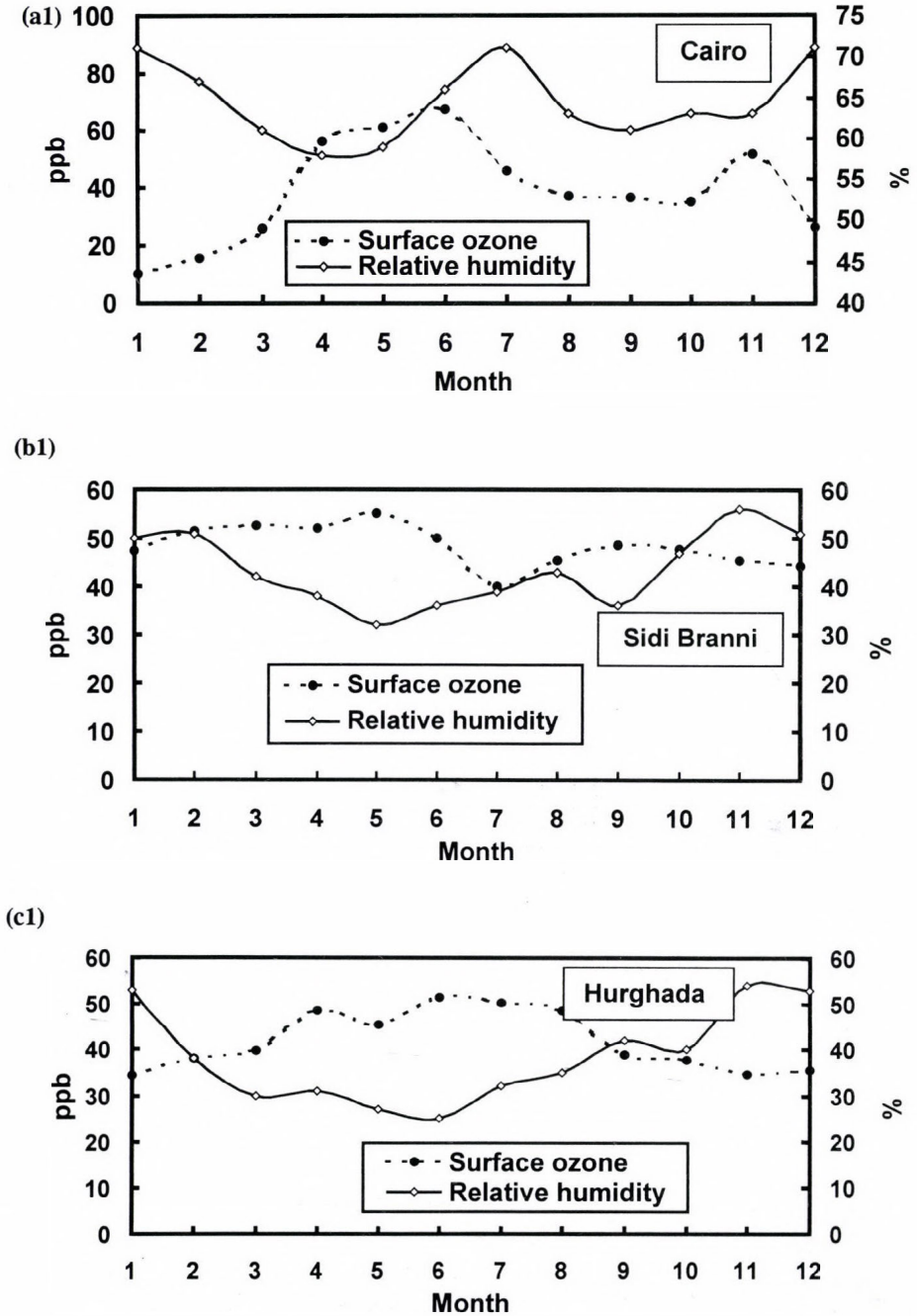

Fig. 6.a1–c1. Monthly variation of surface ozone and relative humidity.

(a2)

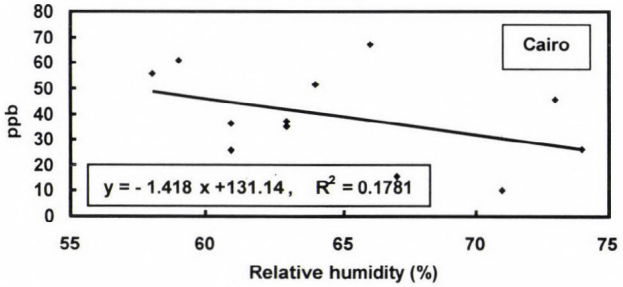

(b2)

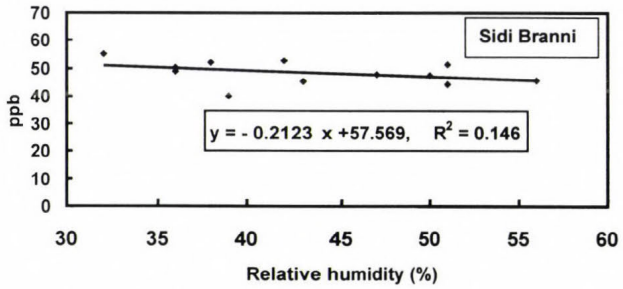

(c2)

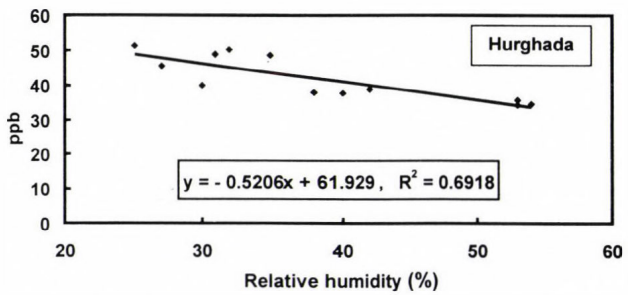

Fig. 6.a2–c2. Relation between surface ozone and relative humidity.

3.6 Relationship between surface ozone and temperature

Figs. 7.a1, 7.b1, and *7.c1* represent the monthly variation of surface ozone concentration and temperature at Cairo, Sidi Branni, and Hurghada, respectively, while *Figs. 7.a2, 7.b2*, and *7.c2* show the relation between surface ozone and temperature at the same stations. It is noticed, that there is a strong similarity among the family of curves, trends, correlation of surface ozone concentration against surface air temperature, and correlation of surface ozone concentration against solar radiation. This is due to the strong relationship between solar radiation and air temperature over Egypt (*El-Hussainy* and *Essa*, 1997).

(a1)

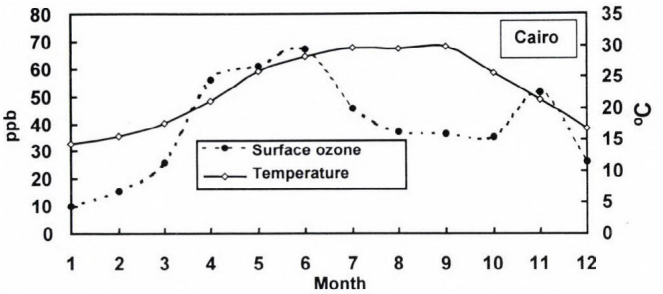

(b1)

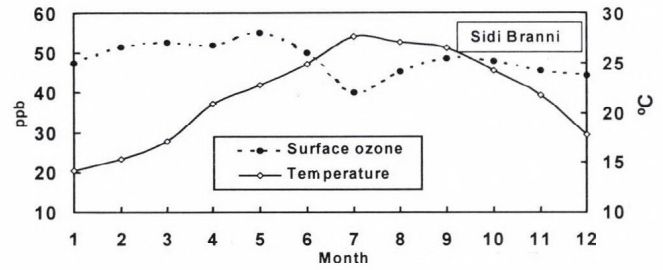

(c1)

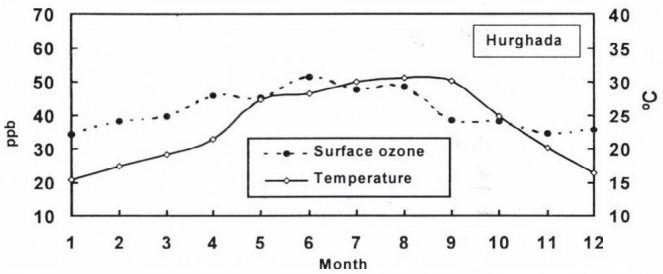

Fig. 7.a1-c1. Monthly variation of surface ozone and temperature.

(a2)

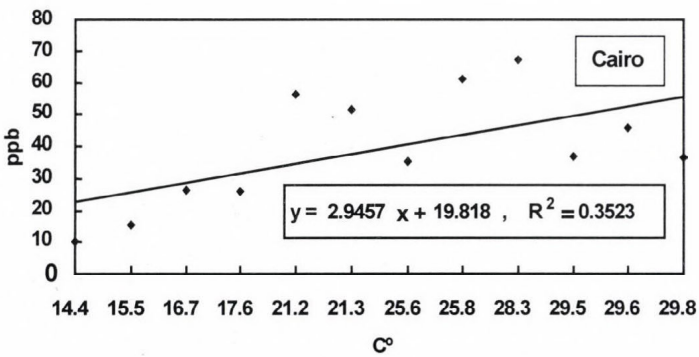

→

(b2)

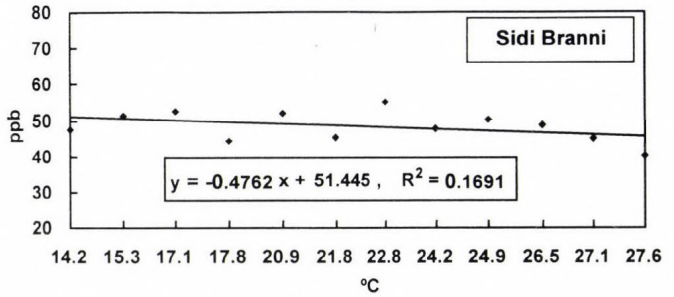

(c2)

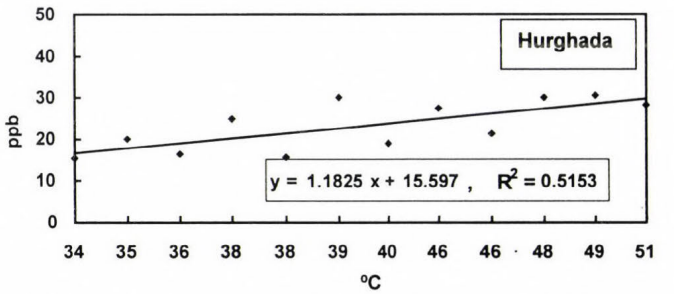

Fig. 7.a2–c2. Relation between surface ozone and temperature.

3.7 Relative importance of different weather elements affecting surface ozone

The relative importance of solar radiation (R), air temperature (T), relative humidity (H), wind speed (S), and wind direction (D) in the formation of surface ozone (Z) will be studied by using multiple regression analysis (*Snedecor* and *Cochran,* 1980) as

$$Z = b_0 + b_1 X_1 + b_2 X_2 + b_3 X_3 + b_4 X_4 + b_5 X_5 + E, \tag{6}$$

where X_1 , X_2 , X_3 , X_4, and X_5 represent R, T, H, S, and D, respectively. E represents the residual (errors).

The equations for Cairo, Sidi Branni, and Hurghada, respectively, are

$$Z = 16.39 + 2.40R + 1.71T - 0.48H + 2.60S, \tag{6a}$$
$$Z = 59.83 + 0.25R - 0.65T - 0.06H + 0.03S, \tag{6b}$$
$$Z = 45.48 + 0.16R + 0.29T - 0.19H + 1.12S - 0.05D. \tag{6c}$$

The standard deviation of errors for Eqs. (6a) to (6c) are 6.01, 6.08, and 5.94, respectively.

The variance for Eq. (6) is

$$\sigma^2_Z = b^2_1\,\sigma^2_1 + b^2_2\,\sigma^2_2 + b^2_3\,\sigma^2_3 + b^2_4\,\sigma^2_4 + b^2_5\,\sigma^2_5 + \sigma^2,$$

where σ^2_i denotes the variance of X_I, and σ^2 denotes the variance of the residual.

The quantity $b^2_I\,\sigma^2_i\,/\sigma^2_Z$ measures the fraction of the variance of Z (surface ozone) attributable to its linear regression on X_i. This fraction can reasonably be regarded as measure of the relative importance of X_I as shown in *Table 4*.

Table 4. Relative importance of different weather elements affecting surface ozone formation at Cairo, Sidi Branni, and Hurghada

Stations	Wind direction	Wind speed	Relative humidity	Temperature	Solar radiation	Residual
Cairo	0.00	0.01	0.05	0.15	0.23	0.56
Sidi Branni	0.00	0.00	0.01	0.22	0.07	0.71
Hurghada	0.06	0.06	0.12	0.06	0.01	0.70

Cairo and Sidi Branni have lowest values in wind speed and direction. This means that wind speed and direction have high relative importance in the formation of surface ozone concentration. While the solar radiation has high relative importance at Hurghada.

4. Conclusions

It is found that photochemical reactions are the effective sources at Cairo and mainly at Hurghada, whereas the upper troposphere is the effective source at Sidi Branni. Higher values of concentration of surface ozone at Sidi Branni and Hurghada comparing to Europe (20–40 ppb) are due to the Azores high belt, which lies at this area making large scale subsidence which causes the transportation of ozone from upper air. For areas of anthropogenic activity (Cairo), the amplitude of diurnal variation is large, and concentrations at daytime can affect the human health (i.e., concentration exceeding 80 ppb).

There is a positive/negative trend for surface ozone concentration against solar radiation/relative humidity for all stations. The relation between wind speed and surface ozone concentration takes a positive trend in the range of 2-7 m/s.

Acknowledgements–The authors thank the Egyptian Meteorological Authority for the data and valuable assistance to prepare this material. Also, thank *Dr. A. S. Zaki* and *Mr. M. A. Dawood* for cooperation and help.

References

Butkovic, V., Cvitas, T., and *Klasinc, L.,* 1990: Photochemical ozone in the Mediterranean. *Sci. Total Environ. 99,* 145-151.

Costal, D.L., Highfill, E.G., Stevens, J., and *Tepper, J.S.,* 1989: Pulmonary function studies in the rate addressing concentration versus time relationship of ozone. In *Atmospheric Ozone Research and its Policy Implications* (eds.: *T. Schneider, S.D. Lee, G.J.R. Wolters* and *L.D. Grant*), 733-743.

Crutzen, P.J., Delany, A.C., Greenberg, J., Haagenson, P., Heidt, L., Lueh, R., Pollack, W., Seiler, W., Wurthurg, A., and *Zimmeimem, P.,* 1985: Tropospheric chemical composition measurement in Brazil during the dry season. *J. Atmos. Chem. 2,* 233-256.

El-Hussainy, F.M., 1986: The spectral composition of the global solar radiation at Cairo and Bahtim. *ASRE 86, 1,* 13-23 *March* 1986, *Cairo, Egypt.*

El-Hussainy, F.M. and *Essa, K.S.M.,* 1997: The phase lag of temperature behind global solar radiation over Egypt. *Theor. Appl. Climatol. 58,* 79-86.

Frenkiel, F.N., 1959: Tropospheric ozone. Symposium on Atmospheric Ozone. July 1959, Oxford. *IUGG Monograph* No. 3, 33-36.

Gusten, H., Heinrich, G., Weppner, J., Abdel-Aal, M.M., Abdel-Hay, F.A., Ramadan, A.B., Tawfik, F.S., Ahmed, D.M., Hassan, G., Cvitas, T., Jeftic, J., and *Klasinc, L.,* 1994: Ozone formation in the greater Cairo area. *The Science of the Total Environment 155,* 285-295.

Helas, G. and *Warneck, P.,* 1981: Background NO_x mixing ratio in air masses over North Atlantic Ocean. *J. Geophys. Res. 86,* 7283-7290.

Jain, S.L. and *Arya, B.C., 2000*: Measurement of surface ozone at NPL, New Delhi. *Q. Ozone Symposium. Atmospheric Ozone.* July 2000, Sapporo, Japan.

Jonson J.E., Kylling, A., Berntsen, T., Isaksen, I.S.A., Zerefos, C.S., and *Kourtidis, K.,* 2000: Chemical effects of UV fluctuations inferred from total ozone and tropospheric aerosol variations. *J. Geophys. Res. 105,* 14561-14574.

Kouvarakis, G., Tsigaridis, K., Kanakidou, M., and *Mihalopoulos, N.,* 2000: Temporal variations of surface regional background ozone over Crete Island in southeast Mediterranean. *J. Geophys. Res. 105,* 4399-4407.

Lippman, M., 1989: Health effects of ozone: a critical review. *J. Air. Pollut. Control Ass. 39,* 672-695.

Ogawa, T. and *Kamala, N.,* 1989: Diurnal and seasonal variations of the tropospheric ozone in tropical Asia. Ozone in the atmosphere. *Ozone Symposium.* Göttingen, Germany, 437-440.

Piotrowicz, S.R., Boran, D.A., and *Fischer, C.J.,* 1986: Ozone in the boundary-layer of the equatorial Pacific-Ocean. *J. Geophysical Res. 91,* 13113-13119.

Randriambelo, T., Baray, J.L., Baldy, S., Bremaud, P., and *Cautenet, S.,* 1999: A case study of extreme tropospheric ozone contamination in the tropics using in-situ, satellite and meteorological data. *Geophy. Res. Let. 26,* 1287-1290.

Routhier, F., Dennett, R., Daves, D.D., Wartburg, A., Haagenson, P., and *Delany, A.C.,* 1980: Free tropospheric and boundary-layer airborne measurement of ozone over the latitude of 58 S to 70 N. *J. Geophysical Res. 85,* 7307-7321.

Seinfeld, J.H. and *Sypros, N.,* 1998: *Atmospheric Chemistry and Physics from Air Pollution to Climate Change.* John Wiley and Sons. Inc., New York, London, Sydney, Toronto.

Snedecor, G.W. and *Cochran, W.G.,* 1980: *Statistical Analysis.* 7th edition. The Iowa State University Press.

Titlon, B.E., 1989: Health effects of tropospheric ozone. *Environment Science Technology 23,* 257-263.

Woodman, J.N., 1987: Pollution induced injury to North American forests and suspicions. *Tree Physiol 3,* 1-15.

IDŐJÁRÁS

Quarterly Journal of the Hungarian Meteorological Service
Vol. 107, No. 2, April–June 2003, pp. 153–170

Temporal change of some statistical characteristics of wind direction field over Hungary

Károly Tar[1] and **Emese Verdes**[2]

[1]*Department of Meteorology, University of Debrecen*
P.O. Box 13, H-4010 Debrecen, Hungary; E-mail: tark@tigris.klte.hu

[2]*Department of Sociology, University of Debrecen*
P.O. Box 11, H-4010 Debrecen, Hungary; E-mail: verdese@tigris.klte.hu

(Manuscript received March 26, 2002; in final form January 22, 2003)

Abstract–The objective of this study is to assess whether changes in the surface pressure field over Europe are reflected in the statistical structure of the wind direction field over Hungary. The data basis consists of hourly wind direction data measured at ten meteorological stations of the country in 1968–1972 and 1991–1995. Relative frequency, relative energy, average speed, and average duration of the wind directions were analysed in the above two periods, in winter and summer, over plains and mountains of the country. We investigated the difference of the relative frequencies with the so-called pi-star index. We gave the definition of the characteristic wind directions and we investigated their energy content and average speed compared to those of the non-characteristic wind directions. Then we detailed the quality of connections between the above-mentioned four parameters of the wind directions. Our main result is that the alterations of the statistical structure of wind direction field over Hungary depend on the features of the terrain and seasons.

Key-words: wind directions, relative frequency of wind directions, relative energy content of wind direction, pi-star index, characteristic wind directions.

1. Introduction

The rise in global surface air temperature, due to the increase of the atmospheric concentration of greenhouse gases, has probably induced a redistribution of the surface pressure field. According to *Schönwiese et al.* (1994) and *Meyhöfer et al.* (1996), this process has occurred in Europe: in the winter half-year the average values of surface pressure, converted to sea level, increased in the south and decreased in the north of the continent between 1961 and 1990, whereas in the summer half-year there were no significant changes.

On the other hand, *Metaxas* et al. (1991) and *Bartzokas* and *Metaxas* (1996) found that the average intensity of influx of cold air masses in summer, coming from the north and north-west to the south-east of Europe, had increased. Therefore, according to their investigations, the summer circulation system is also changing, as a consequence of the redistribution of the surface pressure field in summer, as well. In the above-mentioned authors' view, it is clear that such changes may affect Central-Europe to a relatively less degree than the northwestern and southeastern regions of our continent.

In continental Europe, in winter, the direction of the average pressure gradient is from south to north (*Justyák*, 1994). Thus, according to the previously mentioned results, this gradient itself is also increasing, which might also give rise to changes in the circulation system, e.g., the frequency or average speed of westerly winds may increase during this season. The spatial distribution of annual and monthly average sea level pressure fields in Hungary is due to the so called "basin character": roughly in the middle of the Great Hungarian Plain, a pressure minimum can be found. This is caused by strong warming in summer and frequent passing through of the Mediterranean cyclones in winter (*Dobosy* and *Felméry*, 1971).

The aim of our former investigations (*Tar*, 1998a, 1998b, 1999, 2001; *Mika et al.*, 1999; *Tar et al.*, 2000, 2001a, 2001b; *Makra et al.*, 2000a, 2000b) was to decide whether or not the observed changes in the pressure field over Europe could be detected in the statistical structure of the wind field over Hungary, in spite of the specific pressure field over the country. Change in the wind field, apart from climatic effects, also produces changes, among other things, of deflation and wind energy.

Our aim in this paper is to demonstrate possible marked changes in the statistical structure of the wind direction field over Hungary. The data basis of our investigations consists of hourly wind direction data of ten meteorological stations in Hungary, measured in periods 1968–72 and 1991–95. *Fig. 1* shows the locations and geographical coordinates of the stations. Since our data basis is not continuous, trends, autocorrelations, etc., cannot be determined.

2. Distribution of the wind directions and pi-star index

From the relative frequencies of wind directions of two critical seasons, over the ten stations, in the two five-year periods, we can see that the bigger deviations are in the winter, the significant differences are not presumable in a few cases in the summer.

The statistical test performed to evaluate differences was the χ^2 test of homogeneity. As the observed hours of different wind directions turned to be

quite large numbers, this test showed significant difference in the distributions in each case, which was not very surprising taking into account the sensitivity of the χ^2 test for sample size. The critical value of the χ^2 distribution at 0.05 significance level with 14 degrees of freedom is 23.65, which was highly exceeded in our examples, so we can conclude that wind direction field has changed remarkably. Note, however, that there were very big differences in the computed χ^2 values, which means that the magnitude of difference in hours of wind directions depended on the locations, seasons, and year very much, as *Table 1* shows.

Station	φ	λ	h_1 (1968-72)	h_2 (1991-95)	h_{a1} (1968-72)	h_{a2} (1991-95)
Szombathely	47°16'	16°38'	224	224	9	9
Keszthely	46°46'	17°14'	117	117	15	15
Győr	47°41'	17°38'	119	116	10	10
Pécs	46°00'	18°14'	202	202	10	10
Budapest	47°27'	19°13'	130	130	12	12
Szeged	46°15'	20°06'	83	83	9	9
Miskolc	48°08'	20°48'	118	233	15	15
Békéscsaba	46°41'	21°10'	88	88	9	10 and 20.6
Debrecen	47°30'	21°38'	111	108	10	10
Kékestető	47°52'	20°01'	1010	1010	26	26

h_1, h_2: height of the observatory above the sea level (m);
h_{a1}, h_{a2}: height of the anemometer above ground level (m)

Fig. 1. Location and geographical coordinates of the meteorological stations.

To remove the effect of sample size, we performed an another test, which is not so traditional as the χ^2 test, but has the advantages of not depending on sample size and giving a nice impression of discrepancy between model and data. This test is not a test of significance, rather an index between zero and one, and it is called pi-star index.

Table 1. Results of the χ^2 test

Station	Winter	Spring	Summer	Autumn	Year
Békéscsaba	710	271	148	259	528
Debrecen	1177	468	249	841	1613
Szeged	1178	468	232	398	813
Budapest	1036	627	617	630	2036
Győr	1848	1035	1489	1602	4695
Szombathely	1691	979	576	433	2671
Keszthely	1517	1437	941	1524	4484
Pécs	1451	240	618	611	1511
Miskolc	843	734	662	873	2044
Kékestető	1374	484	315	267	979

The pi-star index of fit was introduced by *Rudas et al.* (1994) for contingency table analysis. The original definition is

$$\pi^* = \pi^*(P, M) = \inf\{\pi : P = (1-\pi)F + \pi Q, \quad F \in M, \quad 0 \le \pi \le 1\}, \tag{1}$$

where P, F and Q denote cell probabilities of two-way contingency tables of the same size and M is a model. Although this definition is for two-way tables, it can be extended to contingency tables of any size with any model, moreover, to any known statistical model.

Roughly speaking, here the observations are decomposed into two parts: a first part, that fits the model exactly, and a second one, which is unrestricted, so that the sum of the observations in the first part will be maximal. Then the ratio of the observations in the second part is the pi-star index. This is the fraction of the sample that cannot be described by the model in the best case. Hence, if the pi-star index is small, we will conclude, that we are close to the model, as only a small fraction of the sample cannot be described by the model. On the contrary, if π^* is big, we will conclude, that we are not so close to the model.

In our case the null hypothesis was that the distribution of the hourly wind direction was the same in the two time periods. Putting it in another way, we had to examine in what extent the measurements in the second period could be described by those of the first period. Again, small π^* values indicated smaller differences, and bigger π^* values meant greater discrepancy in the distributions. According to this, we could conclude, that even removing the effect of sample size, we found big differences in the distributions due to quite big π^* values, but here also we could make differences among the ten stations and seasons examined.

Table 2. Values of π^*

Station	Winter	Spring	Summer	Autumn	Year
Békéscsaba	0.59	0.28	0.24	0.44	0.28
Debrecen	0.55	0.48	0.40	0.58	0.39
Szeged	0.55	0.48	0.39	0.31	0.25
Budapest	0.60	0.65	0.65	0.49	0.60
Győr	0.72	0.64	0.62	0.47	0.54
Szombathely	0.71	0.49	0.47	0.44	0.44
Keszthely	0.71	0.61	0.53	0.61	0.51
Pécs	0.73	0.41	0.47	0.45	0.47
Miskolc	0.46	0.59	0.56	0.55	0.53
Kékestető	0.67	0.50	0.53	0.31	0.50

Seasonal and yearly values of π^* are listed in *Table 2*. It can be seen from the table, that these values are bigger in the majority of cases in winter. This confirms that we wrote about this season in the introduction. The values also show that the temporal change of the distribution of wind directions is more marked in Transdanubian stations. In summer, values commensurable with winter ones can be seen in the no lowland-stations (Szombathely, Keszthely, Pécs, Miskolc, Kékestető), e.g., in the more complex geographical/orographical environment. All these suggest the alteration of directional distributions of summer wind, too, during about 20 years. This also is claimed by Mediterranean authors, *Metaxas* et al. (1991), *Bartzokas* and *Metaxas* (1996). First of all they are speaking about the Etesian wind, which can be considered as part of the summer monsoon circulation. It is possible that the change of features of this wind causes the increase of frequency of northerly directions over Hungary, too. In spring and autumn, the values of π^* cannot be classified from geographical/orographical or other point of view. It is possible that the measure of marked alteration of frequency distribution of wind directions can rather be connected to the circulation/macrosynoptic situations.

Conclusions about the above differences were made by these two (χ^2 and π^*) statistical analyses. Most of the cases they show similar results, however, sometimes they do not move paralelly, because they measure different things. The χ^2 statistic is a sum of the deviances in the observations in the 16 cells measured in two time periods, however, the pi-star index measures the amount of maximum deviance in the above cells.

3. Some other statistical characteristics of wind direction

By our former investigations (*Tar,* 2001), the frequency distribution of wind directions can be in close relation with the relative energy content, average

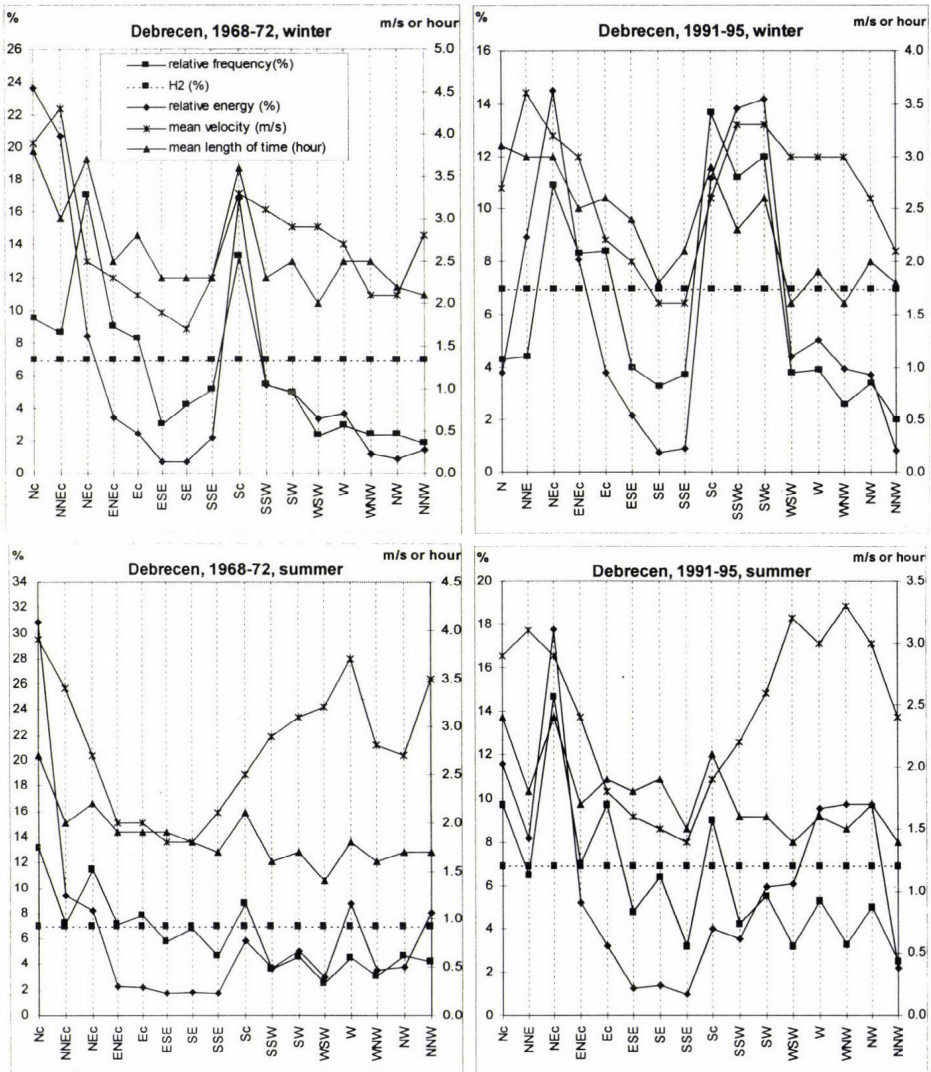

Fig. 2. Some statistical characteristics of wind direction in Debrecen (*c:* characteristic wind direction).

speed, and average duration of wind directions. This can be seen in *Fig. 2* and *Fig. 3.* These figures show the above-mentioned characteristics in winter and summer, in a lowland and a Transdanubian station (Debrecen and Szombathely), which are on about the same geographical latitude. One can see, there are some wind directions where these characteristics differ markedly from the characteristics of other directions.

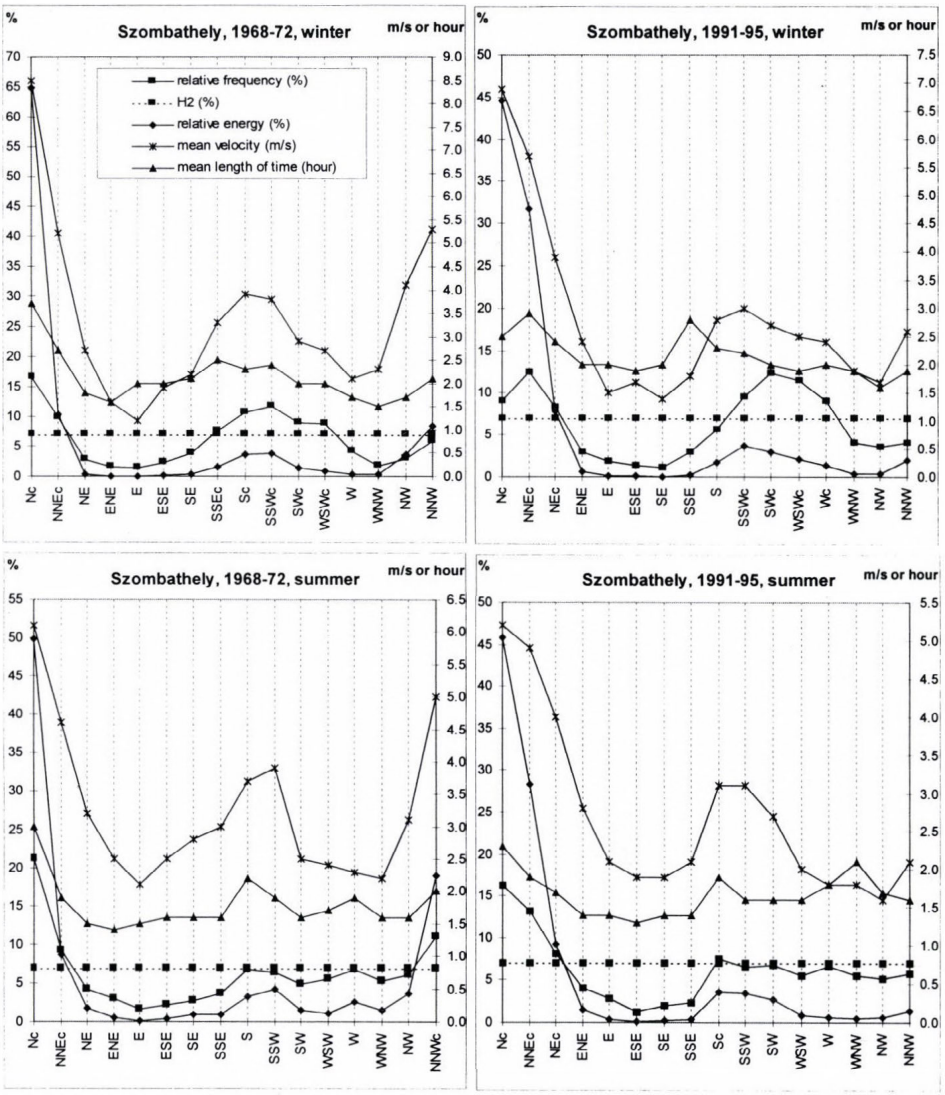

Fig. 3. Some statistical characteristics of wind direction in Szombathely (*c:* characteristic wind direction).

3.1 Characteristic wind directions

The hypothesis on the evenness of the frequency distribution of wind direction was verified in the following way (*Tar*, 1991): let h_1 and h_2 be

$$h_1 = p_0 n - u_\varepsilon \sqrt{n p_0 (1 - p_0)}, \tag{2}$$

$$h_1 = p_0 n + u_\varepsilon \sqrt{n p_0 (1 - p_0)}, \tag{3}$$

where p_0 is equal to $1/16=0.0625$, as we used 16 wind directions, n is the number of cases. u_ε satisfies the equation

$$2\Phi(u_\varepsilon) - 1 = 1 - \varepsilon, \tag{4}$$

where Φ(x) is the distribution function of standard normal distribution. So, if $\varepsilon=0.0027$ (*Péczely*, 1957), then $u_\varepsilon=2.28$.

Let f_D be the relative frequency of direction D, where $D=\{$N, NNE, NE, ENE, E, ESE, SE, SSE, S, SSW, SW, WSW, W, WNW, NW, NNW$\}$. If $f_D \geq h_2$, then D is called characteristic wind direction (CWD), else it is a non-characteristic wind direction (NWD) on $1-\varepsilon$ probability level. If f_D is given in percents, then the limits of the critical interval are $H_1=100\ h_1/n$, $H_2=100\ h_2/n$. *Fig. 2* and *Fig. 3* show the value of H_2, where the characteristic wind directions are denoted by „c" on axis x.

In the following we will compare the energy content and average speed of characteristic wind directions to those of the other wind directions. The average energy content of a D wind direction for a time period (season, year) can be determined with the mean specific wind power, namely with the equation

$$P_{f1}(D) = \frac{\rho}{2} \sum_{j=1}^{k} \frac{f_{Dj}}{N} v_j^{\,3}. \tag{5}$$

Here f_{Dj} is the frequency of the speed of D wind within the $(v_j - 0.5\Delta v, v_j + 0.5\Delta v)$ interval, k is the number of intervals and N is the number of the days of time period, respectively. Let P_{f1} denote the mean specific wind power of time period, which is independent of the wind directions, then the ratio

$$p(D) = \frac{P_{f1}(D)}{P_{f1}} \tag{6}$$

is equal to the relative energy content of the given D wind direction. The average speed of this direction is

$$\bar{v}(D) = \sum_{j=1}^{k} \frac{f_{Dj}}{N} v_j. \tag{7}$$

Value of the last parameter strongly depends on the height of anemometer. This height is regularly 10 meters at the meteorological stations, but it can happen that the wind speed is measured on a lower or higher level. In these cases the height correction is done by the following equation:

$$v_h = v_{10}\,[0.233 + 0.656\,\lg(h + 4.75)] \tag{8}$$

(*Mezősi* and *Simon*, 1981), where v_h is the measured wind speed on $h \neq 10$ m and v_{10} is the calculated wind speed on 10 m. In some selected cities it had happened that the measurements were carried out on height differing from 10 m, or the stations was moved to another place, or the instrument was changed for an automatic one. In the last two cases the height of the sensor was changed, too. In all of these stations we produced the 10-meter wind speed by the above equation.

We investigated in detail the number of characteristic wind directions (CWD), common relative frequencies (CWD_F), common and mean relative energy contents (CWD_E and CWD_{E1}), and average speeds (CWD_{V1}) of these wind directions, mean relative energy content (NWD_{E1}) and average speed (NWD_{V1}) of non-characteristic wind directions, and the seasonal (independently of the wind directions) average wind speed (AWD_{V1}), respectively, in winter and summer of the two five-year periods. The stations were grouped by the following way: stations over plain terrain (Debrecen, Békéscsaba, Szeged, Budapest, Győr), which are opened by geographically, stations over hilly or mountainous territory (Szombathely, Keszthely, Pécs, Miskolc), in which the orography modifies the airflow strongly, and Kékestető, because it belongs to an other current of air, that we have to take into consideration comparing the average wind speeds. We are able to compare only the relative quantities of Miskolc, because the meteorological station was removed to the Avas-mountain in the second time period, and its height above sea level increased markedly.

Our results at stations over plain terrain show that

- the value of CWD is between 3 and 9, CWD_F is between 33 and 81% (Békéscsaba, 1968–72, winter and Győr, 1991–95, winter, respectively),
- CWD_E is between 91% (Győr, 1991–95, winter) and 42% (Debrecen, 1991–95, summer),
- CWD_{E1} (the energy content of one CWD) is between 18.6% (Győr, 1991–95, summer) and 8.3% (Debrecen, 1991–95, summer),
- the maximum values of the above parameters are in Győr, but the minimum value of CWD_{V1} is also here (1991–95, summer). The maximum of the latest parameter is in the Great Hungarian Plane, Szeged, 1968–72, winter,

- relative energy content of an other, non-characteristic wind direction (NWD_{E1}) is between 5.3% (Debrecen, 1991–95, summer) and 1.2% (Győr, 1991–95, winter). The time and place of extreme values of NWD_{V1} agree with those of CWD,
- the average wind speed of seasons (AWD_{V1}) alters from 3.5 m/s (Szeged, 1968–72, winter) to 1.9 m/s (Győr, 1991–95, summer).

Table 3. Territorial averages: average values of CWD, common relative frequency (CWD_F) and relative energy content (CWD_E) of characteristic wind directions, average energy content (CWD_{E1}) and average speed (CWD_{V1}) of one characteristic wind direction, average energy content (NWD_{E1}) and average speed (NWD_{V1}) of one non-characteristic wind direction, averages of wind speed (AWD_{V1})

Average of	CWD	CWD_F (%)	CWD_E (%)	CWD_{E1} (%)	CWD_{V1} (m/s)	NWD_{E1} (%)	NWD_{V1} (m/s)	AWD_{V1} (m/s)
Stations over plain terrain								
Yearly	**5.3**	**53.7**	**63.5**	**12.4**	**2.9**	**3.4**	**2.4**	**2.7**
1968–72	5.3	53.0	63.8	12.2	3.1	3.4	2.5	2.8
1991–95	5.3	54.3	63.3	12.5	2.8	3.3	2.3	2.6
Winter	**5.5**	**55.1**	**66.3**	**12.4**	**3.1**	**3.1**	**2.4**	**2.8**
1968–72	5.0	51.7	62.8	12.7	3.2	3.3	2.6	2.9
1991–95	6.0	58.6	69.7	12.1	3.0	2.9	2.3	2.8
Summer	**5.1**	**52.2**	**60.8**	**12.4**	**2.7**	**3.6**	**2.4**	**2.6**
1968–72	5.6	54.3	64.7	11.7	3.0	3.4	2.5	2.7
1991–95	4.6	50.1	56.9	13.0	2.5	3.8	2.2	2.4
Stations over no-plain terrain								
Yearly	**5.1**	**54.2**	**68.9**	**14.3**	**3.6**	**2.8**	**2.6**	**3.2**
1968–72	4.6	51.8	65.1	14.9	4.0	3.0	2.9	3.5
1991–95	5.3	56.6	72.6	13.6	3.3	2.6	2.3	2.9
Winter	**5.5**	**58.2**	**68.1**	**12.4**	**3.8**	**3.0**	**2.8**	**3.4**
1968–72	5.0	56.4	62.9	12.6	4.1	3.3	3.1	3.6
1991–95	6.0	60.1	73.3	12.3	3.5	2.6	2.6	3.2
Summer	**5.0**	**50.2**	**69.6**	**16.1**	**3.5**	**2.6**	**2.4**	**2.9**
1968–72	4.2	47.3	67.3	17.2	4.0	2.7	2.7	3.3
1991–95	5.0	53.0	72.0	14.9	3.1	2.6	2.1	2.5

Table 3 shows the average values. (The average number of CWD is important from the point of view of other parameters only.) Based on the part concerning the stations over plain terrain of this table we can say that

- there is no considerable difference between the "yearly" (winter +summer) parameters, given in percents, in the two five-year periods at these stations. The ratio of energy content of one CWD to that of one

NWD (CWD_{E1}/NWD_{E1}) is 3.6 in the first five-year period and 3.8 in the second five-year period. The average speed of CWD (CWD_{V1}) is larger than NWD_{V1} with 0.5 m/s, and with 0.2 m/s than the "yearly" average wind speed,

- note, that the decrease of different average wind speeds is 0.2–0.3 m/s to the second period,
- the number of CWD increased with 1, CWD_F and CWD_E also increased with about 7% according to this in winter,
- on the other hand CWD_{E1}, NWD_{E1}, and all the average speed decreased, the latest parameters with 0.1–0.3 m/s in winter,
- the ratio of energy content of different direction groups increased with 3.8–4.2 to the second period, it is equal to 4 on average in winter,
- the number of CWD decreased with 1, CWD_F and CWD_E also decreased with about 4 or 8% according to this in summer,
- the different average wind speeds decreased with 0.3–0.5 m/s in summer, i.e., more considerably than in winter,
- the ratio of energy content of different direction groups increased somewhat to the second period, it is equal to 3.4 on average in two summers.

Our results at stations over no-plain terrain show that

- the number of CWD is between 3 (Szombathely, 1968–72, summer) and 7, the last number occurs in more cases,
- CWD_F is between 74% (Szombathely, 1968–72, summer) and 41% (in more cases), CWD_E is between 94 and 38%,
- CWD_{E1} and CWD_{V1} are between 26–7.6%, and 5.5–1.8 m/s, respectively. In the last case we considered only 3 stations (Szombathely, Keszthely, and Pécs). Note, however, that the average speeds in Szombathely are commensurable with those in Kékestető,
- the maximum of above-mentioned parameters occurs in Szombathely. This value of NWD_{E1} occurs in Pécs (1968–72, winter) among the five stations, and here is the maximum of NWD_{V1} among the considered three stations,
- average wind speed of the seasons is the largest in Szombathely, too. It is interesting that these values decreased in the first three stations in all cases and in Kékestető in summer with 0.9–0.2 m/s to the second period, but they stagnate in Kékestető in the winter.

Based on the part concerning the stations over no-plain terrain of *Table 3*, we can find the following results.

In "yearly average" (winter+summer),

- the number of CWD, CWD_F, and CWD_E increased in order with about 1, 5 and 7%, but in contrast with this

- CWD_{E1} decreased by 1.3% to the second period,
- the above yearly value exceeds that of the stations over plain terrain by about 2% in average, 2.7% in the first, and 1.1% in the second period,
- the value of NWD_{E1} also decreased,
- the ratio CWD_{E1}/NWD_{E1} is equal to 5.1 at these stations in contrast with 3.6 at stations over plain terrain.

In winter,

- the number of CWD increased by 1, CWD_F and CWD_E also increased by about 4%, and 10%, according to this, respectively,
- the values of CWD_{E1} did not change,
- these values are equal to the corresponding values of plain terrain in average and by periods, too,
- NWD_{E1} somewhat decreased. The ratio CWD_{E1}/NWD_{E1} increased here and now, too, but to essentially higher degree than on the plain terrain.

In summer,

- the average number of CWD increased, CWD_F and CWD_E also increased by about 6%, and 5%, according to this, respectively,
- the value of CWD_{E1} decreased by more than 2%, but
- the above mentioned numbers are larger than those at the stations over plain terrain. Therefore, at the stations over no-plain one characteristic wind direction carries more than 3% energy in average. This surplus is 5.5% in summers of 1968–72 and about 2% in summers of 1991–95,
- for the stations over plain terrain there is no considerable difference in the winter and summer values of the above mentioned parameters. For the stations over no-plain terrain, the value of CWD_{E1} is larger by about 4% in summer.
- the ratio CWD_{E1}/ NWD_{E1} is the largest over no-plain terrain in summer, it is 6.2 in average of periods, 6.4 for summers of 1968–72, 5.7 for summers of 1991–95. It is in contrast with the stagnating summer values on plain terrain.

Different average wind speeds are determined, except Miskolc. Based on the part concerning the stations over no-plain terrain of *Table 3*, we can find that,

- in the "yearly average", the value of CWD_{V1} is larger by exactly 1 m/s than NCW_{V1} and 0.4 m/s than the average wind speed of the "year" (in last column, AWD_{V1}: average speed of all wind directions),
- in the period 1991–95 these differences are the same, in the period 1968–72 they are 1.1, and 0.5 m/s, respectively,
- these differences do not change essentially in winter,

- but in summer the difference CWD_{V1}-NCW_{V1} is equals to or larger than 1 m/s, CWD_{V1}-AWD_{V1} is equal to or larger than 0.6 m/s. The maximum of two differences is in the summers of 1968–72,
- all average wind speeds are decreasing, to the highest degree, 0.9 m/s, in the case of summer characteristic wind directions. This value is equal to 0.5 m/s on the plain terrain.

In *Table 4* we give the ratios of time and terrain average energy content of one characteristic and one non-characteristic wind direction (CWD_{E1}/NWD_{E1}). It can be established, that these ratios

- have orographic differences on the annual and summer averages,
- are larger on the plain terrain in winter, and on the no-plain terrain in summer, respectively.

The yearly ratios of two five-year periods do not show considerable differences in the two groups of stations. But these ratios have significant differences in the two groups in winter and on the no-plain terrain stations in summer. According to the table, the ratio does not increase period-by-period in summer, even it decreases on the no-plain terrain stations in this season.

Table 4. The ratios of CWD_{E1}/NWD_{E1}

	Stations over	
	Plain terrain	**No-plain terrain**
Yearly	3.6	5.1
1968–72	3.6	5.0
1991–95	3.8	5.2
Winter	4.0	4.1
1968–72	3.8	3.8
1991–95	4.2	4.7
Summer	3.4	6.2
1968–72	3.4	6.4
1991–95	3.4	5.7

3.2 Relationship between the frequency, energy content, average speed, and average duration of wind directions

As it can be seen in *Fig. 2* and *3*, some curves of values connected to wind directions (frequency, energy content, average speed, and average duration) are roughly parallel to each other. This refers to the linearity of their stochastic connection, so we determined the values of linear correlation coefficient (r). They are given in *Table 5* and *6* in stations over plain and no-plain terrain to the winter and summer of the two five-year periods. The critical value of r, belonging to 16 number of cases, on 0.05 significance level, $r_{0.05}$ equals to 0.4973 (*Dobosi* and *Felméry*, 1971).

Table 5. Values of the linear correlation coefficient in stations over plain terrain (*italic:* significant value)

Debrecen, winter					**Debrecen, summer**				
1968-72	**rel.freq.**	**rel. energ.**	**mean sp.**	**mean dur.**	**1968-72**	**rel.freq.**	**rel. energ.**	**mean sp.**	**mean dur.**
rel.freq.		*0.5984*	0.3266	*0.8722*	**rel.freq.**		*0.6453*	0.0253	*0.9547*
rel. energ.	*0.8580*		*0.8741*	*0.7982*	**rel. energ.**	*0.5676*		*0.6794*	*0.7868*
mean sp.	0.3889	*0.7524*		0.4922	**mean sp.**	0.0193	*0.7619*		0.1816
mean dur.	*0.5929*	*0.5554*	0.3183		**mean dur.**	*0.9114*	0.4940	-0.0481	
1991-95	**rel.freq.**	**rel. energ.**	**mean sp.**	**mean dur.**	**1991-95**	**rel.freq.**	**rel. energ.**	**mean sp.**	**mean dur.**
Békéscsaba, winter					**Békéscsaba, summer**				
1968-72	**rel.freq.**	**rel. energ.**	**mean sp.**	**mean dur.**	**1968-72**	**rel.freq.**	**rel. energ.**	**mean sp.**	**mean dur.**
rel.freq.		*0.8674*	*0.5139*	*0.9484*	**rel.freq.**		*0.6820*	0.2999	0.4669
rel. energ.	*0.9836*		*0.8280*	*0.8628*	**rel. energ.**	*0.8444*		*0.8541*	-0.0084
mean sp.	*0.7940*	*0.7765*		*0.5285*	**mean sp.**	*0.5861*	*0.8606*		-0.4259
mean dur.	*0.8558*	*0.8419*	*0.5264*		**mean dur.**	*0.8486*	*0.6944*	0.4484	
1991-95	**rel.freq.**	**rel. energ.**	**mean sp.**	**mean dur.**	**1991-95**	**rel.freq.**	**rel. energ.**	**mean sp.**	**mean dur.**
Szeged, winter					**Szeged, summer**				
1968-72	**rel.freq.**	**rel. energ.**	**mean sp.**	**mean dur.**	**1968-72**	**rel.freq.**	**rel. energ.**	**mean sp.**	**mean dur.**
rel.freq.		*0.8793*	*0.7232*	*0.7775*	**rel.freq.**		*0.9213*	*0.8119*	*0.8711*
rel. energ.	*0.8099*		*0.9113*	*0.7324*	**rel. energ.**	*0.9241*		*0.9093*	*0.6938*
mean sp.	0.4926	*0.7570*		*0.6297*	**mean sp.**	*0.5521*	*0.7566*		*0.5368*
mean dur.	*0.9016*	*0.7501*	0.4186		**mean dur.**	*0.8172*	*0.6425*	0.2182	
1991-95	**rel.freq.**	**rel. energ.**	**mean sp.**	**mean dur.**	**1991-95**	**rel.freq.**	**rel. energ.**	**mean sp.**	**mean dur.**
Budapest, winter					**Budapest, summer**				
1968-72	**rel.freq.**	**rel. energ.**	**mean sp.**	**mean dur.**	**1968-72**	**rel.freq.**	**rel. energ.**	**mean sp.**	**mean dur.**
rel.freq.		0.3862	0.2789	*0.9285*	**rel.freq.**		*0.8212*	*0.6517*	*0.9041*
rel. energ.	0.4469		*0.9248*	*0.5818*	**rel. energ.**	*0.8022*		*0.9347*	*0.8050*
mean sp.	0.3089	*0.9473*		0.4348	**mean sp.**	0.3678	*0.7413*		*0.6852*
mean dur.	*0.9011*	0.3372	0.2072		**mean dur.**	*0.9394*	*0.7206*	0.3576	
1991-95	**rel.freq.**	**rel. energ.**	**mean sp.**	**mean dur.**	**1991-95**	**rel.freq.**	**rel. energ.**	**mean sp.**	**mean dur.**
Győr, winter					**Győr, summer**				
1968-72	**rel.freq.**	**rel. energ.**	**mean sp.**	**mean dur.**	**1968-72**	**rel.freq.**	**rel. energ.**	**mean sp.**	**mean dur.**
rel.freq.		*0.7970*	0.3713	*0.6007*	**rel.freq.**		*0.9345*	0.4608	*0.8253*
rel. energ.	*0.7994*		*0.7886*	*0.5146*	**rel. energ.**	*0.8652*		*0.6831*	*0.8373*
mean sp.	*0.6648*	*0.8829*		0.2303	**mean sp.**	0.4389	*0.6314*		*0.5187*
mean dur.	*0.6867*	*0.6164*	*0.5108*		**mean dur.**	*0.9025*	*0.8393*	0.4449	
1991-95	**rel.freq.**	**rel. energ.**	**mean sp.**	**mean dur.**	**1991-95**	**rel.freq.**	**rel. energ.**	**mean sp.**	**mean dur.**

The most important conclusions from *Table 5* concerning to stations over the plain terrain are:

- All number of significant cases ($r > r_{0.05}$) are 74% in the year, 75% in winter, and 73% in summer. Therefore, there is no considerable seasonal difference.
- The numbers of significant cases do not differ considerably from each other in the seasons of two periods: it is 77% in 1968–72 and 73% in

Table 6. Values of the linear correlation coefficient in stations over no-plain terrain (*italic:* significant value)

Szombathely, winter					**Szombathely, summer**				
1968-72	**rel.freq.**	**rel. energ.**	**mean sp.**	**mean dur.**	**1968-72**	**rel.freq.**	**rel. energ.**	**mean sp.**	**mean dur.**
rel.freq.		*0.6786*	*0.7797*	*0.8492*	**rel.freq.**		*0.9560*	*0.8751*	*0.9284*
rel. energ.	0.4830		*0.8566*	*0.8420*	**rel. energ.**	*0.9022*		*0.8531*	*0.8918*
mean sp.	*0.6253*	*0.9557*		*0.8218*	**mean sp.**	*0.8655*	*0.8877*		*0.8224*
mean dur.	0.3392	*0.5975*	*0.6234*		**mean dur.**	*0.8319*	*0.6764*	*0.5469*	
1991-95	**rel.freq.**	**rel. energ.**	**mean sp.**	**mean dur.**	**1991-95**	**rel.freq.**	**rel. energ.**	**mean sp.**	**mean dur.**
Keszthely, winter					**Keszthely, summer**				
1968-72	**rel.freq.**	**rel. energ.**	**mean sp.**	**mean dur.**	**1968-72**	**rel.freq.**	**rel. energ.**	**mean sp.**	**mean dur.**
rel.freq.		*0.6606*	*0.6539*	*0.8576*	**rel.freq.**		*0.8653*	*0.7997*	*0.8377*
rel. energ.	*0.7496*		*0.9347*	*0.7963*	**rel. energ.**	*0.8224*		*0.9159*	*0.8103*
mean sp.	*0.6966*	*0.8792*		*0.7209*	**mean sp.**	*0.5748*	*0.8159*		*0.7999*
mean dur.	*0.9010*	*0.8937*	*0.8891*		**mean dur.**	*0.7705*	*0.8052*	*0.7653*	
1991-95	**rel.freq.**	**rel. energ.**	**mean sp.**	**mean dur.**	**1991-95**	**rel.freq.**	**rel. energ.**	**mean sp.**	**mean dur.**
Pécs, winter					**Pécs, summer**				
1968-72	**rel.freq.**	**rel. energ.**	**mean sp.**	**mean dur.**	**1968-72**	**rel.freq.**	**rel. energ.**	**mean sp.**	**mean dur.**
rel.freq.		0.4683	0.1163	*0.8819*	**rel.freq.**		*0.8411*	*0.5724*	*0.6756*
rel. energ.	*0.5967*		*0.8659*	*0.5679*	**rel. energ.**	*0.7262*		*0.8737*	*0.6381*
mean sp.	0.1946	*0.7915*		0.3267	**mean sp.**	0.3151	*0.8094*		*0.5874*
mean dur.	*0.7193*	0.4252	0.2774		**mean dur.**	*0.8260*	*0.7219*	0.3534	
1991-95	**rel.freq.**	**rel. energ.**	**mean sp.**	**mean dur.**	**1991-95**	**rel.freq.**	**rel. energ.**	**mean sp.**	**mean dur.**
Miskolc, winter					**Miskolc, summer**				
1968-72	**rel.freq.**	**rel. energ.**	**mean sp.**	**mean dur.**	**1968-72**	**rel.freq.**	**rel. energ.**	**mean sp.**	**mean dur.**
rel.freq.		*0.5031*	0.0466	*0.7001*	**rel.freq.**		*0.8412*	0.1503	*0.6116*
rel. energ.	*0.5638*		*0.7380*	*0.6524*	**rel. energ.**	*0.8762*		*0.5916*	*0.5826*
mean sp.	0.4584	0.7941		0.3880	**mean sp.**	0.4432	*0.7148*		0.3475
mean dur.	*0.9115*	*0.6530*	*0.6420*		**mean dur.**	*0.8289*	*0.7290*	*0.5445*	
1991-95	**rel.freq.**	**rel. energ.**	**mean sp.**	**mean dur.**	**1991-95**	**rel.freq.**	**rel. energ.**	**mean sp.**	**mean dur.**
Kékestető, winter					**Kékestető, summer**				
1968-72	**rel.freq.**	**rel. energ.**	**mean sp.**	**mean dur.**	**1968-72**	**rel.freq.**	**rel. energ.**	**mean sp.**	**mean dur.**
rel.freq.		*0.8857*	*0.6121*	*0.8336*	**rel.freq.**		*0.9483*	*0.6743*	*0.8953*
rel. energ.	*0.9161*		*0.8550*	*0.6888*	**rel. energ.**	*0.8767*		*0.8038*	*0.8972*
mean sp.	*0.8441*	*0.8478*		0.3769	**mean sp.**	*0.7431*	*0.7700*		*0.7733*
mean dur.	*0.6222*	*0.7576*	*0.7428*		**mean dur.**	*0.8204*	*0.8552*	*0.7377*	
1991-95	**rel.freq.**	**rel. energ.**	**mean sp.**	**mean dur.**	**1991-95**	**rel.freq.**	**rel. energ.**	**mean sp.**	**mean dur.**

- 1991–95, in winter and summer. Namely, the ratio of significant cases decreased by about 4% to the second period at stations over the plain terrain.

The most important conclusions from *Table 6* concerning the stations over the no-plain terrain are:

- All number of significant cases are 80% in winter, 92% in summer, 86% altogether. Therefore, there is considerable seasonal difference at these stations.

- The ratios of significant cases differ from each other in the seasons of two periods: it is 80% in winter, 93% in summer of 1968–72, 80% in winter, 90% in summer of 1991–95. Namely, the number of significant cases did not change considerably to the second period in the seasons at these stations.

The most important conclusions from the two tables are:

- The connection of the relative frequency and relative energy content is not significant only in four cases. They are all winter cases. There are no orographical and temporal differences.
- There is no seasonal difference in connection of the relative frequency and mean velocity. There is a temporal difference in the stations over no-plain terrain: the number of significant cases decreased by 10% to the second period. The orographical differences are marked: the number of significant cases are more with 30% (1968–72), 20% (1991–95), and 25% (together), respectively, than those in the stations over no-plain terrain.
- The connection of relative frequency and average duration is significant except two cases, which is not surprising.
- The connection of relative energy and average speed is significant in every case, since they are in a complicated functional relation through the hourly wind speed.
- The connection between relative energy and average duration is completely random, of course. The number of significant cases is larger by 10% in the stations over no-plain terrain, considering all the cases or periods. There is a temporal difference, too: such cases decreased by 10% to the second period in both territories. There are no seasonal differences.
- All three kinds of differences are noticeable in connection of the average speed and average duration. Considering all the cases, we can establish twice as many significant cases in the stations over no-plain terrain than in the other territory (70% and 35%, respectively). The difference is only 10% in the first period, but it is 60% in the second one. Namely, the number of significant cases considerably decreased at the stations over plain terrain and considerably increased at the stations over no-plain terrain to the second period. At the same time, the number of significant connections is more in summer in the first period and in winter in the second period.

4. General conclusions

Temporal change of the frequency distribution of wind directions, which is in connection with the global warming, during the two selected period (1968–72, 1991–95), is not investigable by traditional statistical tests. The χ^2-test cannot

be applied because of the large sample size. The π^* index shows seasonal and orographical differences but only in the comparison of its values, there is no significant threshold value. Its outstanding winter values, in Győr, Szombathely, Keszthely, and Pécs, refer rather to geographical differences than orographical ones. They indicate the connection with the NW steering flow, i.e., the seasonal large-scale processes (for example with the change of the see-level pressure in Europe). Its summer values are less, they show the less marked change without geographical and/or orographical differences.

The energy carried by the wind directions depends on the season and orography. This is verified by our investigations concerning the characteristic wind directions: in summer their energy content is less at the stations over plain terrain, more at the stations over no-plain terrain than in winter. The energy content of a characteristic wind direction increases in both territory in winter, decreases in the no-plain terrain in summer, to the second period. One characteristic wind direction carries about four times more energy than one non-characteristic wind direction on the yearly and winter averages, and about five times more than the summer average in Hungary.

There are seasonal and orographical differences in relations of the different parameters (relative frequency, relative energy content, average speed, average duration) of wind directions. In summer the number of significant cases is more than in winter in the plain terrain, they are almost equal to each other in the no-plain terrain. We could not establish considerable temporal differences between the two periods.

With the above results and establishments we would like to contribute to more exact and detailed knowledge of wind climate in our country, and to scientifically/climatologically established utilization of the wind energy .

Acknowledgements–The authors wish to express thanks to OTKA (Hungarian Scientific Research Found) and the Ministry for Environmental Protection for the sponsorship of researches connected the subject of this study, as well as to the Hungarian Meteorological Service for putting the data basis at their disposal.

References

Bartzokas, A. and *Metaxas, D.A.*, 1996: Northern Hemisphere gross circulation types. Climatic change and temperature distribution. *Meteorol. Zeitschrift*, N.F. 5, 99-109.

Dobosi, Z. and *Felméry, L.*, 1971: *Climatology* (in Hungarian), Tankönyvkiadó, Budapest, 500 p.

Justyák, J., 1994: *The Climate of Europe* (in Hungarian). Egyetemi Jegyzet. Debreceni Egyetem, 135 p.

Makra, L., Tar, K., and *Horváth, Sz.*, 2000a: Some statistical characteristics of the wind energy over the Great Hungarian Plane. *Int. J. Ambient Energy 21*, No. 2, 85-96.

Makra, L., Tar, K., and *Lukácsovicsné Horváth, Sz.*, 2000b: Analysis of wind speed data series in Hungary by using a new statistical test and conclusions in connection with climate change.

Scientific Meeting on Detection and Prediction of Contemporary Climate Change and their Effects in a Regional Scale, Tarragona, Spain, 29-31st May, 2000.

Metaxas, D.A., Bartzokas, A., and *Vitsas, A.*, 1991: Temperature fluctuations in the Mediterranean area during the last 120 years. *Int. J. Climatol. 11*, 897-909.

Meyhöfer, S., Rapp, J., and *Schönwiese, C.D.*, 1996: Observed three-dimensional climate trends in Europe 1961-1990. *Meteorol. Zeitschrift*, N.F. 5, 90-94.

Mezősi, M. and *Simon A.*, 1981: The theory and practice of meteorological wind measurements (in Hungarian). *Meteorológiai Tanulmányok*, No. 36. Országos Meteorológiai Szolgálat, Budapest.

Mika, J., Kircsi, A., and *Tar K.*, 1999: Some statistical characteristics of daily maximum wind gusts in the Great Hungarian Plain (in Hungarian). *Meteorológiai Tudományos Napok 1999*. Orsz. Meteorológiai Szolgálat, 207-213.

Rudas, T., Clogg, C.C., and *Lindsay, B.G.*, 1994: A new index of fit based on mixture methods for the analysis of contingency tables. *J. Royal Statistical Society*, Ser. B 56, 623-639.

Schönwiese, C.D., Rapp, J., Fuchs, T., and *Denhard, M.*, 1994: Observed climate trends in Europe 1891-1990. *Meteorol. Zeitschrift*, N.F. 3, 22-28.

Tar, K., 1998a: Statistical characteristics of the wind field over Hungary, in connection with the global warming (in Hungarian). In *Klimaváltozás és következményei*. Orsz. Meteorológiai Szolgálat, 249-258.

Tar, K.,1998b: Alteration of the statistical structure of the wind field in Hungary in connection with the climatic change. *2nd European Conference on Applied Climatology*, Central Institute for Meteorology and Geodinamics, Nr. 19, (CD-ROM, ISSN 1016-6254) Vienna, Austria.

Tar, K., 1999: Temporal change of statistical charcateristics of wind field over the Great Hungarian Plain (in Hungarian). *Change of landscape in the Carpathian Basin*. Proc. of Scientific Conference, Nyíregyháza, November 4-6, 1998. (ed.: *Gy. Füleky*), Gödöllő, 225-230.

Tar, K., 2001: Alteration of the statistical structure of the wind field in Hungary in connection with the conditional climatic change. *OTKA Research Paper* (T023765), University of Debrecen (in Hungarian).

Tar, K., Makra, L., and *Horváth, Sz.*, 2000: Some statistical characteristics of the wind energy in Hungary in connection with climatic change. *3rd European Conference on Applied Climatology* (CD-ROM, ISBN 88-900502-0-9), Pisa, Italy

Tar, K., Makra, L., and *Kircsi, A.*, 2001a: Temporal change of some statistical characteristics of wind speed in Hungary. In *Detecting and Modelling Regional Climate Change* (eds.: *M.B. India* and *D.L. Bonillo*). Springer-Verlag, 251-262.

Tar, K., Makra, L., Horváth, Sz., and *Kircsi, A.*, 2001b: Temporal change of some statistical characteristics of wind speed in the Great Hungarian Plane. *Theoretical and Applied Climatology*, Vol. 69, No. 1-2, 69-79.

BOOK REVIEW

Barry, R. G. and *Carleton, A. M.*, 2001: **Synoptic and Dynamic Climatology.** Routledge (Taylor and Francis Group), London and New York, 620 pages, with 15 color and black-and-white plates, nearly 300 figures and didactic illustrations, extended topical index.

The book provides a comprehensive account of the dynamical behavior and mechanisms of the global climate system and its components, together with a modern survey of synoptic scale weather systems in the tropics and extratropics, including the methods and applications of synoptic classification.

Roger G. Barry is Professor of Geography and Director of the National Snow and Ice Data Center at the University of Colorado. *Andrew M. Carleton* is Professor of Geography at Pennsylvania State University. This fact largely determines the key value of the book for meteorologists and other scientists. Scrolling through the book, the reader gets a scholarly description of the atmospheric circulation from the smallest to largest scales of atmospheric motions.

Twenty-seven years have elapsed since the publication of *Synoptic Climatology: Methods and Applications* (*Barry* and *Perry*, 1973), and the field has advanced considerably during that time. Computer-based classifications have become the rule, and the ready availability of extensive climatic data bases has permitted diverse analytical studies to be carried out. Results from these studies now allow us to state more confidently the most useful procedures for the synoptic classification and analysis of regional or local climatic conditions. The book differs very much from the one appeared three decades before. Only the last Chapter ("Synoptic climatology and its applications") remind us to the book-ancestor which is not coincidental and is accompanied by displaying *Prof. Allen H. Perry*, as co-author of the present chapter, as well.

The widespread practical applications of these studies is illustrated, with particular emphasis on the linkages between regional and global-scale climate processes. The latter relation, most likely an unresolved task required by climate change impacts but not yet available with fully dynamical models, makes the book especially valuable. Downscaling studies frequently based on objective classifications of the circulation systems, but sometimes using just formal statistics and (easily available) low resolution fields, could improve a lot by assimilation of the corresponding chapters, too.

Part I provides an introduction to the global climate system and the space-time scales of weather and climate processes, followed by a chapter on climate

data and their analysis. *Part 2* describes and explains the characteristics of the general circulation of the global atmosphere, planetary waves and blocking behavior, and the nature and causes of global teleconnection patterns. *Part 3* discusses synoptic weather systems in the extra-tropics and tropics, and satellite based climatologies of synoptic features. It also describes the methods and applications of synoptic climatology and summarizes current climatic research and its directions.

The scale and scope of this undertaking is remarkable. Each chapter makes it clear what is known and what has still to be investigated. This is coupled with a fascinating insight into the development of ideas over the past centuries and the way in which investigations have become increasingly scientific, utilizing the most sophisticated technologies available. Some of the figures are interesting because we know other interpretations expressing the same idea. A part of the figures are a little old, however, which is acceptable with tolerance in case of a textbook. In some cases, however, the print of the drawings does not correspond to the present typographical technology.

Summarizing, the authors provided a much-needed bridge between classical synoptic climatology and the more recent developments in dynamical and statistical meteorology. This book will serve as a valuable reference for climate researchers. It will also provide an excellent textbook for climate related courses at the graduate and post-graduate levels.

J. Mika

GUIDE FOR AUTHORS OF *IDŐJÁRÁS*

The purpose of the journal is to publish papers in any field of meteorology and atmosphere related scientific areas. These may be

- research papers on new results of scientific investigations,
- critical review articles summarizing the current state of art of a certain topic,
- short contributions dealing with a particular question.

Some issues contain "News" and "Book review", therefore, such contributions are also welcome. The papers must be in American English and should be checked by a native speaker if necessary.

Authors are requested to send their manuscripts to

Editor-in Chief of IDŐJÁRÁS

P.O. Box 39, H-1675 Budapest, Hungary

in three identical printed copies including all illustrations. Papers will then be reviewed normally by two independent referees, who remain unidentified for the author(s). The Editor-in-Chief will inform the author(s) whether or not the paper is acceptable for publication, and what modifications, if any, are necessary.

Please, follow the order given below when typing manuscripts.

Title part: should consist of the title, the name(s) of the author(s), their affiliation(s) including full postal and E-mail address(es). In case of more than one author, the corresponding author must be identified.

Abstract: should contain the purpose, the applied data and methods as well as the basic conclusion(s) of the paper.

Key-words: must be included (from 5 to 10) to help to classify the topic.

Text: has to be typed in double spacing with wide margins on one side of an A4 size white paper. Use of S.I. units are expected, and the use of negative exponent is preferred to fractional sign. Mathematical formulae are expected to be as simple as possible and numbered in parentheses at the right margin.

All publications cited in the text should be presented in a *list of references*, arranged in alphabetical order. For an article: name(s) of author(s) in Italics, year, title of article, name of journal, volume, number (the latter two in Italics) and pages. E.g., *Nathan, K.K.,* 1986: A note on the relationship between photo-synthetically active radiation and cloud amount. *Időjárás 90,* 10-13. For a book: name(s) of author(s), year, title of the book (all in Italics except the year), publisher and place of publication. E.g., *Junge, C. E.,* 1963: *Air Chemistry and Radioactivity*. Academic Press, New York and London. Reference in the text should contain the name(s) of the author(s) in Italics and year of publication. E.g., in the case of one author: *Miller* (1989); in the case of two authors: *Gamov* and *Cleveland* (1973); and if there are more than two authors: *Smith et al.* (1990). If the name of the author cannot be fitted into the text: *(Miller,* 1989); etc. When referring papers published in the same year by the same author, letters a, b, c, etc. should follow the year of publication.

Tables should be marked by Arabic numbers and printed in separate sheets with their numbers and legends given below them. Avoid too lengthy or complicated tables, or tables duplicating results given in other form in the manuscript (e.g., graphs)

Figures should also be marked with Arabic numbers and printed in black and white in camera-ready form in separate sheets with their numbers and captions given below them. Good quality laser printings are preferred.

The text should be submitted both in manuscript and in electronic form, the latter on diskette or in E-mail. Use standard 3.5" MS-DOS formatted diskette or CD for this purpose. MS Word format is preferred.

Reprints: authors receive 30 reprints free of charge. Additional reprints may be ordered at the authors' expense when sending back the proofs to the Editorial Office.

More information for authors is available: antal.e@met.hu

Information on the last issues: http://omsz.met.hu/irodalom/firat_ido/ido_hu.html

Published by the Hungarian Meteorological Service

Budapest, Hungary

INDEX: 26 361

HU ISSN 0324-6329